Verification of a Combined Variable Approach for the Microbiological Validation of Monochromatic- and Polychromatic UV Systems

Zur Erlangung des akademischen Grades eines
DOKTORS DER NATURWISSENSCHAFTEN

von der KIT-Fakultät für Chemieingenieurwesen und Verfahrenstechnik des Karlsruher Instituts für Technologie (KIT)
genehmigte

DISSERTATION

von

Tim Schwarzenberger

Tag der mündlichen Prüfung: 25.07.2025

Erstgutachter: Prof. Dr. Harald Horn

Zweitgutachter: Prof. Dr.-Ing. Matthias Franzreb

Declaration of Originality

I confirm that the submitted thesis is original work and was written by me without further assistance. Appropriate credit has been given where reference has been made to the work of others.

Tim Schwarzenberger

Zusammenfassung

Die vorliegende Doktorarbeit untersucht zentrale Aspekte der Validierung von UV-Desinfektionssystemen, die mit Nieder- oder Mitteldruck-Quecksilberdampflampen betrieben werden. In Deutschland müssen diese Systeme vor dem kommunalen Einsatz validiert werden. Akkreditierte Laboratorien führen hierzu Biodosimetrie im Großmaßstab durch, um die keimtötende Wirkung zu überprüfen und Betriebsparameter festzulegen. Dabei wird ein gut charakterisierter, nicht pathogener Testmikroorganismus verwendet, aktuell *Bacillus subtilis* Sporen.

Mit der Einführung neuer DIN-Normen für Mitteldrucklampensysteme und LED-basierte Systeme ergibt sich die Notwendigkeit, das veraltete Wirkungsspektrum von *Bacillus subtilis* Sporen mit modernsten Techniken neu zu definieren. Daraus ergibt sich die erste Hypothese:

Hypothese 1:

Bacillus subtilis ist für zukünftige Teststandards möglicherweise nicht mehr als Ersatzmikroorganismus geeignet. Dies gilt insbesondere für die Validierung von polychromatischen UV-Desinfektionssystemen (mit Mitteldrucklampen oder LEDs). In dieser Studie wurde das Wirkungsspektrum von *Bacillus subtilis* Sporen bei 19 monochromatischen Wellenlängen zwischen 220 nm und 320 nm mit einem abstimmbaren, laserbasierten Aufbau bestimmt, der ein hochauflösendes Spektrum, insbesondere zwischen 260 nm und 285 nm, ergab. Eine vergleichende Analyse mit Literaturdaten [Cabaj et al., 2002] zeigte eine signifikant höhere UV-Empfindlichkeit zwischen 260 nm und 280 nm sowie einen starken Abfall der Inaktivierung oberhalb von 280 nm, wobei ab 290 nm keine weitere Inaktivierung mehr beobachtet wurde.

Die zweite Hypothese dieser Arbeit befasst sich mit der Optimierung der derzeit in Europa angewandten Methodik des biodosimetrischen Verfahrens und wird wie folgt formuliert:

Hypothese 2:

Der „combined variable"-Ansatz, der Methodik für die Biodosimetrie aus dem amerikanischen UV-Desinfektionshandbuchs (UVDGM), bietet eine größere Flexibilität, Effizienz und Sicherheit bei der Validierung und Überwachung von UV-Systemen im Vergleich zum traditionellen europäischen „intensity setpoint"-Verfahren. Bei diesem Testverfahren werden die reaktorspezifischen Fluenzverteilungen berücksichtigt, indem die spezifische UV-Empfindlichkeit (D_L) von Mikroorganismen einbezogen wird. Dadurch kann eine präzisere Desinfektionswirksamkeit für wasserrelevante Pathogene abgeschätzt werden. Bei polychromatischen Systemen wird die Methodik zusätzlich durch einen Korrekturfaktor erweitert, um die Abhängigkeit der Desinfektionswirksamkeit von der Wellenlänge für verschiedene Mikroorganismen einzuberechnen.

Die Anwendbarkeit dieses alternativen Testverfahrens wurde theoretisch mittels Simulationswerkzeugen bewertet. Die theoretischen Ergebnisse bestätigten die erheblichen Vorteile des alternativen Ansatzes und zeigten Defizite in der bestehenden Methodik auf.

Diese Arbeit leistet einen wesentlichen Beitrag zur Weiterentwicklung und Optimierung der UV-Desinfektionstechnologie und trägt zur Verbesserung der öffentlichen Gesundheit und Sicherheit bei.

Abstract

This dissertation examines key aspects of the validation of UV disinfection systems that use low-pressure or medium-pressure mercury vapor lamps. These systems must be validated before their municipal use in Germany. Accredited laboratories conduct large-scale biodosimetry to verify germicidal efficacy and establish operating parameters. A well-characterized, non-pathogenic surrogate microbe, currently *Bacillus subtilis* spores, is used for this purpose.

With the introduction of new DIN standards for medium-pressure lamp systems and LED-based systems, it becomes necessary to redefine the outdated action spectrum of *Bacillus subtilis* spores using state-of-the-art techniques. This leads to the first hypothesis:

Hypothesis 1:

Bacillus subtilis may no longer be suitable as a surrogate microbe for future test standards, particularly for the validation of polychromatic UV disinfection systems (using medium-pressure lamps or LEDs). In this study, the action spectrum of *Bacillus subtilis* spores was determined at 19 monochromatic wavelengths between 220 nm and 320 nm using a tunable laser-based setup that provided a high-resolution spectrum, especially between 260 nm and 285 nm. A comparative analysis with literature data [Cabaj et al., 2002] revealed significantly higher UV sensitivity between 260 nm and 280 nm, with a sharp decline in inactivation above 280 nm, and no further inactivation observed from 290 nm onwards.

The second hypothesis of this work deals with the optimization of the biodosimetric method currently used in Europe and is formulated as follows:

Hypothesis 2:

The "combined variable" approach, a methodology for biodosimetry from the American UV Disinfection Guidance Manual (UVDGM), offers greater flexibility, efficiency, and safety in the validation and monitoring of UV systems compared to the traditional European "intensity setpoint" approach. This method takes reactor-specific fluence distributions into account by incorporating the specific UV sensitivity (D_L) of microbes, allowing for a precise estimation of disinfection efficacy for waterborne pathogens. For polychromatic systems, the methodology is further refined by an action spectrum correction factor (ASCF) to account for the dependence of the disinfection efficacy on the wavelength of various microbes.

The effectiveness of this alternative testing method was evaluated theoretically using simulation tools. The theoretical results confirmed the significant advantages of the alternative approach and highlighted deficiencies in the existing methodology.

This work makes a substantial contribution to the advancement and optimization of UV disinfection technology, thereby enhancing public health and safety.

Vorwort

Bereits seit Abschluss meines Masterstudiums stand für mich fest: Eines Tages verfasse ich eine Dissertation. Ich bin überglücklich, dass ich diesen Traum nun verwirklicht habe!

Die vorliegende Arbeit ist nicht nur das Ergebnis wissenschaftlicher Forschung, sondern auch das eines jahrelangen Werdegangs in einem Arbeitsbereich, der mich immer fasziniert hat und in dem ich mit Freude arbeite. Bereits seit 2014 bin ich beim TZW beschäftigt und habe in dieser Zeit mit Begeisterung und Engagement ein tiefgehendes Wissen im Bereich UV-Desinfektion aufgebaut. Wir haben gemeinsam Entwicklungen angestoßen und zahlreiche Herausforderungen gemeistert. 2020 begann ich schließlich, meinen lang gehegten Traum der Promotion zu verwirklichen.

Gerade die Doppelbelastung zwischen Hauptarbeit und Dissertation erforderte immer wieder Disziplin und Motivation. Es gab zahlreiche Herausforderungen, wie z.B. lange Labortage (während Corona mit Maske...) und zahlreiche Reisen, die nicht immer reibungslos verliefen – doch am Ende habe ich auf jedem Schritt des Weges etwas dazugelernt.

An dieser Stelle möchte ich all denen danken, die mich auf diesem Weg unterstützt haben. Mein besonderer Dank gilt meinem Arbeitgeber, der mir die Möglichkeit gegeben hat, diese Dissertation neben meiner Haupttätigkeit durchzuführen. Danke auch an meine Kolleginnen und Kollegen sowie Freunde am TZW, insbesondere Karl-Heinz, Adrian, Jutta und Dirk, für die Unterstützung im Labor und für euren wertvollen Input.

Ein herzlicher Dank gilt den Mitarbeitenden der PTB in Braunschweig, die mich mit ihrer Gastfreundschaft herzlich aufgenommen haben. Felix, Peter, Kerstin und Saulius, vielen Dank für die gemeinsame Zeit – und Felix, danke für die legendären Bowlingabende, die immer wieder für Ausgleich sorgten. Christian und Ian möchte ich für ihre wissenschaftliche Unterstützung und die konstruktiven Diskussionen danken, die mir geholfen haben, komplexe Themen zu durchdringen. Eure Hilfe beim Gegenlesen der Arbeit war unbezahlbar.

Ebenso danke ich meinem Betreuer, Professor Horn, für seine wertvollen Anregungen bei der Zusammenstellung der Arbeit und die Unterstützung als Lektor. Meinem Zweitgutachter Professor Franzreb bin ich ebenfalls sehr dankbar, dass er so kurzfristig eingesprungen ist.

Ein großer Dank geht auch an meine Freunde Andi, Tobse und Zotti, die immer ein offenes Ohr hatten und regelmäßig nach dem Stand der Dinge gefragt haben. Eure Unterstützung und euer Interesse haben mir sehr geholfen.

Mein größter Dank jedoch gilt meiner Familie. Meinen Eltern danke ich dafür, dass sie mir immer alle Freiheiten gelassen und keinen Druck ausgeübt haben – gerade das hat mich dazu ermutigt, meinen eigenen Weg zu gehen. Nina danke ich von Herzen für ihren unermüdlichen Ansporn, auch abends oder am Wochenende an meiner Dissertation weiterzuarbeiten. Und meine Tochter Lotta hat mir auf ihre

eigene Weise gezeigt, worauf es im Leben wirklich ankommt: Freude, Leichtigkeit und der unermüdliche Glaube daran, dass man seine Ziele erreichen kann. Schließlich danke ich dem Rest meiner Familie – meinem Bruder, meinen Großeltern, Tanten, Onkeln, Cousins und Cousinen –, die stets voller Stolz und Neugier gefragt haben, wann die Verteidigung stattfindet. Ihr habt mich dadurch immer wieder motiviert.

Diese Dissertation ist das Ergebnis vieler kleiner Schritte, viel harter Arbeit und der Unterstützung eines wunderbaren Netzwerks. Es ist nicht allein das Erreichen des Ziels, das zählt, sondern der Weg, den man dabei zurücklegt – und diesen Weg werde ich stets in guter Erinnerung behalten.

Table of Contents

List of Tables

List of Figures

List of Abbrevations

AS_λ	Action spectrum constant for wavelength λ
ASCF	Action spectrum correction factor
BPL	Ballast power level
CB	Collimated beam
CFD	Computational fluid dynamics
cfu	Colony forming units
DIN	German Institute for Standardization
D_L	UV sensitivity of a microbe
DNA	Deoxyribonucleic acid
DVGW	German Technical and Scientific Association for Gas and Water
EPA	Environmental Protection Agency
FBH	Ferdinand-Braun-Institute
FHWM	Full-width-at-half-maximum
FNU	Formazin nephelometric units
GAP	Microbiological laboratory in Canada
H_{UV}	UV fluence applied with a collimated beam device
LED	Light emitting diode
LP	Low pressure (referring to UV lamps)
MP	Medium pressure (referring to UV lamps)
MS2	MS2 phage (a type of bacteriophage used as a surrogate)
OPO	Optical parametric oscillator
PFU	Plague forming units
PI	Prediction interval

PTB	German Metrology Institute
Qß	Qß phage (a type of bacteriophage used as a surrogate)
Re	Reynolds number
REF	Reduction equivalent Fluence
RNA	Ribonucleic acid
SD	Standard deviation
T1UV	T1UV phage (a type of bacteriophage used as a surrogate)
TZW	German Water Centre
U_{IN}	Uncertainty of interpolation
UVDGM	UV Disinfection Guidance Manual
UV	Ultraviolet radiation
UVA	UV absorbance of water or a suspension
UVT	UV transmission of water or a suspension
WPE	Wall plug efficiency
WTV	Water supplier of the TZW test facility

.

1. Introduction

1.1. Research objectives

The overall aim of this thesis was to review the current methodology for the validation of UV systems in Europe. This involved two main focuses: assessing the suitability of *Bacillus subtilis* spores as a surrogate for the biodosimetric validation of UV systems with polychromatic UV sources, and validating, evaluating, and comparing the American biodosimetric combined variable approach [EPA (United States Environmental Protection Agency), 2020] with the UV intensity setpoint approach [DVGW Deutsche Vereinigung des Gas- und Wasserfaches e.V., 2006] widely used in Europe.

The objectives and hypothesis of this work are as follows:

Research objective 1:

Determine the wavelength dependence (disinfection efficacy of wavelengths in the UV-C and UV-B range) of *Bacillus subtilis* spores, the only surrogate microbe currently used for biodosimetric UV system validation in Europe. Additionally, to compare the wavelength dependence of the main surrogate MS2 phage used for UV system validation in America with state-of-the-art literature data. This objective involves establishing a state-of-the-art action spectrum using a tunable laser-based setup to provide a high-resolution spectrum.

Hypothesis 1:

Based on the defined action spectrum of *Bacillus subtilis* spores, which shows significantly higher UV sensitivity between 260 nm and 280 nm, a sharp decline in inactivation above 280 nm, and no further inactivation from 290 nm onwards, *Bacillus subtilis* spores may not be suitable as a surrogate for the validation of UV systems with polychromatic UV sources. The use of *Bacillus subtilis* spores leads to higher measurement uncertainties during biodosimetry and results in decreased performance of UV systems during operation. Utilizing MS2 phage as a surrogate would mitigate these issues and allow for more efficient operation of UV systems.

Research objective 2:

Validate the combined variable approach. Using simulation tools to validate the theoretical foundation of this concept.

Hypothesis 2:

Adopting the combined variable approach as the standard method for biodosimetric testing in Europe offers greater flexibility during validation testing depending on application requirements. This scientific approach for testing enables more efficient operation of UV systems while ensuring safe operation and meeting disinfection requirements.

1.2. Basic principles on ultraviolet radiation

This chapter briefly summarizes the basics of the UV radiation used for disinfection processes. Since this thesis has a strong focus towards the experimental work, the physical and biological fundamentals are not described to the fullest extent. For a more detailed review of the fundamentals, the work of Harm (1980) and Mayor-Smith (2014) are recommended.

1.2.1. The ultraviolet spectrum

The UV spectrum is categorized into four regions: vacuum UV (100 nm to 200 nm); UV-C (200 nm to 280 nm); UV-B (280 nm to 315 nm); and UV-A (315 nm to 400 nm) [Meulemans, 1987]. Only the UV-C and UV-B parts can be considered as the germicidal wavelength range for practical purposes [Bolton, 2010], with different specific limits depending on the literature, e.g. 200 nm to 300 nm [EPA (United States Environmental Protection Agency), 2006] or 240 nm to 290 nm [DVGW Arbeitsblatt W 294-1, 2006].

1.2.2. UV sources

Mercury vapor lamps are commonly used for UV disinfection of drinking water [Chevremont, Boudenne, Coulomb, & Farnet, 2013a]. The technical standards relevant for testing UV disinfection systems mainly consider mercury vapor lamps. The construction and the functionality of gas discharge lamps are well descirbed by Lister at al. (2004) and will be outlined below.

The A gas discharge lamp typically consists of a gas-filled quartz glass body, as well as an anode and a cathode at the ends of the lamp. In mercury vapor lamps, mercury is present in liquid form (as elemental mercury) or in solid form (as mercury alloy). Upon applying a certain operating voltage, electrons are emitted at the cathode, colliding with inert gas atoms, leading to their ionization. This process generates a plasma through which an electric current flows, heating the gas. As a result, the mercury transitions to the gaseous phase, leading to collisions between the gaseous mercury and electrons in the plasma. This excites the mercury atoms, causing them to briefly enter a higher-energy state. Upon returning to the ground state, energy is released in the form of radiation within the mercury-specific UV emission spectrum.

Two types of mercury vapor lamps are widely used for UV disinfection, primarily differing in the amount of available mercury and operating parameters and thus the prevailing mercury partial pressure within the lamp. These are known as low-pressure and medium-pressure lamps (LP and MP), and they exhibit certain distinct characteristics [Bolton & Cotton, 2008].

The amalgam lamp, where mercury is present in solid form as an alloy, is practically the only optimized form of the low-pressure lamp used today. This results in advantages in terms of lifespan and reduced

temperature sensitivity during operation. In the following, the term LP-lamps exclusively refers to amalgam lamps. In MP-lamps the mercury is in liquid form.

The most noticeable difference between LP- and MP-lamps lies in their respective emission spectra [Bolton & Cotton, 2008]. LP-lamps emit monochromatically in the germicidal range (240 nm and 290 nm according to DVGW [DVGW Arbeitsblatt W 294-1, 2006]), with their main emission at the characteristic mercury line of 253.7 nm. In contrast, MP-lamps exhibit a polychromatic emission spectrum with multiple emission lines (see Figure 1, shaded in green). In comparison to LP-lamps, MP-lamps have a significantly higher proportion of emissions in the UV-B-, UC-A-, visible-range (≈290 nm to 800 nm) and in heat radiation (≈ > 800 nm). Consequently, the conversion efficiency (≡ wall plug effiency (WPE)) of electrical input power to emitted radiation in the microbicidal range is significantly lower for MP-lamps.

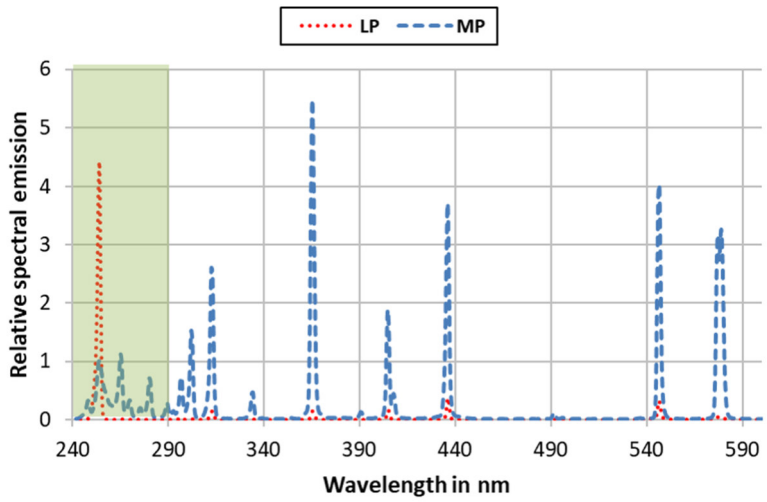

Figure 1: Spectral emission of LP-lamp (red dotted line) and MP-lamp (blue dashed line). The green shaded area defines the germicidal range (data from measurements at TZW: DVGW-Technologiezentrum Wasser).

Table 1 gives an overview of the relevant characteristics of LP- and MP-lamps.

Table 1: Different characteristics of LP- and MP-lamps [DVGW Deutsche Vereinigung de Gas- und Wasserfaches e.V., 2023].

Parameter	LP-lamp	MP-lamp
Mercury	Amalgam < 15 mg	Liquid ≤ 90 mg per kW
Electrical power consumption	≈ 1 W/cm to 10 W/cm (max. of 1 kW per lamp)	≈ 50 W/cm to 250 W/cm (max. of 15 kW per lamp)
Wall plug efficiency (WPE)	≈ 30 % to 35 %	≈ 10 % to 15 %
Operating temperature	80 °C to 120 °C	600 °C to 900 °C
End of lifetime (at 70 %)	12,000 hrs to 16,000 hrs	9,000 hrs to 12,000 hrs
Steady-state time	≈ 3 min to 7 min	≈ 1 min

Due to the progressing ban of mercury according the directive 2011/65/EU on the restrictions of the use of certain hazardous substance in electrical and electronic equipment [European Union, 2011] there is a need for alternative UV sources. Light-emitting-diode (LED) technology is emerging as a viable alternative to mercury lamps and is continuously advancing towards the UV range [Song, Mohensi, & Taghipour, 2016; Chen, Loeb, & Kim, 2017]. Although the emission spectra of UV-LEDs can be tailored to specific peak-wavelengths, their full-width-at-half-maximum (FWHM) typically spans a few nanometers, precluding them from being considered monochromatic [Chen, Loeb, & Kim, 2017]. UV-LEDs are constructed as chips, with dimensions ranging from 12 mm² to 36 mm² depending on the packaging [Einfeldt, 2022]. This chip-based design offers opportunities for novel UV system configurations [Chen, Loeb, & Kim, 2017; Nyangaresi, Rathnayake, & Beck, 2023]. The UV output per chip available on the market varies widely, ranging from 1 mW to 100 mW [Einfeldt, 2022]. Regarding the wall plug efficiency, it is currently challenging to standardize this value for UV-LEDs due to inconsistent measurement procedures across different datasheets. However, based on measurements conducted during LED projects at TZW: DVGW-Technologiezentrum Wasser (TZW) and available literature data, WPE values typically range between approximately 3 % and 7 %, varying depending on the wavelengths [Harris, Pagan, & Batoni, 2013; Simons, Lawal, & Pagán, 2022]

1.3. Molecular damage/Inactivation mechanism

UV disinfection is a physical disinfection method that alters the genetic material (Deoxyribonucleic Acid (DNA) and Ribunucleic Acid (RNA)) of microbes rendering the pathogenic microbes inactive and thus inhibiting their ability to reproduce themselves [Harm, 1980]. In contrast to oxidatively acting chemical disinfectants such as chlorine (as chlorine dioxide or hypochlorite) or ozone, practically no reaction products are formed during UV water disinfection that would have an impact on water quality [Bernhardt, et al., 1994; DVGW Arbeitsblatt W 294-1, 2006].

In the germicidal-effective range, UV radiation is particularly strong in its absorption by nucleic acids such as DNA and RNA, with the maximum occurring at a wavelength of about 260 nm (refer to Figure 2) (modified from [Jagger, 1967]).

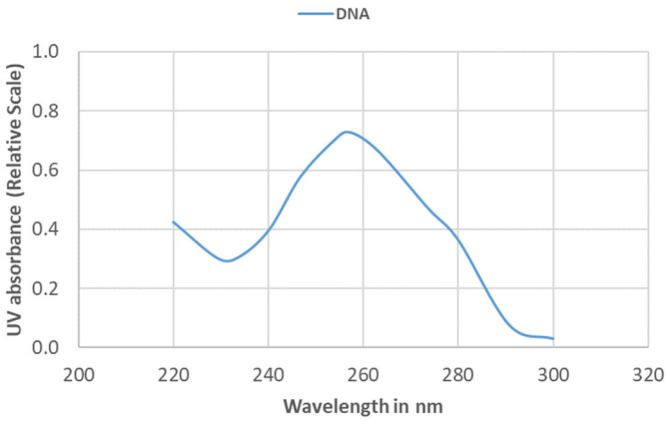

Figure 2: UV absorbance spectrum of DNA at pH 7 (modified from [Jagger, 1967]).

In general, the better a wavelength is absorbed by a biological component, the greater the potential in damaging genetic material. Since each microbe has its unique genetic information and composition of nucleic acids, the sensitivity to UV irradiation differs [Kowalski, Bahnfleth, & Hernandez, 2009]. Nucleic acids carry genetic information in either single stranded or double stranded Deoxyribonucleic Acid (DNA). DNA consists of the bases guanine, cytosine, adenosine, and thymine, while Ribonucleic Acid (RNA), whether single or double-stranded, shares the same bases, except for the presence of uracil instead of thymine. Pyrimidines include cytosine, thymine, and uracil, and purines consist of adenine and guanine. The different absorbance spectrum of the pyrimidine and purine bases are shown in Figure 3. This leads to the conclusion that a microbe DNA or RNA differs depending on its bases composition.

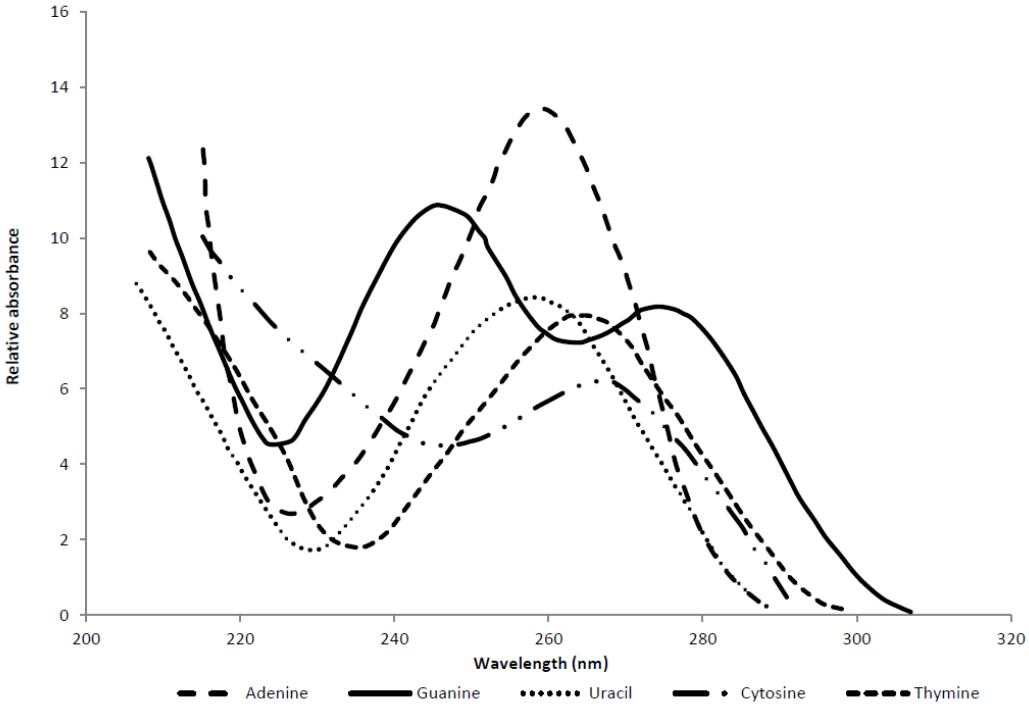

Figure 3: Absorbance of Purine and Pyrimidine bases at pH7 in the ultraviolet range [Mayor-Smith, 2014; Davidson, 1965]

Purines and pyrimidines exhibit strong UV light absorption, but the susceptibility to UV-induced damage is notably higher in pyrimidines [Smith & Hanawalt, 1969]. The absorption of UV light gives rise to six types of damage in the pyrimidines of nucleic acids [Setlow, 1967; Snowball & Hornsey, 1988; Pfeifer, 1997], with the extent of damage varying according to the UV fluence. The subsequent three forms of damage contribute significantly to the inactivation of microbes:

- The formation of pyrimidine dimers occurs when covalent bonds exist between adjacent pyrimidines on the same DNA or RNA strand, representing the most prevalent damage resulting from UV disinfection.
- Pyrimidine (6-4) pyrimidone photoproducts resemble pyrimidine dimers and emerge at the same sites.
- Covalent bonds in the form of protein-DNA cross-links may play a vital role in disinfecting specific microbes.

However previous studies suggested that not only the absorbance of DNA or RNA might be responsible for inactivation effects by UV [Cabaj, Sommer, Pribil, & Haider, 2002; Mamane-Gravetz, Linden, Cabaj, & Sommer, 2005]. Also Kowalski, Bahnfleth, & Hernandez [2009] mentioned various additional intrinsic factors, which might have an impact on the UV sensitivity (under constant ambient conditions, such as temperature and humidity). These factors can include physical size, molecular weight, DNA conformation, presence of chromophores, tendency for clumping, presence of repair enzymes or dark/photo-repair mechanisms, hydrophilic surface properties, relative index of refraction, specific UV spectrum, guanin and cytosin content, and the percentage of potential pyrimidine dimers.

1.4. Inactivation kinetics

For chemical disinfectants, inactivation kinetics are often described using the first-order disinfection model by Chick (1908) and Watson (1908). This model states that the rate of inactivation is directly proportional to the number of microbes present at any given time. The Chick-Watson model is represented by Equation 1:

$$\frac{N_0}{N} = exp^{k \cdot t} \tag{1}$$

With:

N_0/N	Inactivation ratio, with N_0 being the initial concentration of the microbe and N the concentration at time t after treatment, unit less

k	Inactivation rate constant (depending on disinfectant, disinfectant concentration and microbe), in min^{-1}
t	Contact time, in min

This model is also applicable to UV disinfection. In this context, microbial inactivation is usually expressed as log inactivation (logI), and the correlation between logI and UV fluence is give by:

$$\log_{10}\left(\frac{N_0}{N}\right) = logI = k \cdot H_{UV} \quad (2)$$

With:

$Log_{10}(N_0/N)$	Logarithmic inactivation, with N_0 as the initial concentration and N the concentration after applying UV fluence H_{UV}, unit less
k	Inactivation rate constant (depending on UV source and microbe), in m^{-2}/J
H_{UV}	Applied UV fluence, in J/m^2

Typically, UV fluence is used instead of UV dose, as measuring dose is practically not feasible. A UV dose is the energy or amount of photons (in the UV wavelength range) absorbed per volume or mass, in J/m^3 [International Union of Pure and Applied Chemistry, 2006], whereas UV fluence is the integral of a fluence rate over the duration of an irradiation process, in W/m^2 [International Union of Pure and Applied Chemistry, 2006]. The fluence rate, in W/m^2, is something which can be measured rather easily by using a UV sensor. Nevertheless this thesis will use the term dose-response curve, but the thesis will continue to use the term UV fluence. While the term dose-response curve may not be entirely accurate from a technical standpoint, it is employed in this work due to its frequent use and recognition.

Two notable deviations from the first-order inactivation model in Equation 2 have been documented in literature. Several researchers [Knudson, 1985; Sommer, Haider, Cabaj, Pribil, & Lhotsky, 1998; Mamane-Gravetz, Linden, Cabaj, & Sommer, 2005] have reported that at low fluences, bacteria or bacterial spores show no inactivation, likely due to repair mechanisms [Sutherland, 2002]. However, at higher UV fluences, the inactivation follows a typical log-linear correlation. This is described as a shoulder behaviour.

The second deviation from linear kinetics, known as tailing, occurs when no further increase in inactivation is observed at high fluences [Cerf, 1977]. This effect can be attributed to clustering [Kowalski, Bahnfleth, Raguse, & Moeller, 2020] or to the presence of UV-resistant sub-populations of the microbe [Parker & Darby, 1995]. Clustering happens when microbes aggregate due to factors such as hydrophobic interactions, ionic surface charges, or specific physical surface characteristics [Mamane-Gravetz & Linden, 2005; Raguse, et al., 2016; Gerba & Betancourt, 2017].

In this thesis, the first-order inactivation model will be used in modified forms. These adjustments are necessary due to the shoulder behavior of microbes, combined with other effects that compromise straight linear behavior. These factors include tailing effects, specific phage/host interactions, inhomogenous radial mixing in the bench scale setup, and inherent microbiological variations in the assay [Havelaar, Nieuwstad, Meulemans, & van Olphen, 1991; Hijnen, Beerendonk, & Medema, 2006; Mayor-Smith, 2014].

1.5. Regulation and validation of UV systems for water disinfection

1.5.1. Field of application

In the late 1990s, it became evident that UV disinfection of drinking water efficiently inactivates protozoan parasites such as *Cryptosporidium* and *Giardia* [Clancy, Hargy, Marshall, & Dyksen, 1998]. This effectiveness contrasts with the limited efficacy of chlorine or chlorine dioxide [Campell, Tzipori, G., & Angus, 1982; Korich, Mead, Madore, Sinclair, & Sterling, 1990]. UV disinfection has since grown in significance and is now recognized as effective for inactivating bacteria, protozoa, and viruses. Presently, UV disinfection finds widespread application across various sectors. In the water industry, it is employed for disinfecting drinking water, wastewater, industrial water, ballast water, and reuse water, among other purposes. UV disinfection systems in the water sector vary widely in size, ranging from point-of-use (PoU) applications handling only a few liters per minute to municipal and industrial installations processing several tens of thousand of liters per minute. Outside of the water sector, UV disinfection is utilized for air and surface purification, as well as in medical applications. However, this thesis focuses exclusively on UV disinfection within the water sector.

1.5.2. Overview national standards

The key benchmarks for validating UV systems in the treatment of drinking water (municipal) include the American UV Disinfection Guidance Manual (UVDGM) [EPA (United States Environmental Protection Agency), 2006] with its extended document [EPA (United States Environmental Protection Agency), 2020], the German DVGW W 294-2 (DVGW Arbeitsblatt W 294-2., 2006) , the Austrian ÖNORM M5873-1 [ÖNORM M 5873-1, 2020] and the DIN-19294-1 [DIN (Deutsches Institut für Normung e.V.), 2020]. These standards stand as the most universally acknowledged criteria for validat-

ing UV systems in drinking water contexts. Furthermore, they serve as foundational references for numerous secondary guidelines across various applications in the water sectors, e.g. water reuse [NATIONAL WATER RESEARCH INSTITUTE, 2012], food and beverage [U.S. Department of Health and Human Services, 2013] and public aquatic faciliter like pools [U.S. Department of Health and Human Services, 2014]. The acceptance of the various standards and guidelines is usually regulated at the national level. With regards to the drinking water sector the validation protocols from DVGW, ÖNORM, DIN and USEPA have either been adapted by other countries or they accept at least one of the mentioned validation protocols. For most countries a validation of UV systems is mandatory before operating in the field. Some countries like Germany are stricter and demand in addition to a validation a subsequent certification process resulting in a certificate for the specific UV system type. This certification process includes monitoring audits on a regular basis (every other year) at the manufacturer of a type-tested product, checking e.g.:

- the internal quality management
- the purchase of components (serial numbers as stated in the validation report, usage of components as stated in the validation report)
- the production site (measurement of component dimensions, hygienic certificates of materials in contact with water (o-rings etc), final inspection)

1.6. Validation of UV systems

This chapter outlines the procedure for validating a UV system, dividing it into biodosimetric and technical testing. Biodosimetric testing takes center stage in evaluating the disinfection performance of a UV system, while technical testing characterizes the relevant components of the system. The emphasis will be on municipal (drinking) water treatment and validations guided by DIN 19294-1 [DIN (Deutsches Institut für Normung e.V.), 2020] and UVDGM [EPA (United States Environmental Protection Agency), 2006] with its extended document of the innovative approaches [EPA (United States Environmental Protection Agency), 2020].

1.6.1. UV system design and components

In the context of this thesis, a UV system is defined as a closed vessel system featuring both an inlet and an outlet, typically constructed of stainless steel. This system comprises a UV source (or multiple sources), the electronic lamp drivers referred to as ballasts, UV sensors for monitoring UV irradiance, a measurement window, and quartz sleeves (for lamp-based systems). Figure 4 illustrates an example of a single-lamp UV system with an L-shaped inlet/outlet configuration (indicated by the blue arrows). Other common configurations include Z-shaped, U-shaped, or straight flow. Additionally, the UV system depicted in Figure 4 showcases the UV lamp (purple) housed within the quartz sleeve (yellow) and

the measurement window (green) with a UV sensor (brown). Moreover, most UV systems also incorporate static elements such as baffle plates (blue) or other flow control elements to enhance hydraulic performance.

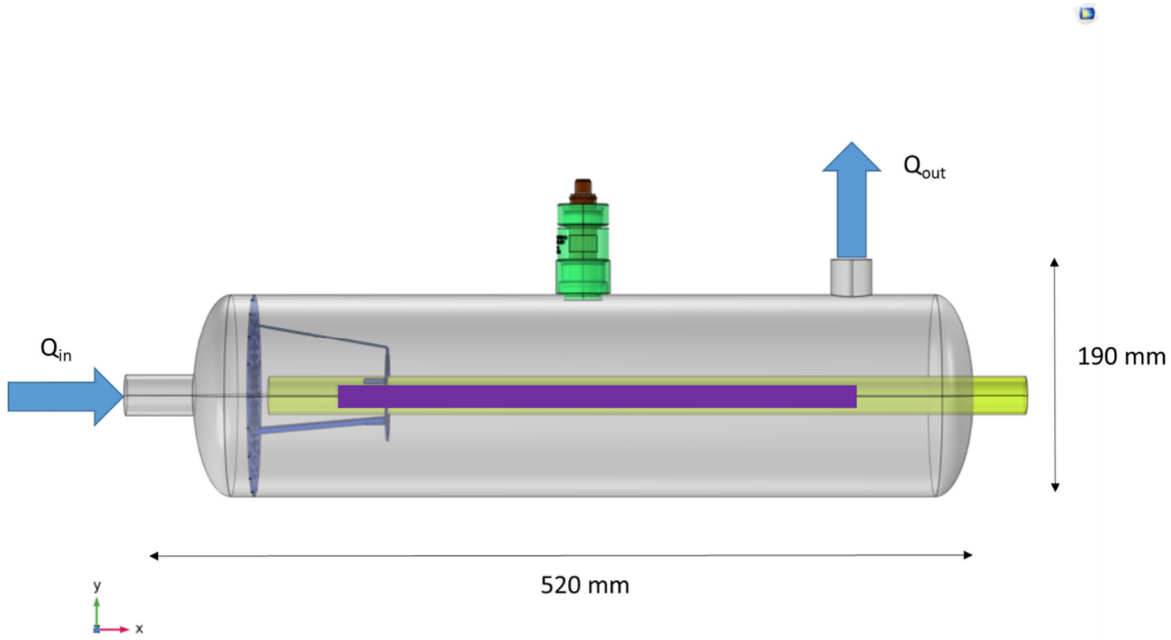

Figure 4: Example of a single lamp UV system with a UV lamp (purple), quartz sleeve (yellow), measurement window (green), UV sensor (brown) and baffle plate (blue). The blue arrows indicate the direction of flow.

For the components including lamps, ballasts , UV sensors (referred to as duty sensor within the UV system), measurement windows, and quartz sleeves, specific requirements are outlined in DIN 19294-1 [DIN (Deutsches Institut für Normung e.V.), 2020]. The dimensions and specific characteristics of duty sensors and measurement windows are standardized and must be followed during the validation process. In contrast, the UVDGM [EPA (United States Environmental Protection Agency), 2006] provides more flexibility for duty sensors and measurement windows and does not specify fixed dimensions or characteristics.

1.6.2. Biodosimetric testing

The fundamental principle for validating the disinfection performance is consistent across most standards (refer to Figure 5). The subsequent paragraphs will elaborate on this underlying principle.

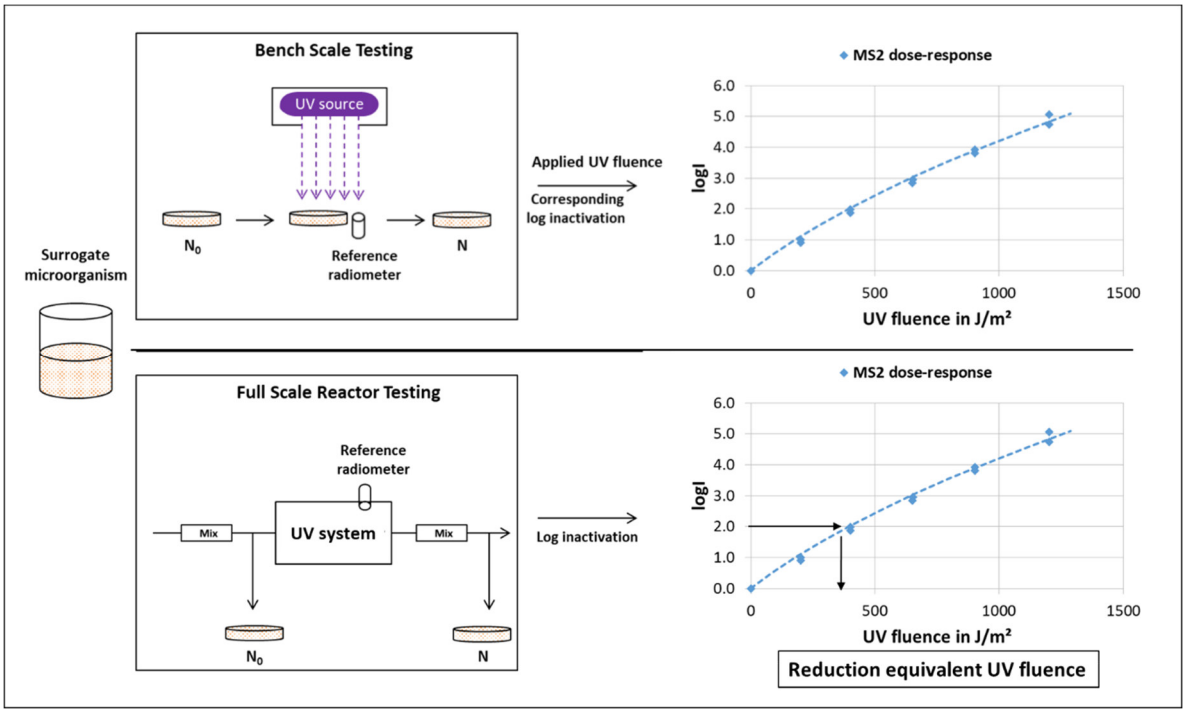

Figure 5: Fundamental principles for biodosimetry.

Since direct measurement of UV fluence within UV systems using physical methods onsite is not feasible [Sommer, Cabaj, & Haider, 1996], biological methods are employed. This process, known as biodosimetry, encompasses both bench scale testing and full scale reactor testing [Qualls & Johnson, 1983; Sommer & Cabaj, 1993; Blatchley & Hunt, 1994]. Non-pathogenic surrogate microbes serve as biodosimeters (refer to Chapter 1.6.4).

- **Bench Scale Testing:** Using a collimated beam apparatus (CB), the surrogate microbes are exposed to UV under specific conditions of fixed UV irradiance and volume, with no influence from hydraulics. Collimated beam tests are conducted at various fluences by adjusting the exposure time. Consequently, the UV dose-response relationship (UV fluence versus log inactivation (logI)) of the challenge microbe is established, leading to a dose-response equation. This relationship varies for each species. A common protocol for a standard operating procedure of the bench scale testing is described by Bolton et al. [Bolton, Beck, & Linden, 2015]. This protocol was used for the experiments presented in this work.
- **Full Scale Reactor Testing:** In these investigations, a known concentration of the surrogate microbe is injected upstream of the UV system. Subsequently, samples are collected upstream (N_0) and downstream (N) from the UV system, and the microbe's concentration in each sample is determined to calculate the log inactivation ($logI = logN_0/N$). The log inactivation measured

during full-scale reactor testing can be transformed into a reduction equivalent fluence (REF) using the dose-response equation obtained from bench scale testing. The REF must always be correlated with the particular surrogate employed during validation testing and connected to the UV source utilized in the collimated beam apparatus (in most cases this is related to a LP source). By conducting these tests across specific ranges, such as water flow and UV-transmission of the water (UVT), it is possible to define the operating range of a UV system. In this study, the term UVT will consistently refer to a 10 mm path length. Unless specified otherwise, the term UVT will denote the value measured at 254 nm. The UVT is a critical parameter for characterizing the water to be disinfected, as it indicates the concentration of humic substances in the water. A lower UVT signifies that more UV radiation is absorbed by the water, leading to shorter contact times and consequently lower overall UV fluences within the UV system. This reduction in fluence can only be compensated by either increasing the UV output of the lamps (if they are not already operating at full power) or reducing the water flow through the system. Determining the suitable operating range in terms of water flow and UVT is the primary goal of biodosimetric testing.

While the outlined procedure is generally consistent across the researched standards, variations exist in the stipulations regarding disinfection efficacy for UV systems and the selection of surrogate microbes. For instance, in the DIN (and also DVGW and ÖNORM) standard, achieving a UV fluence of at least 400 J/m² (based on *Bacillus subtilis* spores as the surrogate microbe and LP CB) is deemed sufficient for the disinfection efficacy of a UV system at a specific flow rate and UVT. This threshold value must ensure the removal of all pertinent pathogens in the drinking water application by a minimum of a 4-log level [Bernhardt, et al., 1994; Hoyer, 1998]. In contrast, the UVDGM does not specify a fixed UV fluence. For UVDGM validation, one can target a particular log inactivation for specific pathogens such as *Cryptosporidium*, *Giardia* and viruses (refer to Table 2). Depending on the application, the requirements and criteria for log inactivation credits may vary.

Table 2: Required UV fluence for certain log inactivation of Cryptosporidium, Giardia *and viruses [EPA (United States Environmental Protection Agency), 2006].*

Target Pathogens	**Required UV fluence in J/m² to achieve indicated log inactivation**			
	1-log	**2-log**	**3-log**	**4-log**
Cryptosporidium	25	58	120	220
Giardia	21	52	110	220
Viruses	580	1000	1430	1860

1.6.3.UV Fluence distribution within a UV system

In this context, the more appropriate term would be "UV dose distribution". However, recognizing that the dose is generally assumed to be proportional to the fluence, the term "UV fluence" is used to minimize confusion.

In a UV reactor with optimal hydraulics, all microbes passing through receive an identical UV fluence. This uniform distribution of UV fluence is represented by a single value, known as the ideal fluence distribution. For instance, in scenarios such as the assessment of a UV dose-response using a collimated beam apparatus or within an ideal plug-flow reactor, where the suspension is perfectly stirred, the administered fluence is determined by the average UV irradiance within the reactor multiplied by the residence time. Therefore, in an ideal reactor, the REF determined with a challenge microbe serves as an indicator of the REF provided to all microbes, as each one receives an equivalent fluence.

However, real UV systems do not exhibit such uniform fluence distributions. Instead, the REF depends on the dose-response curve of the surrogate or target microbe [Cabaj, Sommer, & Schoenen, 1996]. In fact, the fluence distributions in a UV system vary depending on factors such as UVT, UV lamp output, and flow rate.

1.6.4.Surrogates

Due to impracticality and concerns for public health, it is not feasible to handle a target pathogen directly during validation testing. Therefore, non-pathogenic surrogate microbes with a specific sensitivity to UV radiation are used during UV system validations. The selection of a surrogate for the validation of a UV system varies depending on the standard. The two major surrogates will be described in more detail below.

Since the early 1990s, *Bacillus subtilis* spores have been utilized in Europe, particularly in Germany and Austria, to validate the disinfection performance of UV systems in drinking water applications through biodosimetry [Bernhardt et al., 1994]. While the accurate scientific name for this strain is *Bacillus spizizenii*, for enhanced recognition, *Bacillus subtilis* is used in the subsequent document.

Spores of various *Bacillus* species are formed through sporulation, a process triggered by nutrient depletion in the environment [Piggot & Hilbert, 2004]. This results in a cell type that remains dormant and metabolically inactive, capable of surviving long periods without nutrients [Setlow P. , 2006]. Some researchers [Kennedy, Reader, & Swierczynski, 1994; Vreeland, Rosenzweig, & Powers, 2000] report that spores can survive even millions of years, suggesting the evolution of multiple protective mechanisms to preserve cell structure during dormancy, such as resistance to chemicals, heat and radiation [Nicholson, Munakata, Horneck, Melosh, & Setlow, 2000; Henriques & Moran, 2007]. *Bacillus subtilis* spores are typically about 1–2 micrometers in diameter [Nicholson, Munakata, Horneck, Melosh, &

Setlow, 2000] with a complex structure that includes double-stranded DNA and a large genome consisting of about 40,000 base pairs [ATCC genome, https://www.atcc.org/products/6633].

The spores of *Bacillus subtilis* meet essential requirements as a surrogate. They are not naturally present in drinking water, are non-pathogenic, easy to handle and process in the lab, and are quite resistant to UV [Setlow P., 2006]. This surrogate has been incorporated as the only surrogate microbe in the DVGW worksheet W 294-2 [DVGW Arbeitsblatt W 294-2, 2006], published in 2006, which governs the validation of UV systems for municipal drinking water applications in Germany. This standard has been applied for various UV system validations, covering both low-pressure and medium-pressure lamp-based systems. For low-pressure (LP) system validations, W 294-2 was replaced by DIN 19294-1 in 2020 [DIN (Deutsches Institut für Normung e.V.), 2020], still utilizing *Bacillus subtilis* spores as a surrogate.

In contrast to the European approach the UVGDM allows for various surrogates including MS2 phage, Qß phage, PRD-1 phage, B40-8 phage, ϕx174 phage, *Escherichia coli*, T7 phage, T1 phage, T1UV phage, *Bacillus pumilus* spores and *Bacillus subtilis* spores [EPA (United States Environmental Protection Agency), 2006; EPA (United States Environmental Protection Agency), 2020]. Nevertheless MS2 phage has been established as the predominant surrogate of choice. MS2 phage is a well-studied single-stranded RNA virus that infects enterobacteria such as *Escherichia coli* and *Salmonella typhimurium*. It is classified as a member of the *Fiersviridae* family and is notable for its small size (27 nm to 28 nm) and simple structure, with a genome of approximately 4000 base pairs [Valegård, Fridborg, & Unge, 1990]. The UV resistance of MS2 phage is likely due to the protective role of its protein capsid and the stable packaging of its RNA genome [Valegård, Fridborg, & Unge, 1990]. The compact structure of the capsid absorbs and dissipates UV radiation, preventing or at least lower the direct damage to the RNA.

The UV sensitivity of *Bacillus subtilis* spores is comparable to that of the MS2 phage. Both *Bacillus subtilis* spores and MS2 bacteriophage require approximately 200 J/m² per log-inactivation (logI) [Sommer, Haider, Cabaj, Pribil, & Lhotsky, 1998; Malayeri, Mohensi, & Bolton, 2016]. The primary distinction lies in the characteristic shoulder behavior of *Bacillus subtilis* spores observed below 100 J/m², where, depending on batch-to-batch variability, no inactivation may be observed. This phenomenon is not evident for MS2 phage, where the log-inactivation function plotted against UV fluence follows a polynomial trend from the origin [Sommer, Haider, Cabaj, Pribil, & Lhotsky, 1998].

In general the criteria for a surrogate to be considered suitable, according the EPA guidelines, are as follows:

- The surrogate and host bacteria (if surrogate is a phage) should not be pathogenic to humans.
- The surrogate should have a similar dose-response curve as the target pathogen.
- Easy to handle and process in the lab.

- Samples with the surrogate should remain stable over time to allow shipment of the samples, without any loss in concentration or changes in the dose-response behavior.

1.6.5.Germicidal spectral response (action spectrum)

From now on, the germicidal spectral response will be referred to as the action spectrum (AS). As mentioned in Chapter 1.3, the spectral sensitivity of different microbes varies depending on the wavelength of the UV radiation, leading to a microbe-specific action spectrum. Figure 6 illustrates this variation using MS2 phage, *Cryptosporidium*, and Adenovirus as examples. The y-axis scale indicates the spectral sensitivity (AS_λ) as the ratio of inactivation effectiveness at a specific wavelength to the inactivation effectiveness at 254 nm, which represents the characteristic main emission line of a LP-lamp at 253.7 nm.

For most microbes, the peak action spectrum occurs between 260 nm to 270 nm, with a local minimum observed between 230 nm to 240 nm, and it diminishes to zero near 300 nm [Hoyer, 1998; Mamane-Gravetz, Linden, Cabaj, & Sommer, 2005; Beck, Wright, Hargy, Larason, & Linden, 2015]. While the action spectra of various microbes can be quite similar at wavelengths above 240 nm, notable differences can arise at wavelengths below 240 nm, as depicted in Figure 6.

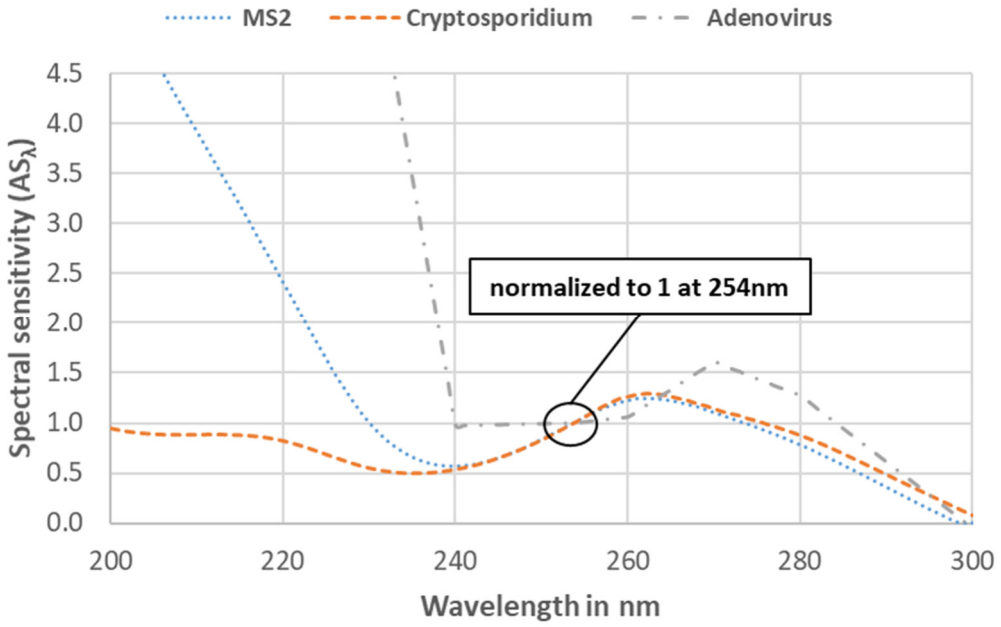

Figure 6: Action spectrum of MS2 phage, Cryptosporidium *and Adenovirus (adapted from [Beck, Wright, Hargy, Larason, & Linden, 2015]).*

In UV systems employing polychromatic UV sources, the disparities in action spectra can significantly influence the performance of UV systems which then is either be overestimated or underestimated during operation. This impact is contingent on several factors outlined in the innovative approach document [EPA (United States Environmental Protection Agency), 2020]:

1. Action spectra of the surrogate during validation and of the target pathogens during application.
2. UV absorption of the water during validation and of the water during application.
3. Change of the UV emission of the UV sources due to aging.
4. Change of the UV transmittance of the quartz sleeves due to aging and fouling.

The wavelength range, especially between 200 nm and 240 nm, can introduce notable disparities between validated performances and actual performances during operation [Linden, Wright, Collins, Cotton, & Beck, 2015]. A comprehensive exploration of the detailed impact and how to account for the factors outlined from 1. to 4. was conducted in a project supported by the Water Research Foundation [Linden, Wright, Collins, Cotton, & Beck, 2015]. Given that the German DIN standards for polychromatic sources will specifically exclude the wavelength range between 200 nm and 240 nm, this thesis will not delve into these impacts. Instead, the focus will be on elaborating further on factors 1. and 2., and discussing their respective impacts for wavelengths above 240 nm.

The primary rationale for excluding wavelengths between 200 nm and 240 nm, achieved through the use of doped quartz sleeves, is to prevent the formation of nitrite. This precaution is necessary due to the heightened absorption of wavelengths below 235 nm by nitrate ions, as highlighted in the study by Bernhardt et al. (1994).

The Ultraviolet Disinfection Guidance Manual (UVDGM) introduced an Action Spectra Correction Factor (ASCF) designed to be applied to polychromatic UV sources to address variations in action spectra between surrogates and pathogens. For this study, the definition of this factor has been slightly modified and can be expressed as Equation 3.

$$ASCF = \frac{P_G}{P} = \frac{\sum_{\lambda=240nm}^{300nm} P(\lambda) \cdot AS(\lambda) \cdot \delta\lambda}{\sum_{\lambda=240nm}^{300nm} P(\lambda) \cdot \delta\lambda} \quad (3)$$

With:

ASCF	Action spectra correction factor, unitless
P_G	Germicidal UV output of the UV source, in W
P	UV output of the UV source, in W
P(λ)	Spectral UV output of the UV source as a function of the wavelength, in W/nm
AS(λ)	Spectral sensitivity of the microbe, unitless

1.6.6. Full Scale reactor testing: theory of the combined variable approach

The test method used for biodosimetry in this work is based on the principle of the "combined variable" approach, which was published in 2020 [EPA (United States Environmental Protection Agency), 2020] as an extension of the UVDGM [EPA (United States Environmental Protection Agency), 2006]. The theory behind it has been applied and confirmed through numerical flow simulations and over 35 UV system validations over a period of 15 years in the U.S. [EPA (United States Environmental Protection Agency), 2020] resulting in an empirical equation. These studies demonstrated that the logI of a target or test microbe at a given UVT can be expressed as a function of a combined variable and is typically defined by an equation as a power function (refer to Equation 4). The background and derivation of the final formula presented below are included in Appendix A in the innovative approaches document [EPA (United States Environmental Protection Agency), 2020]. The foundational assumption of this approach is, that the trajectories of particles remain constant regardless of changes in the water flow rate [Lawryshyn, 2018]. Given the empirical nature of this equation, the quantities are utilized with illustrative units in the subsequent context, and a unit correction factor is introduced. Additional unit correction factors will be applied in this thesis as needed based on the dependence of A' and B'.

$$logI_{pred} = A' \cdot \vartheta_C{}^{B'} = A' \cdot \left(\frac{S/S_0 \cdot \omega}{Q \cdot D_L}\right)^{B'} \quad (4)$$

With:

$logI_{pred}$	Predicted log inactivation of a target microbe, unitless
A' and B'	Empirical coefficients as a function of the UVT, unitless
ϑ_c	The combined variable
S	Irradiance measured with a duty sensor, in W/m²
S_0	Predicted irradiance at 100 % UV output setting of the UV source and current UVT, in W/m²
Q	Water flow through the UV system, in m³/h
D_L	UV sensitivity of a target microbe, in J/m² per logI

ω	Unit correction factor, in m·J/h

The key feature of this method is the combined variable, composed of the relative UV output of the UV source (S/S_0) as defined by the duty sensor readings, the water flow through the UV reactor (Q), and the UV sensitivity of the microbe (D_L). The D_L of a microbe is the microbe-specific REF required to achieve a certain logI (D_L = REF/logI). The constants A' and B' depend on the UVT and can be determined based on the validation results. For each single UV system, the logI is specifically determined as a function of the combined variable and UVT with optimized functions for A' and B'.

The significant advantage of this approach lies in its remarkable flexibility, leveraging validation results across diverse applications to operate and monitor UV systems in the most efficient manner. It considers the impact of fluence distributions by incorporating the specific UV sensitivity of the microbe. In the case of polychromatic systems, the combined variable term can be expanded by the Action Spectra Correction Factor to account for the specific wavelength dependence of various microbes. This is illustrated in Equation 5.

$$logI_{pred} = A' \cdot \vartheta_c^{B'} = A' \cdot \left(\frac{{}^{S}/_{S_0} \cdot \omega}{Q \cdot D_L \cdot {}^{1}/_{ASCF}}\right)^{B'} \quad (5)$$

With:

ASCF	Action Spectra Correction Factor of the microbe, unit less

1.6.7. Full scale reactor testing: technical testing

The primary focus of this thesis will center around biodosimetric testing, while technical testing will be summarized concisely, highlighting key aspects. This typically includes:

- Reviewing manufacturers' technical data sheets and drawings to ensure compliance, with a focus on measuring dimensions where possible for the UV system vessel and all relevant components.
- Assessing manufacturers' hygienic data sheets for all materials in contact with drinking water within the UV system.
- Characterizing UV lamps and ballasts.

- Characterizing duty sensors.
- Investigating the relationship between duty sensor readings, UVT, and ballast power levels (BPL).

These procedures may vary depending on whether the system is validated according to DIN 19294-1 [DIN (Deutsches Institut für Normung e.V.), 2020] or the UVDGM [EPA (United States Environmental Protection Agency), 2006].

2. Determination of the action spectrum of *Bacillus subtilis* spores with a tunable laser-based setup

As outlined in Chapter 1.6.4, *Bacillus subtilis* spores have been traditionally employed for UV system validation over an extended period, particularly in Europe. However, with the introduction of new DIN standards for medium-pressure lamp systems and LED-based systems, there is a need to reevaluate the outdated action spectrum of *Bacillus subtilis* spores using state-of-the-art techniques and methodologies. Additionally, an assessment of its suitability in light of these advancements is essential.

In contrast to LP-lamps, MP-lamps and LEDs exhibit broad emission spectra and cannot be categorized as monochromatic sources in the UV-C spectral range. While MP-lamps are distinctly defined as polychromatic UV sources with various emission peaks in the UV-C range, LEDs may be constrained to specific small spectral ranges at a particular peak-wavelength, characterized by a defined full width at half maximum (FWHM) of a few nanometers. These optical characteristics and variations, compared to the physics-limited LP-lamp emitting solely at 253.7 nm in the UV-C range, introduce complexity to the biodosimetric procedure and necessitate more detailed data on the spectral sensitivity of the surrogate. To accurately and safely interpret biodosimetric results from a polychromatic UV system validation, a more comprehensive action spectrum of *Bacillus subtilis* spores is essential. In the general German disinfection approach, surpassing a REF of 400 J/m², tested with a surrogate, is mandated. This threshold value ensures the removal of all relevant pathogens in drinking water applications by at least a 4-log level [Bernhardt, et al., 1994]. Understanding the action spectrum of the surrogate allows maintaining the REF at the same level, even when specific pathogens are not targeted.

In contrast, the U.S. approach does not assign fixed log-inactivation credits for particular pathogens. Instead, it allows for flexible log-inactivation credits depending on the requirements of a particular application or location. Action spectra for various surrogates and pathogens have been investigated by Beck [Beck, et al., 2015] using a tunable laser setup in this context. The results of this work are directly incorporated into the “Guidance for Implementing Action Spectra Correction with Medium Pressure UV Disinfection” [Linden K. , Wright, Collins, Cotton, & Beck, 2015] which is used to validate UV systems in accordance with UVDGM to account for different emission spectra of UV sources. Notably, *Bacillus subtilis* spores were not examined in these studies.

Therefore, a detailed action spectrum of *Bacillus subtilis* spores was determined using a tunable laser-based setup. These investigations address a significant gap in current scientific knowledge by providing up-to-date data on the spectral sensitivity of *Bacillus subtilis* spores. The results will contribute to a better understanding of the spore's behavior under various UV sources and enhance the accuracy and reliability of UV system validations.

2.1. Material and methods

2.1.1. Irradiation experiments

UV irradiation bench-scale experiments have played a pivotal role in scientific research for decades [Lindenauer & Darby, 1994; Bolton & Linden, 2003; Kuo, Chen, & Nellor, 2003]. Within the realm of UV system validation, these experiments are essential for establishing the UV sensitivity of surrogates and pathogens, leading to the development of characteristic dose-response curves. These curves form the foundation of biodosimetric UV system validation (refer to chapter 1.6.2), ensuring the secure operation of UV systems in real-world applications. Generally, these bench-scale systems are referred to as collimated beam apparatus (CB), utilizing LP- or MP-lamps as UV sources.

To determine the wavelength dependence of surrogates and pathogens, additional effort and resources are required. This can be achieved, for instance, by employing polychromatic UV sources in combination with bandpass filters [Cabaj, Sommer, Pribil, & Haider, 2002] or, in a more precise approach, by utilizing a tunable laser-based setup. In this thesis, the latter method was employed to determine a high-resolution action spectrum of *Bacillus subtilis* spores.

The following sections will provide an overview of the bench-scale units based on LP- and MP-lamps, along with details of the tunable laser-based setup utilized in this research.

2.1.2. UV irradiations with LP- and MP-collimated beam apparatus

In the experiments, a LP-CB served as the reference bench-scale system. This apparatus is widely used as the basis for most dose-response curves applied in full-scale UV system validation [Bolton & Linden, 2003]. Concurrently running irradiance experiments with this reference system alongside the laser-based irradiances served two purposes: monitoring the stability of *Bacillus subtilis* spores during the experiments and validating the laser-based setup initially (refer to Chapter 2.2.1).

At this point, the distinction between "UV fluence" and "UV dose" emerges. This occurs because it is impractical to directly measure the energy per unit volume using radiometers that gauge irradiance (equivalent to fluence rate).

The LP-CB setup used in this thesis is depicted in Figure 7. The distance from the top surface of the Petri dish (9) to the axial centerline of the UV lamp (3) is 660 mm. A monitoring radiometer (8, International Light IL1700 with sensor SED240), calibrated to the reading of a reference radiometer at the center of the Petri dish, is positioned beside the Petri dish to continuously measure irradiance (in W/m²). The irradiance is integrated over time to obtain an accurate UV fluence (in J/m²). Once the desired UV fluence is achieved, the shutter is promptly closed (shutter speed ≈ 0.5 s).

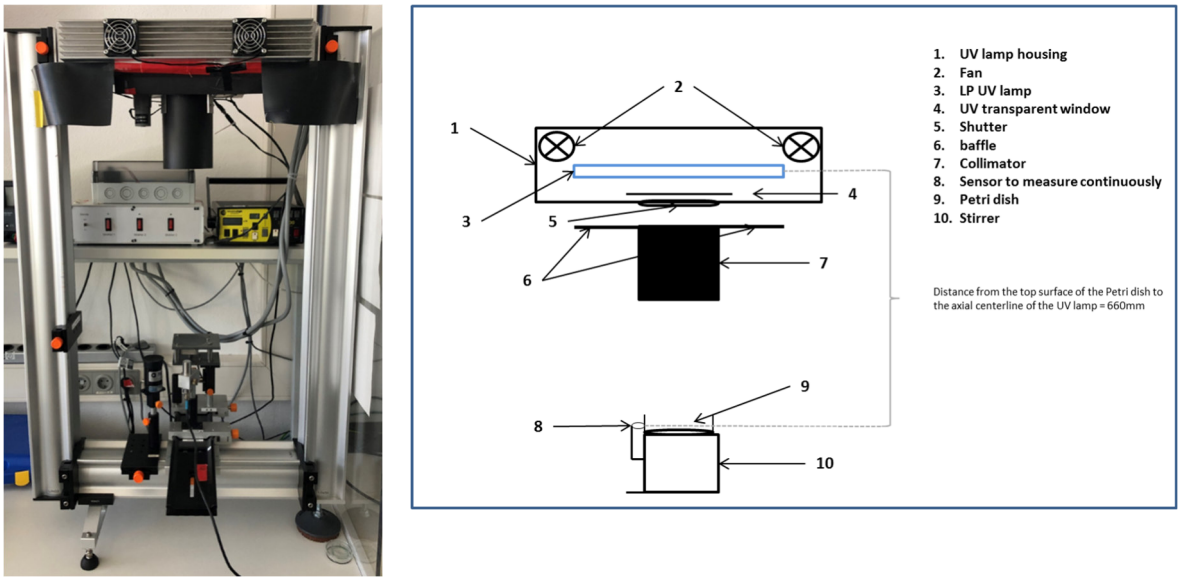

Figure 7: Picture of the LP-CB at TZW (left picture). Schematic structure of a CB (right figure).

Before and after each irradiation, the incident irradiance ($S_{incident}$ in W/m²) on the top surface of the water in the Petri dish is measured, and the radiometer for monitoring is adjusted accordingly. To calculate the average irradiance ($S_{average}$ in W/m²) within the suspension of microbes, four correction factors are applied (refer to Equation 6).

$$S_{average} = S_{incident} \cdot PF \cdot WF \cdot DF \cdot RF \quad (6)$$

With:

$S_{average}$	Average irradiance within the microbe suspension, in W/m²
$S_{incident}$	Incident irradiance on the top surface of the water in the Petri dish, in W/m²
PF	Petri Factor: accounting for the homogeneity of the irradiance distribution across the area of the Petri dish, unit less
WF	Water Factor: accounting for the absorption of UV radiation by the suspension, unit less
DF	Divergence Factor: accounting the reduction in irradiance resulting from an increase in distance within the path length (4.4 mm) inside the suspension
RF	Reflection Factor: accounting for the reflection of vertical beams of the top surface of the suspension (defined as 0.9750)

The factors for the experiments were calculated in accordance with Bolton & Linden (2003) and Bolton, Beck & Linden (2015).

The desired UV fluence (in J/m²) is entered into the control device of the CB, and the current irradiance is integrated over time until the desired UV fluence is achieved. Given the constant irradiance and the absence of hydraulic impacts, the UV fluence can be defined as follows (refer to equation 7):

$$H_{UV} = S_{average} \cdot t \tag{7}$$

With:

H_{UV}	Applied UV fluence at the collimated beam apparatus, in J/m²
$S_{average}$	Average irradiance within the microbe suspension, in W/m²
t	Time of the irradiation, in s

A collimated beam apparatus with a MP-lamp (MP-CB) was constructed in a manner analogous to the LP-CB from Figure 7, except the distance from the top surface of the Petri dish to the axial centerline of the UV lamp was 828 mm. The average irradiance during the experiments for the LP-CB was approximately 2.4 W/m², while for the MP-CB, it was approximately 3.6 W/m². The four correction factors for both LP- and MP-CB are outlined in Table 3. The raw data for individual irradiations can be found in Appendix C.

Table 3: The four correction factors for LP- and MP-CB from Figure 7.

Correction factor	LP CB	MP CB
PF*	0.979-0.987	0.921
WF	0.997-0.998	0.998
DF	0.994	0.995
RF	0.975	0.975

*the Petri factor is reassessed every three months at TZW by scanning the area of the Petri dish every 5 mm with a radiometer

2.1.3. UV irradiations using a tunable laser-based setup

To assess the germicidal spectral response of microbes at various wavelengths, a tunable laser-based setup at the Physikalisch-Technische Bundesanstalt (PTB) was employed for controlled irradiation. The setup integrates a pulsed optical parametric oscillator (OPO) system as a spectrally tunable monochromatic radiation source. The laser beam is directed by folding mirrors to enable vertical irradiation of a Petri dish containing a prepared suspension sample of *Bacillus subtilis* spores. Transforming the beam into a homogeneous field is achieved by a micro-lens array to illuminate the entire Petri dish area. The distance from the micro-lens array to the top of the suspension is 245 mm, and this value was used in calculating the divergence factor. The schematic of this setup is illustrated in Figure 8.

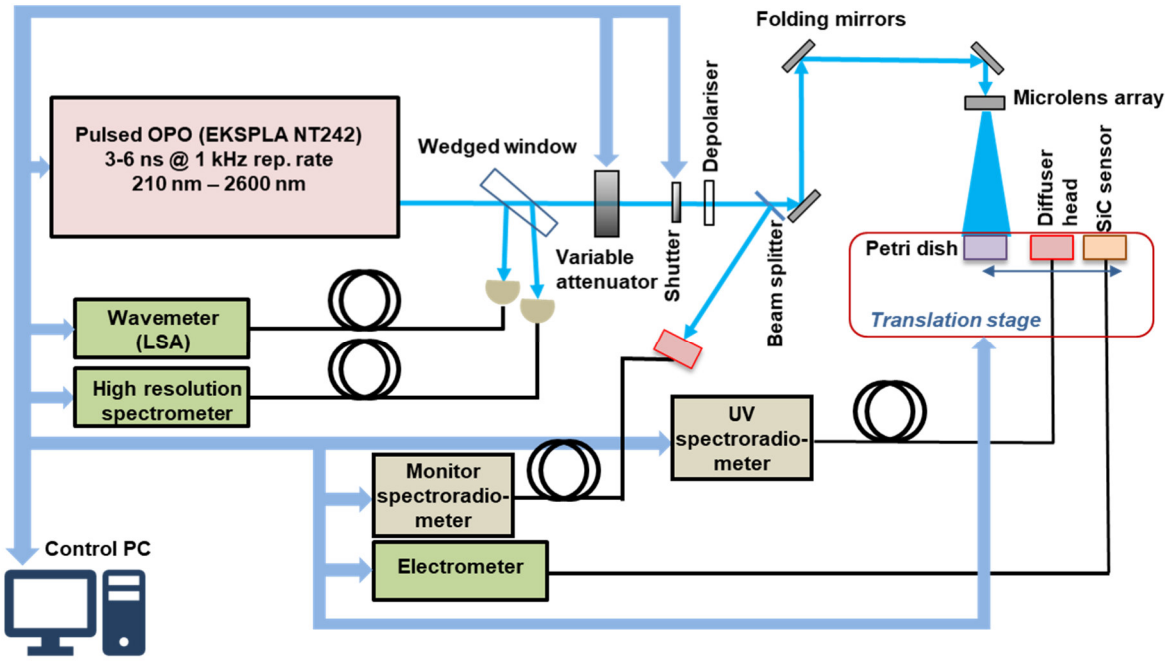

Figure 8: Schematic representation of a tunable laser-based setup at PTB for the irradiation of microbes placed in a Petri dish (schematic designed by PTB).

A linear motorized translation stage facilitates successive measurements by a calibrated array spectroradiometer and a silicon carbide sensor, determining the irradiance values to which the microbe suspension sample in the Petri dish is exposed. Another array spectroradiometer captures a fraction of the beam reflected by a beam splitter, monitoring the stability of the values during the irradiation time corresponding to the aimed fluence of the UV irradiation by the laser-generated field. The maximum irradiances available for the irradiation experiments ranged between 0.27 W/m² and 4.61 W/m². Figure 9 illustrates the average values of the irradiances with the tunable laser for the specific wavelengths during the irradiation campaigns at PTB. The time for exposing the samples is defined by a programmable, computer-controlled shutter of the laser beam. The UV fluences varied from 50 J/m² to 1000 J/m², depending on the wavelength, to achieve a maximum logI of approximately 3.0.

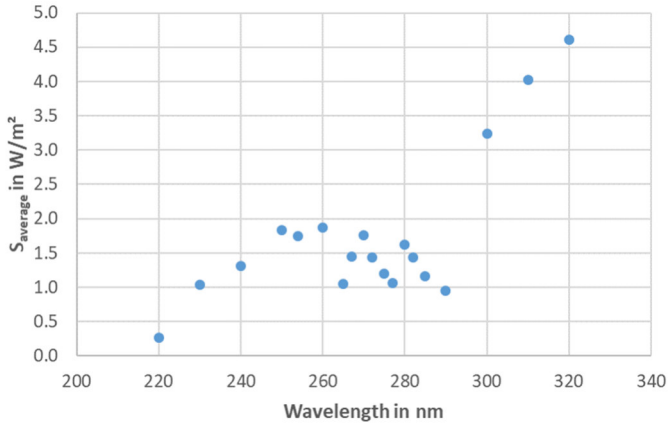

Figure 9: Average irradiance values for the specific wavelengths during the irradiation campaigns at PTB.

Figure 10 displays the irradiance distribution in the irradiation plane at two wavelengths. The field homogeneity, measured at 260 nm, 270 nm, and 280 nm using a detector with a 3 mm entrance optic, yielded a Petri factor (PF) estimated to be 0.98 ± 0.01.

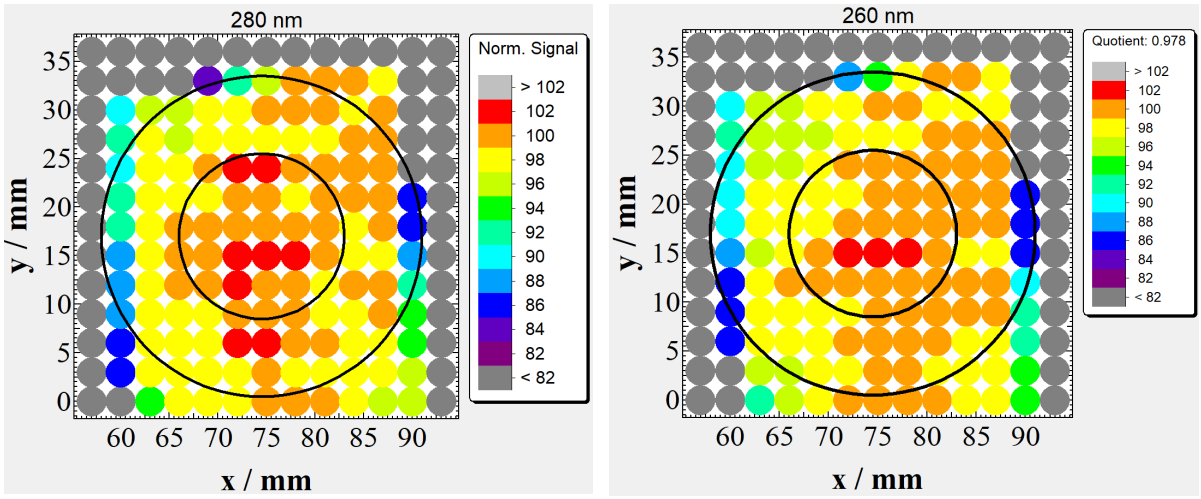

Figure 10: Uniformity of the spectral irradiance distribution in the irradiation plane of the Petri dish measured at two laser wavelengths. The inner and outer circles delineate the areas defined by the measurement sensors and the Petri dish, respectively (schematic designed by PTB).

To consider the water absorbance for calculating the water factor, transmission spectra of the suspension were measured. The absorbance of the water at the specific wavelength was then utilized in the calculation. The four correction factors for UV irradiations using a tunable laser-based setup are listed in Table 4. The raw data for individual irradiations can be found in the Appendix CAppendix C: Raw data Chapter .

Table 4: The four correction factors for the UV irradiations using a tunable laser-based setup.

Correction factor	Laser 220 nm to 320 nm
PF	0.998
WF	0.983-0.998
DF	0.982
RF	0.975

2.1.4.Surrogates *Bacillus subtilis* spores and MS2 phage

The primary objective of the experiments was to establish a new action spectrum for the *Bacillus subtilis* spores strain ATCC 6633. While the accurate scientific name for this strain is *Bacillus spizizenii*, for enhanced recognition, *Bacillus subtilis* is used in the subsequent discussion.

To facilitate a direct comparison of results with existing literature data and thereby assess the laser-based setup, experiments were conducted using the MS2 phage strain ATCC 15597-B1. This single-stranded RNA virus is routinely utilized in UV system validations according to UVDGM. Beck conducted a detailed action spectrum analysis using a tunable laser-based setup [Beck et al., 2015].

2.1.5.Stock preparation and enumeration of *Bacillus subtilis* spores

The preparation process involved initiating a pre-culture on a plate, followed by propagation in a liquid culture. The spore suspension, isolated and purified from this process, is summarized briefly below.

1. Cultivation initiation:
    - Start with a 3-eyelet smear of the pure culture ATCC 6663 on Columbia agar.
    - Incubate for 24 hours at 37 °C.
2. Inoculation and sporulation:
    - Inoculate colonies in sporulation medium.
    - Cultivate for 3 days at 37 °C.
3. Spore harvesting:
    - Harvest spores by centrifugation at 5,000 g, 5 °C to 10 °C for 15 minutes.
    - Wash the spores by resuspending the pellet three times in 20 ml of sterile double-distilled water.
    - The final pellet is resuspended in 400 ml sterile double-distilled water.
    - Pasteurize at 80 °C for 10 minutes to eliminate vegetative cells.
    - Store the final suspension at 4 °C.
4. Spore assay:
    - Conduct the spore assay using yeast extract agar (YEA).
    - Plate samples in triplicate and incubate inverted for 24 to 36 hours at 37 °C.
    - Adjust dilutions and aliquots to achieve a count of 20 to 200 colony-forming units (cfu) per Petri dish.
    - Analyze the ratio of not irradiated samples ($\log N_0$) to irradiated samples (logN) to determine the logI.
    - Perform negative controls each day to ensure the sterility of the working place.
5. Sample assay:
    - Assay each sample the day after collection.
    - Samples are taken at PTB in Braunschweig and sent via overnight express in a cooler to the TZW laboratory in Karlsruhe.

2.1.6.Stock preparation and enumeration of MS2 phage

The MS2 phage were procured from GAP EnviroMicrobial Services located in London, Ontario, Canada (GAP).

The detection of MS2 phage utilized the single-layer method [Association Public Health Association, 2017], wherein the sample is placed into an empty Petri dish, and agar mixed with the host bacteria is poured over the sample. *Salmonella typhimurium* (NCTC 12484) served as the host bacteria. For the assay, bacterial host cultures were incubated for approximately 3 hours at 37 °C to achieve an optical

density at 600 nm (OD600) of 0.45. The bacteria were stored on ice until usage. The media in the bottles were dissolved with a steamer and kept fluid at 42 °C in a water bath. Additional media compounds (CaCl or CaGlucose) as well as bacteria were added to a media bottle directly before use.

The samples were plated in duplicate and incubated at 37 °C for 18 hours. Dilutions and aliquots of the samples were adjusted to count 10 to 300 plaque-forming units (pfu) per Petri dish. Negative controls and positive controls (to ensure the assay's effectiveness) were plated each day.

2.1.7.Scope of experiments with *Bacillus subtilis* spores

The experiments primarily focused on one batch, referred to as Batch 1 of *Bacillus subtilis* spores. However, a second batch, denoted as Batch 2 was utilized during the experiments to validate the results of the main batch on a spot-check basis. Data for Batch 1 were collected on six different days between October 2021 and April 2022, encompassing 19 different wavelengths ranging from 220 nm to 320 nm. Data for Batch were gathered on a single day and involved four different wavelengths.

A summary of the wavelengths used, the number of repetitions, and the total number of UV fluence replicates (n) for both batches of *Bacillus subtilis* spores is provided in Table 5.

Table 5: Summary of the conducted experiments with Bacillus subtilis *spores, including the number of repetitions and the total number of replicates (n) for each wavelength using the tunable laser-based setup from Figure 8.*

Batch 1			Batch 2		
Wavelength in nm	**Repetitions**	**Total n**	**Wavelength in nm**	**Repetitions**	**Total n**
220	2	24	254	1	15
230	2	24	260	1	18
240	2	27	270	1	15
250	2	24	280	1	18
254	6	108			
260	2	36			
265	4	72			
267	2	36			
270	4	81			
272	1	15			
275	4	72			
277	1	18			
280	3	54			
282	1	18			
285	3	42			
290	2	24			
300	1	12			
310	1	12			
320	1	12			

During each one- to three-day test session of the laser irradiations, a dose-response at 254 nm was conducted to verify the stability of the setup conditions at the PTB. Additionally, an irradiation with the reference LP-CB at TZW was carried out as a quality assurance measure to confirm the stability of the spores.

Further experiments included irradiations at 254 nm, 265 nm, and 270 nm with low irradiances (target irradiance of 0.1 W/m²) to validate the reciprocity law within a specific irradiance range. Fluences of 100 J/m² and 400 J/m² were specifically targeted for these experiments.

2.1.8.Scope of experiments with MS2 phage

The experiments involving the MS2 phage were conducted in November 2022 and February 2023, utilizing a laser-based setup with nine different wavelengths. Each wavelength was repeated at least two times. Table 6 provides a summary of the wavelengths used, the number of repetitions, and the total number of UV fluence replicates (n).

Table 6: Summary of the conducted experiments with MS2 phage, including the number of repetitions and the total number of replicates (n) for each wavelength using the tunable laser-based setup from Figure 8.

MS2 phage		
Wavelength in nm	**Repetitions**	**Total n**
254	3	42
260	2	28
265	2	28
267	2	28
270	2	28
275	2	28
277	2	28
280	2	24
290	2	14

In each test session of the laser irradiations, a dose-response at 254 nm was performed to ensure the stability of the setup conditions at the PTB. Furthermore, irradiations with the reference LP-CB (from Figure 7) at TZW was conducted as a quality assurance measure to confirm the stability of the MS2 phage.

2.1.9.Implementation of the irradiation with *Bacillus subtilis* spores

On each day of irradiation, a suspension with a target concentration of 1 x 10^6 colony forming units per milliliter (cfu/ml) was prepared in 500 ml of reverse osmosis water (without a buffer solution). The suspension was continuously stirred throughout the entire experiment. Before commencing the irradiation, 4 ml of the suspension were pipetted into a Petri dish (3.5 cm diameter). A stirring fish (15 mm x 4.5 mm) was added to the Petri dish to ensure homogeneous mixing during the irradiation period. The volume of the stirring fish was considered in the calculations of the water- and the divergence factor due to the increased path length. The Petri dish was placed on the sample table, and the irradiation procedure was initiated. Following irradiation, the solution was transferred to a Falcon tube and refrigerated.

Samples for $logN_0$ were collected at the beginning, middle, and end of each day to observe any potential changes in the initial concentration. Each $logN_0$ sample was plated nine times, resulting in a total of 27 $logN_0$ values per day. The average $logN_0$ values, along with the standard deviation (SD) of the replicates for each day of irradiations and for both batches of *Bacillus subtilis* spores, are detailed in Table 7. It is evident that the measured $logN_0$ concentrations closely align with the target concentration of 6-log. The standard deviations of the replicates also fall well within the defined 0.2 range quality criterion specified in DIN 19294-1 [DIN (Deutsches Institut für Normung e.V.), 2020]. The raw data for $logN_0$ values can be found in the Appendix C.

Table 7: The average $logN_0$ values along with the standard deviation of the replicates are provided for each irradiation day and both batches of Bacillus subtilis *spores.*

	Batch 1		**Batch 2**	
irradiation day	**$logN_0$**	**SD replicates**	**$logN_0$**	**SD replicates**
1	6.09	0.06	6.03	0.17
2	6.00	0.07		
3	6.07	0.07		
4	6.12	0.04		
5	5.98	0.07		
6	6.13	0.07		

2.1.10. Implementation of the irradiation with MS2 phage

The implementation of the irradiation experiments with the MS2 phage followed a methodology analogous to that described in Chapter 2.1.9, with a couple of exceptions. Instead of using reverse osmosis water as the suspension for the MS2 phage, chlorine-free tap water was employed as a buffer solution. Additionally, a separate $logN_0$ was measured and utilized for the dose-response calculation for each single wavelength.

2.1.11. Statistical analysis for *Bacillus subtilis* spores irradiations

For the data analysis, the regression of the 254 nm dose-response curve was determined using an adjusted first-order inactivation model, as outlined in Chapter 1.4. Specifically, the parameter A was included, which represents the y-intercept with a negative value. This is necessary because the curve crosses the fluence axis at the UV fluence where the log-linear correlation begins, as shown in Equation 8:

$$logI_{254nm} = A_{254nm,B.sub.} + B_{254nm,B.sub.} \cdot H_{UV,254nm} \quad (8)$$

With:

$logI_{254nm}$	Measured log inactivation at 254 nm, unit less
$A_{254nm, B.sub.}$ and $B_{254nm, B.sub.}$	Regression parameters defining the UV dose-response at 254 nm, $A_{254nm, B.sub.}$ unit less and $B_{254nm, B.sub.}$ in m²/J
$H_{UV, 254nm}$	Applied UV fluence at 254 nm, in J/m²

The analysis considered only data within the linear range. The calculation of logI corresponding to specific UV fluences was based on the average daily $logN_0$ value (refer to Table 7).

To determine the action spectrum constants for each wavelength, a mapping approach was applied using Equation 9:

$$logI_{\lambda} = A_{254nm,B.sub.} + B_{254nm,B.sub.} \cdot H_{UV,\lambda} \cdot AS_{\lambda} \quad (9)$$

With:

AS_{λ}	Action spectrum constant for wavelength λ, unit less

For wavelengths 290 nm to 320 nm, where there was no significant inactivation, the mapping was done without $A_{254nm, B.sub}$ to force the regression through the origin.

The mapping approach has the advantage of covering action spectrum values over a broad logI range and is not defined by a fixed logI.

For all wavelengths, AS_λ was statistically significant (p-value < 0.05) using linear regression as given in Equation 9. The combined dataset from all repeated measurements was used for each wavelength to determine the action spectrum constant. The standard deviation of the action spectrum constant was calculated by first determining the uncertainty of the interpolation (U_{IN}) for each wavelength's dataset with Equation 10. In the following sections, U_{IN} will also be used as the 95th percentile prediction interval (PI) in the graphs.

$$U_{IN,\lambda} = SD_\lambda \cdot t_\lambda \tag{10}$$

With:

$U_{IN,\lambda}$	Uncertainty of interpolation at wavelength λ, unit less
SD_λ	Standard deviation of the differences between measured logI and predicted logI using Equation 9, unit less
t_λ	Two-sided Student's t-statistic at a 95th percentile level with n-k degrees of freedom, where n is the total number of samples (including replicates) from all repeated measurements and k is the number of parameters used for the regression equation, at wavelength λ

Next, the maximum and minimum action spectrum constants are calculated by combining $U_{IN,\lambda}$ from Equation 10 and inserting it in Equation 11.

$$logI_\lambda \pm U_{IN,\lambda} = A_{254nm,B.sub.} + B_{254nm,B.sub.} \cdot H_{UV,\lambda} \cdot AS_{\lambda,max/min} \tag{11}$$

With:

$AS_{\lambda,\ max/min}$	Maximum and minimum action spectrum constants for wavelength λ, unit less

The differences between AS_{λ} from Equation 9 and $AS_{\lambda,\ max/min}$ from Equation 11 were defined as the uncertainty of the action spectrum constant.

2.1.12. Statistical analysis for MS2 phage irradiations

To statistically analyze of the MS2 dose-response curves, a quadratic function was used, as described in Equation 12. Although, theoretically, a single-stranded RNA virus should adhere to the first-order disinfection model outlined in Equation 1 [Havelaar, Nieuwstad, Meulemans, & van Olphen, 1991], a quadratic function was applied due to various factors discussed in Chapter 1.4, which provided the best fit. Researchers have documented the use of both quadratic and straight linear functions for MS2 dose-response curve [Sommer, et al., 2001; Calgua, et al., 2014; Beck, Wright, Hargy, Larason, & Linden, 2015], and these functions are also recognized in the standard UVDGM framework.

$$logI_{254nm} = A_{254nm,MS2} \cdot H_{UV,254nm} + B_{254nm,MS2} \cdot {H_{UV,254nm}}^2 \quad (12)$$

With:

$A_{254nm,\ MS2}$ and $B_{254nm,\ MS2}$	Regression parameters defining the UV dose-response at 254 nm, $A_{254nm,\ MS2}$ in m^2/J and $B_{254nm,\ MS2}$ in m^4/J^2

To ascertain the MS2 action spectrum constants for each wavelength, a mapping approach was employed using Equation 13.

$$logI_{\lambda} = A_{254nm,MS2} \cdot H_{UV,\lambda} \cdot AS_{\lambda} + B_{254nm,MS2} \cdot (H_{UV,\lambda} \cdot AS_{\lambda})^2 \quad (13)$$

The action spectrum constant was determined using the combined dataset obtained from all repeated measurements for each wavelength. The standard deviation of the action spectrum constant was computed by initially determining the uncertainty of the interpolation (U_{IN}) as introduced in chapter 2.1.11 using Equation 10. In the subsequent analysis, U_{IN} will also be referred to as the 95th percentile prediction

interval in the graphical representations. The process involved calculating the maximum and minimum action spectrum constants by combining $U_{IN,\lambda}$ from Equation 10 and inserting it in Equation 14.

$$logI_\lambda \pm U_{IN,\lambda} = A_{254nm,MS2} \cdot H_{UV,\lambda} \cdot AS_{\lambda,max/min} + B_{254nm,MS2} \cdot (H_{UV,\lambda} \cdot AS_{\lambda,max/min})^2 \qquad (14)$$

The standard deviation of the action spectrum constant was defined by determining the differences between AS_λ calculated using Equation 13 and $AS_{\lambda,\,max/min}$ obtained from Equation 14.

2.2. Results and discussion *Bacillus subtilis* spores irradiations

The following results will refer to the scope listed in Table 5. With the exception of Chapter 2.2.4, the results will pertain to the *Bacillus subtilis* spores from Batch 1.

2.2.1. Comparison of 253.7 nm LP-CB and 254 nm laser-based setup

As outlined in Chapter 1.6.5, the action spectra of microbes are traditionally normalized to the primary emission line of a LP-lamp, precisely at 253.7 nm. This choice is influenced by the fact that the LP-CB apparatus serves as the reference for UV system validation worldwide and is the most commonly used collimated beam apparatus in laboratories globally. However, in the laser-based setup, the wavelength was intentionally set to 254 nm. To demonstrate the comparability and repeatability of the laser-based setup at PTB with the LP-CB reference at TZW, six dose-response curves at 254 nm were conducted with “batch 1” throughout the experiments. For the calculation of the regressions Equation 8 was used.

The results with the laser-based setup are illustrated in Figure 11, showcasing a strong correlation in the combined dataset with a coefficient of determination (R^2) of 0.967.

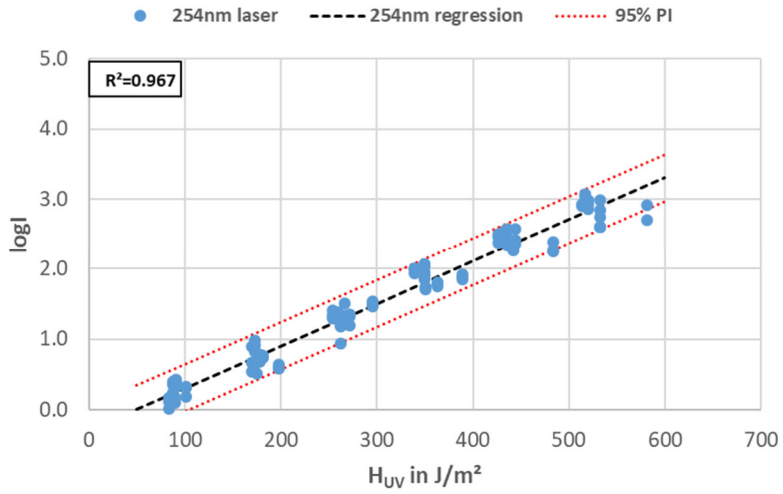

Figure 11: Dose-response curve of Bacillus subtilis *spores from Batch 1 exposed to 254 nm using the laser-based setup. The curve is based on combined data from six individual repetitions. The red dotted lines represent the 95th percentile prediction interval (≡U_{IN}).*

The dose-response curve for the LP-CB was generated from five individual irradiations. The findings are depicted in Figure 12, demonstrating a robust correlation within the consolidated dataset, with a coefficient of determination (R^2) of 0.990.

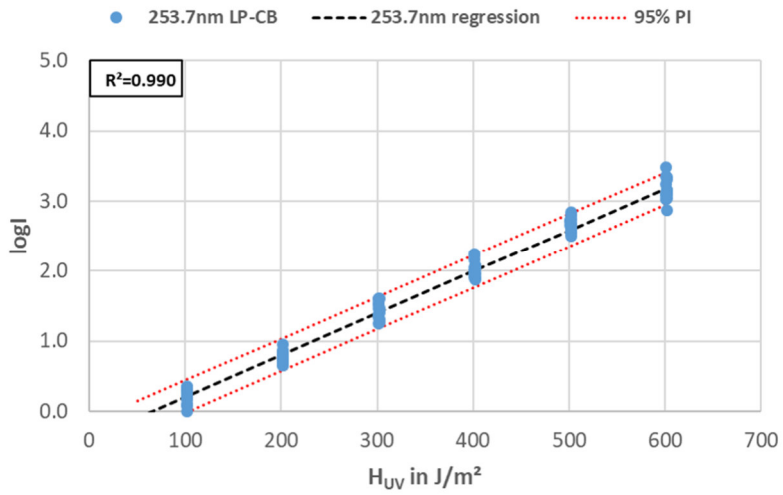

Figure 12: Dose-response curve of Bacillus subtilis *spores from Batch 1 exposed to 253.7 nm using the LP-CB. The curve is based on combined data from five individual repetitions. The red dotted lines represent the 95th percentile prediction interval (≡U_{IN}).*

Figure 13 presents a comparison of the dose-response curves for the 254 nm laser-based and the 253.7 nm LP-CB. The graph affirms that the laser-based regression comfortably falls within the prediction interval of ± 0.23-logI of the conventional 253.7 nm LP-CB, which serves as the reference.

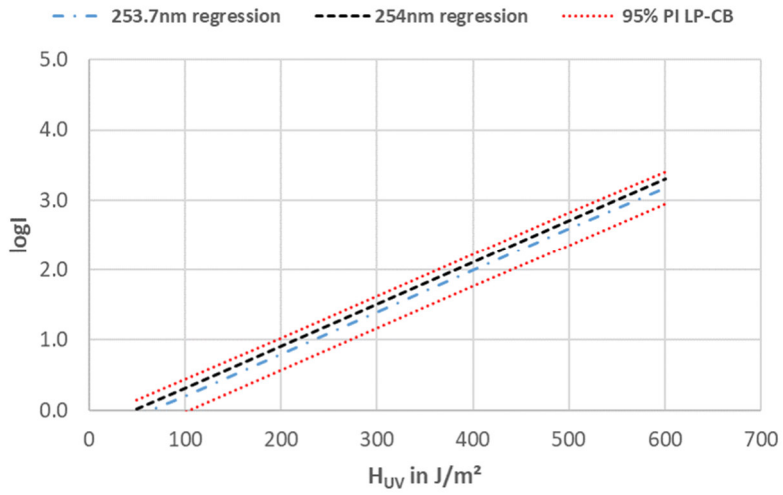

Figure 13: Dose-response curves of Bacillus subtilis *spores Batch 1 to 254 nm from laser-based setup (black dashed line) and 253.7 nm from LP-CB (blue dash-dot line). The red dotted lines define the 95th percentile prediction from the LP-CB data.*

Both curves demonstrate a similar slope and intercept, leading to variations in the UV fluence for 2-logI and 3-logI between the laser-based and LB-CB irradiations below 5 %, as outlined Table 8.

Table 8: UV dose-response results of Bacillus subtilis *spores Batch 1 for the wavelengths 254 nm with the laser-based setup and 253.7 nm with the LP CB for 2- and 3-log inactivation and the regression parameters A and B defining the dose-response curves using Equation 8.*

Wavelength in nm	**H_{UV} in J/m² needed for (± 95 % PI)**		**A**	**B in m²/J**
	2-logI	**3-logI**		
254 nm laser	382 ± 56	550 ± 56	-2.880E-1	5.982E-3
253.7 nm LP-CB	402 ± 38	570 ± 38	-3.847E-1	5.940E-3

These results lead to two conclusions: firstly, the laser-based system exhibited consistent stability throughout the experiments, and secondly, the outcomes were highly comparable to those obtained from the low-pressure collimated beam apparatus.

According to literature data at 253.7 nm for LP-CB [Malayeri, Mohensi, & Bolton, 2016], the dose-response curves of *Bacillus subtilis* spores ATCC 6633 can vary significantly, with an average UV fluence of 320 J/m² and a standard deviation of ± 111 J/m² for 2-log-inactivation. Nevertheless, Batch 1 can be considered as representative of *Bacillus subtilis* spores that fulfill the criteria stated in DIN 19294-1.

2.2.2. Dose-response curves with the different wavelengths from the laser-based setup with Batch 1

The results for various wavelengths using the tunable laser are depicted in Figure 14. The R^2 values consistently exceed 0.980, and the uncertainty of interpolation (as per Equation 10) ranges between 0.09 and 0.44, with an average of 0.21. For wavelengths between 290 nm and 320 nm, the R^2 values are lower due to their minimal efficacy in inactivation, resulting in a slope of approximately 0, which is suboptimal for the applied statistical analysis.

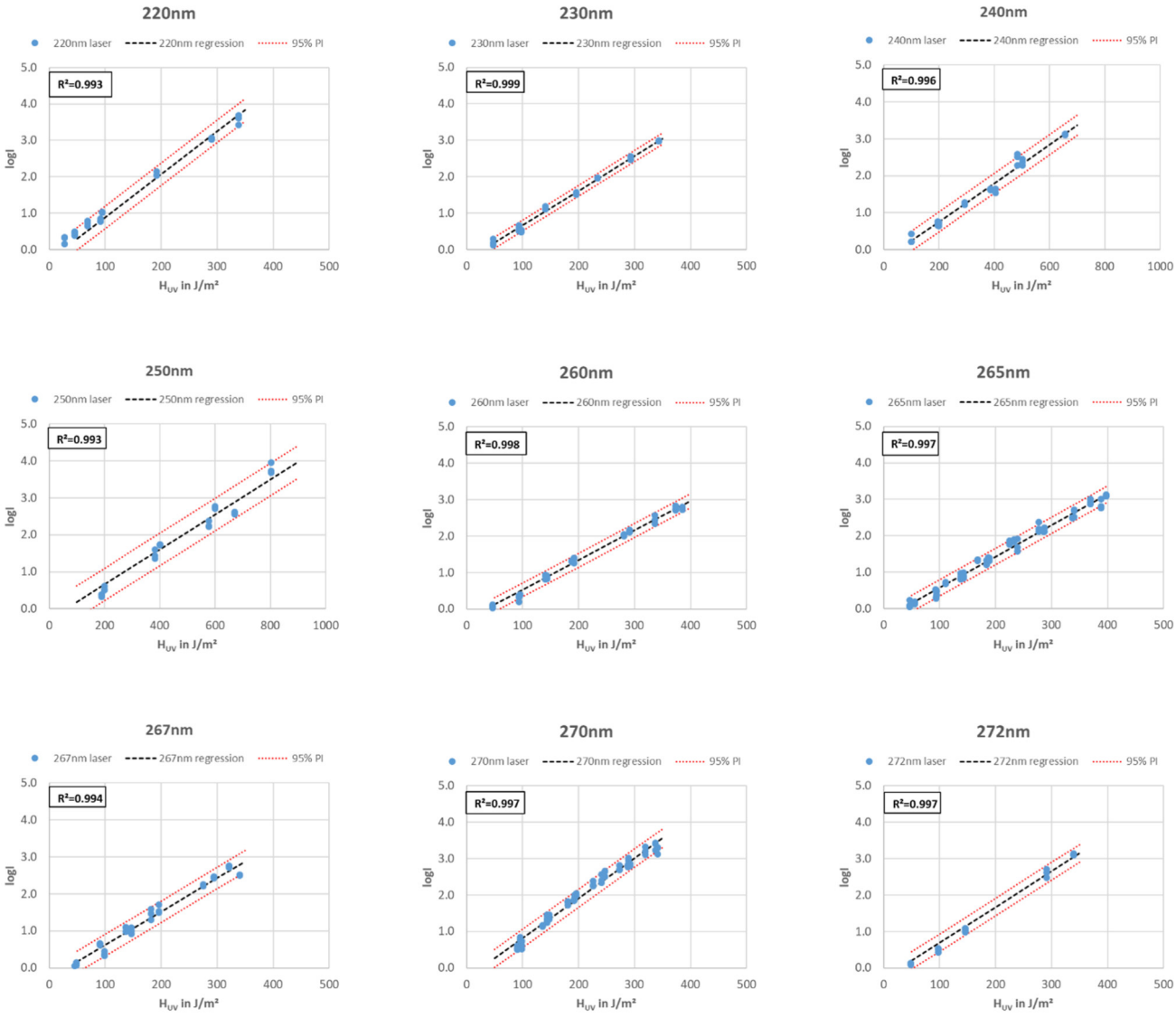

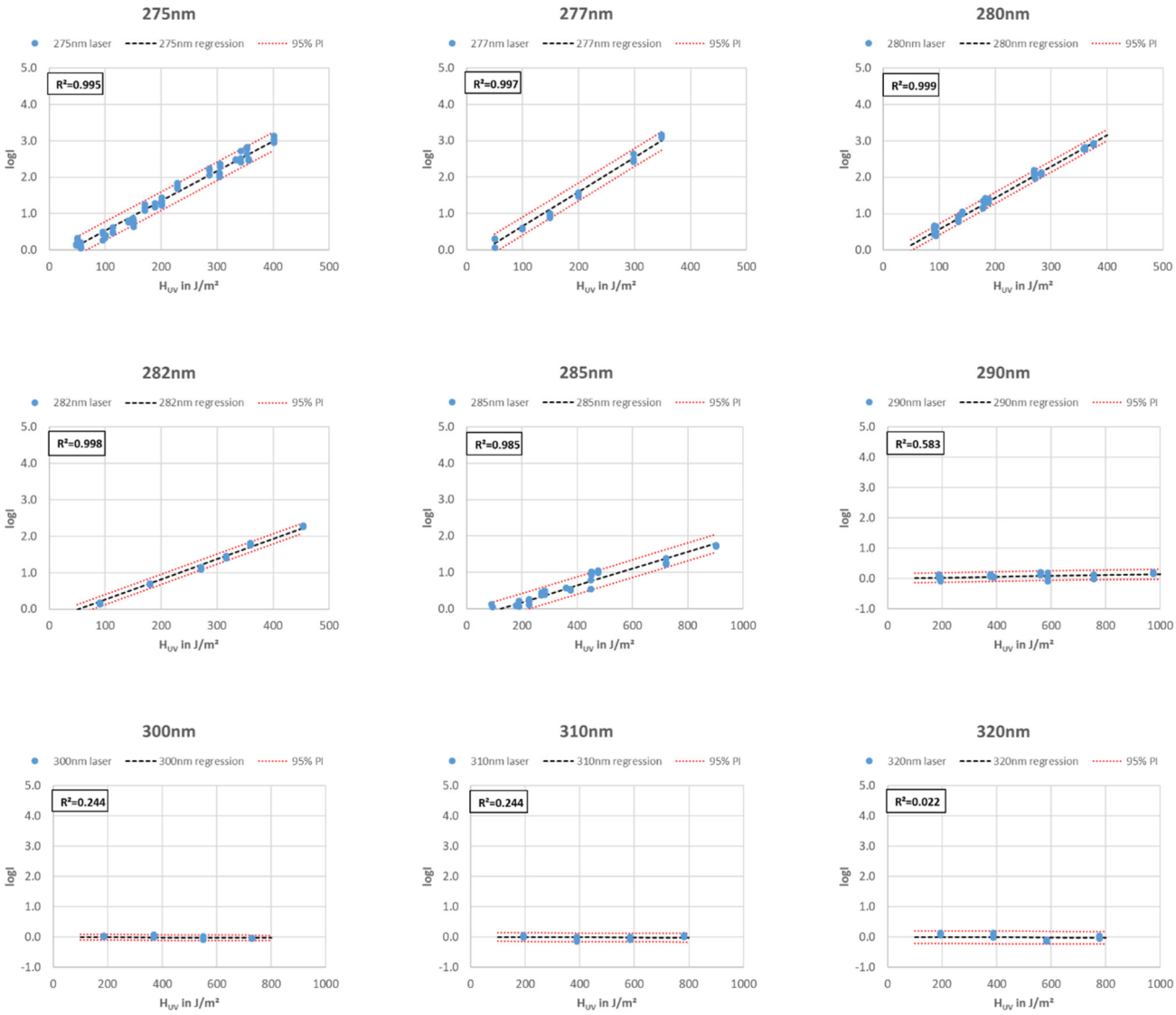

Figure 14: Dose-response curve of Bacillus subtilis *spores Batch 1 to wavelength specific UV light from tunable laser. The blue circles represent the combined data of the specific wavelength with the resulting regression curve (black dashed line). The red dotted lines define the 95th percentile prediction. Note different x-axis values.*

Table 9 provides a summary of the UV dose-response data derived from Figure 14, presenting the UV fluences required for 2-logI and 3-logI across different wavelengths ranging from 220 nm to 280 nm. No inactivation was observed between 300 nm and 320 nm. The highest efficacy, demonstrated by the lowest required UV fluence, was observed at 270 nm, where only 54 % of the UV fluence was needed for the same logI compared to 254 nm.

Table 9: UV dose-response results of Bacillus subtilis *spores Batch 1 covering wavelengths from 220 nm to 285 nm, indicating UV fluences required for 2-log and 3-log inactivation and action spectrum constant for each wavelength (AS_λ).*

Wavelength in nm	**H_{UV} in J/m² needed for (± 95 % PI)**		**$AS_\lambda \pm \Delta$**
	2-logI	**3-logI**	
220	194 ± 26	279 ± 26	1.97 ± 0.23
230	240 ± 16	345 ± 16	1.59 ± 0.11
240	438 ± 52	630 ± 52	0.87 ± 0.10
250	483 ± 92	694 ± 92	0.79 ± 0.13
254	382 ± 56	550 ± 56	1.00
260	281 ± 23	404 ± 23	1.36 ± 0.12
265	267 ± 26	384 ± 26	1.43 ± 0.14
267	253 ± 32	364 ± 32	1.51 ± 0.21
270	208 ± 23	299 ± 23	1.84 ± 0.18
272	233 ± 24	335 ± 24	1.64 ± 0.16
275	280 ± 31	402 ± 31	1.37 ± 0.16
277	243 ± 27	349 ± 27	1.57 ± 0.17
280	266 ± 18	382 ± 18	1.44 ± 0.10
282	412 ± 25	592 ± 25*	0.93 ± 0.07
285	985 ± 105	1415 ± 105*	0.39 ± 0.08
290	-**	-**	0.03 ± 0.00

*data extrapolated

** data not significant for extrapolation

The dose-response data presented in Figure 14 was utilized to derive the action spectrum of *Bacillus subtilis* spores relative to their response at 254 nm, as described in chapter 2.1.11. The resultant action spectrum is displayed in Figure 15.

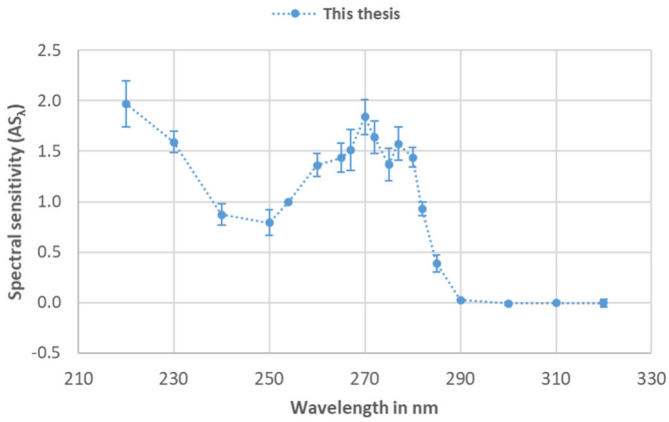

Figure 15: Action spectrum of Bacillus subtilis *spores determined in this thesis.*

A comparison, shown in Figure 16, was made with data from Cabaj et al. (2002), referenced in the DVGW worksheet W 294-3. The action spectrum obtained in this thesis reveals a distinct structure, particularly between 260 nm and 280 nm, showcasing a peak value at 270 nm of 1.84. In contrast, the reference action spectrum from Cabaj et al. (2002) shows a flatter behavior in the 250 nm to 280 nm range with values ranging from 1.00 to 1.15. Additionally, the notable decrease in efficiency to zero at 290 nm distinguishes the action spectrum obtained in this thesis from that of Cabaj et al. (2002).

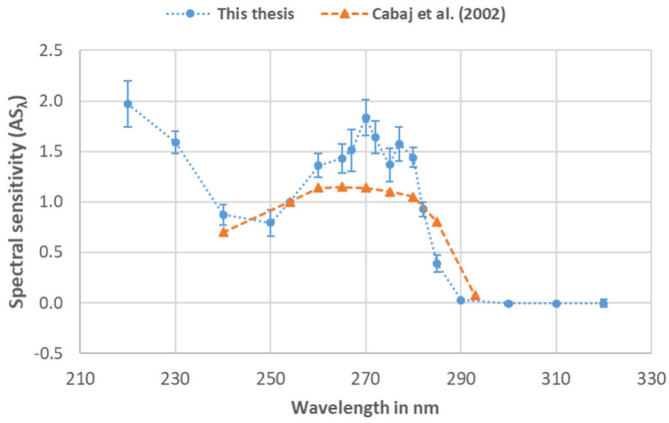

Figure 16: Action spectra of Bacillus subtilis *spores from this thesis (blue circles with dotted line) compared to data from Cabaj et al. (2002) (orange triangles with dashed line).*

Chen et al. (2009) determined absorbance spectra of decoated *Bacillus subtilis* spores which align reasonably well with the action spectrum identified in this thesis, as shown in Figure 17. This absorbance spectrum of the decoated spores does not contain DNA. Past research suggested that factors beyond the DNA absorbance spectrum, such as other components within the spores, might contribute to the UV inactivation process [Cabaj, Sommer, Pribil, & Haider, 2002; Mamane-Gravetz, Linden, Cabaj, & Sommer, 2005]. The consistency between the action spectrum determined in this thesis and the absorption spectrum from Chen et al. (2009), support the concept that inactivation of *Bacillus subtilis* spores is impacted by more than solely the genetic material.

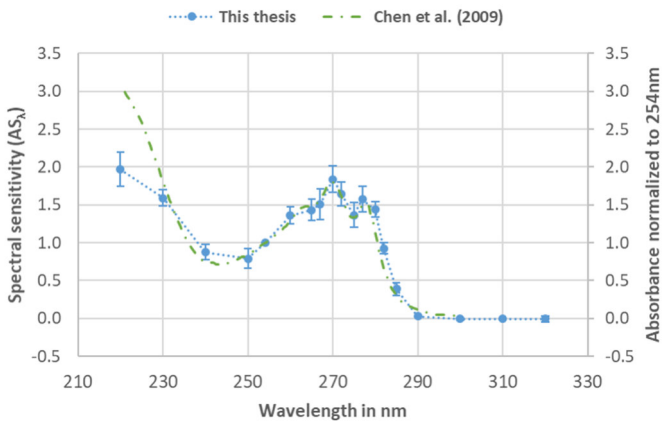

Figure 17: Action spectra of Bacillus subtilis *spores from this thesis (blue circles with dotted line) compared to data from Chen et al. (2009) showing the absorbance spectra from decoated* Bacillus subtilis *spores (green dash-dot line).*

2.2.3. Dose-response curves with low irradiances

For the wavelengths 254 nm, 265 nm, and 270 nm, the laser irradiance was adjusted down to approximately 0.10 W/m², compared to the data presented in chapter 2.1.3. These experiments were undertaken to assess the applicability of the law of reciprocity. In radiation biology, the law of reciprocity posits that, for a constant total dose, the biological effect of radiation remains the same irrespective of the irradiance or the duration of irradiation [Sommer, Haider, Cabaj, Pribil, & Lhotsky, 1998]. In simpler terms, the biological effect is directly proportional to the dose, whether delivered in a short time at high intensity or over a longer period at low intensity.

Due to limitations in increasing irradiance without altering the PTB setup, these experiments were conducted at lower irradiances. The three graphs in Figure 18 suggest that there is no significant difference observed when irradiating with low irradiances.

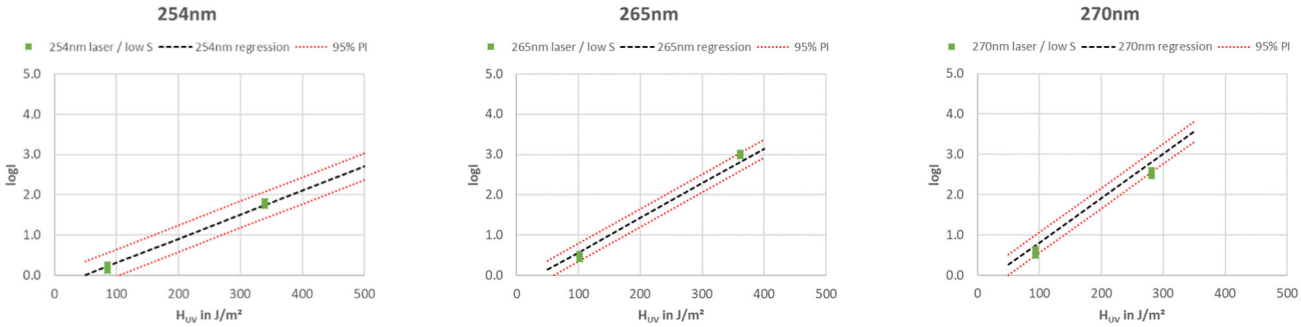

Figure 18: Data points (green squares) of Bacillus subtilis *spores Batch 1 to wavelength specific UV light from tunable laser with low irradiances (≈ 0.1 W/m²). The black dashed lines symbolize the regression curves with regular irradiances. The red dotted lines define the 95th percentile prediction based on the results with the regular irradiances.*

All the recorded data points (depicted as green squares) fall within the 95th percentile prediction interval, as established from the outcomes obtained with standard irradiances (refer to chapter 2.2.1). Table 10

provides a listing of the measured low irradiance UV fluence data points along with documentation of their compliance within the 95th percentile prediction interval.

Table 10: UV fluence data points obtained at low irradiances, along with their corresponding measured logI values accompanied by standard deviation (SD), calculated logI with a 95th percentile prediction interval (PI) based on the low irradiance UV dose data points, and verification of whether the differences in logI lie within the 95th PI.

Wavelength in nm	**H_{UV} in J/m²**	**Measured with low irradiance**	**Calculated with regular irradiance**	**Delta within 95% PI?**
		logI ± SD	**logI ± 95 % PI**	
254	86	0.18 ± 0.08	0.23 ± 0.33	Yes
	339	1.80 ± 0.06	1.74 ± 0.33	Yes
265	102	0.45 ± 0.06	0.59 ± 0.22	Yes
	362	2.99 ± 0.04	2.81 ± 0.22	Yes
270	94	0.58 ± 0.08	0.74 ± 0.25	Yes
	280	2.55 ± 0.07	2.79 ± 0.25	Yes

2.2.4. Dose-response curves with the different wavelengths from the laser-based setup with Batch 2

A distinct batch of *Bacillus subtilis* strain ATCC 6633, referred to as Batch 2, was employed to spot-check and validate the reproducibility of the results obtained from Batch 1. The selection of Batch 2 was based on its initially different absolute UV sensitivity to 254 nm, indicated by significant different regression values as compared to the data from Batch 1. Specifically, for Batch 1, a 22 % higher UV fluence for 2-logI and a 32 % higher fluence for 3-logI were required compared to Batch 2. The regression parameters for both batches are summarized in Table 11.

Table 11: UV dose-response results of Bacillus subtilis *spores Batch 1 and Batch 2 for the wavelengths 254 nm with the laser-based setup for 2- and 3-log inactivation and the regression parameters A and B defining the dose-response curves using Equation 8.*

ID	**H_{UV} in J/m² needed for (± 95 % PI)**		**A**	**B in m²/J**
	2-logI	**3-logI**		
Batch 1	382 ± 56	550 ± 56	-2.880E-1	5.982E-3
Batch 2	313 ± 31	418 ± 31	-9.669E-1	9.480E-3

The dose-response regressions for both batches are illustrated in Figure 19.

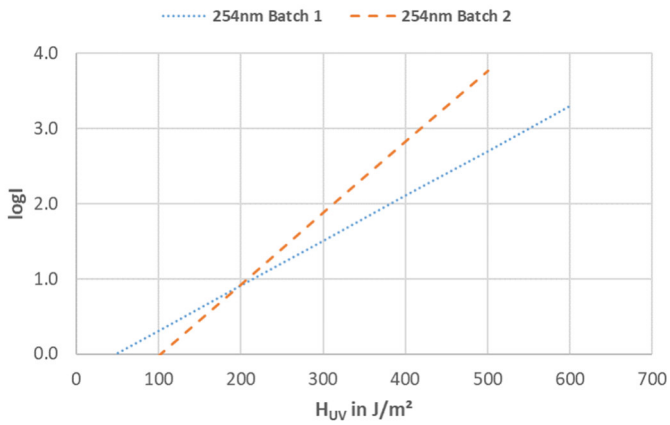

Figure 19: Regressions of the dose- response for Batch 1 (blue dotted line) and Batch 2 (orange dashed line).

The objective was to investigate whether, despite the absolute difference in UV sensitivity between the batches, the relative ratio of disinfection efficacy at other wavelengths to 254 nm remains similar.

The experiments for Batch 2 were carried out using wavelengths of 254 nm, 260 nm, 270 nm, and 280 nm. The results are depicted in Figure 20, where the R^2 values consistently exceed 0.980. The uncertainty of interpolation falls within the range of 0.29 to 0.44.

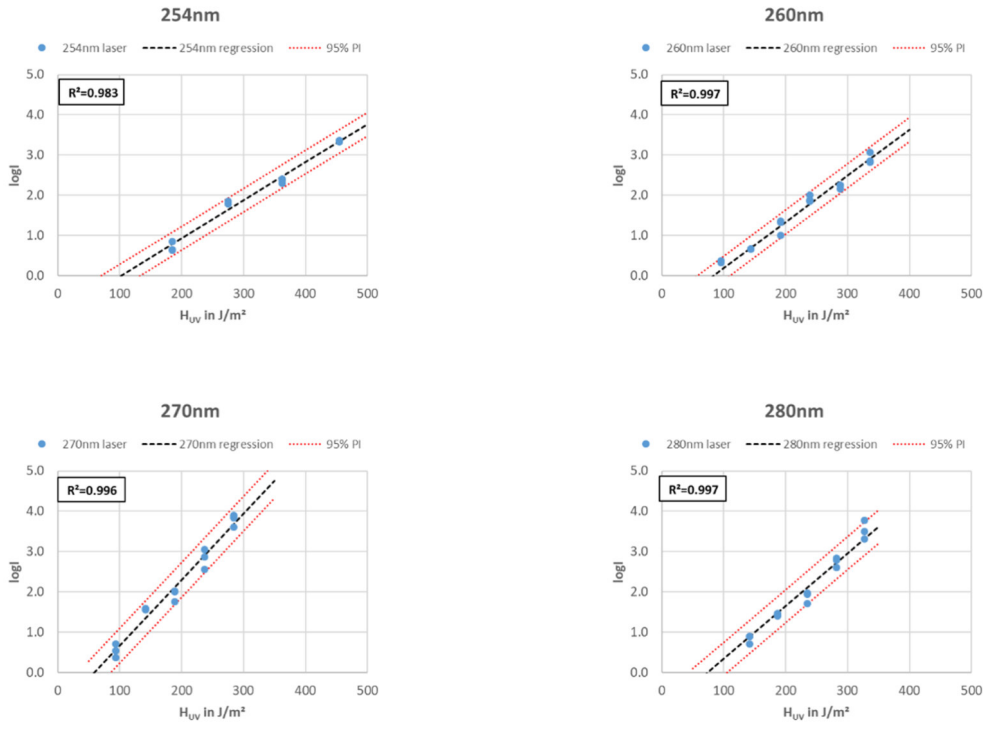

Figure 20: Dose-response curve of Bacillus subtilis *Spores Batch 2 to wavelength specific UV light from tunable laser. The blue circles represent the combined data of the specific wavelength with the resulting regression curve (black dashed line). The red dotted lines define the 95th percentile prediction.*

Similar to Batch 1, the wavelength of 270 nm demonstrated the highest efficiency, as evidenced by Table 12. For the same logI, 58 % of the UV dose compared to 254 nm is required. This closely aligns with the findings from Batch 1, where the corresponding value was 54 %.

Table 12: UV dose-response results of Bacillus subtilis *spores Batch 2 for the different wavelengths for 2- and 3-log inactivation.*

Wavelength in nm	**H_{UV} in J/m² needed for (± 95 % PI)**	
	2-logI	**3-logI**
254	313 ± 31	418 ± 31
260	258 ± 26	345 ± 26
270	182 ± 27	243 ± 27
280	227 ± 32	303 ± 32

Analog to the data analysis of Batch 1, the dose-response data from Figure 20 were employed to calculate the action spectrum values relative to 254 nm. These calculated values are represented in Figure 21 as orange circles with a dashed line.

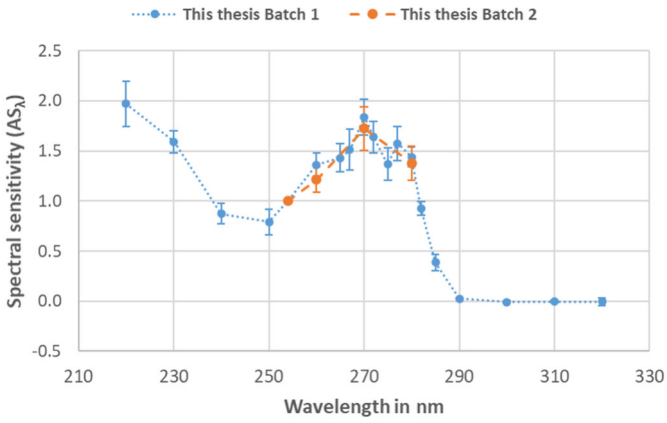

Figure 21: Action spectra of Bacillus subtilis *spores from this thesis with Batch 1 (blue circles with dotted line) and Batch 2 (orange circles with dashed line).*

The data closely align with the results obtained from Batch 1 (depicted as blue circles and a dotted line in Figure 21) and fall well within the standard deviations, as detailed in Table 13, for the wavelengths 260 nm, 270 nm, and 280 nm for both Batch 1 and Batch 2.

Table 13: Action spectra values (α_λ) for the wavelengths 260 nm, 270 nm and 280 nm for Batch 1 and Batch 2 and verification that the differences of the action spectra values lie within the standard deviations (SD).

Wavelength in nm	**Batch 1 $AS_\lambda \pm SD$**	**Batch 2 $AS_\lambda \pm SD$**	**Delta within SD?**
260	1.36 ± 0.12	1.21 ± 0.13	Yes
270	1.84 ± 0.18	1.72 ± 0.22	Yes
280	1.44 ± 0.10	1.38 ± 0.17	Yes

2.2.5. Definition of the interpolation of the action spectrum of *Bacillus subtilis* spores

To establish a new action spectrum for *Bacillus subtilis* spores, as per the findings in chapter 2.2.2, a linear interpolation was performed in 1 nm increments between adjacent data points, following Equation 15.

$$AS_\lambda = b_{\lambda n\ to\ \lambda n+1} + m_{\lambda n\ to\ \lambda n+1} \cdot \lambda \quad (15)$$

With:

AS_λ	Action spectrum value at wavelength λ, unit less
$b_{\lambda n \text{ to } \lambda n+1}$, $m_{\lambda n \text{ to } \lambda n+1}$	Regression parameters between two adjacent data points at wavelengths n and n+1, $b_{\lambda n \text{ to } \lambda n+1.}$ unit less and $m_{\lambda n \text{ to } \lambda n+1.}$ in nm^{-1}
λ	Wavelength, in nm

Table 14 provides the regression parameters for each set of adjacent data points. The complete table, containing action spectrum values spanning from 220 nm to 300 nm in 1 nm increments, is available for reference in Appendix B.

Table 14: Regression parameters between two adjacent data points, for the action spectrum of Bacillus subtilis *spores.*

Wavelength n in nm	**Wavelength n+1 in nm**	$\mathbf{b_{\lambda n \text{ to } \lambda n+1}}$	$\mathbf{m_{\lambda n \text{ to } \lambda n+1}}$ **in nm^{-1}**
220	230	1.033E+1	-3.800E-2
231	240	1.815E+1	-7.200E-2
241	250	2.790E+0	-8.000E-3
251	254	-1.234E+1	5.250E-2
255	260	-1.424E+1	6.000E-2
261	265	-2.280E+0	1.400E-2
266	267	-9.170E+0	4.000E-2
268	270	-2.786E+1	1.100E-1
271	272	2.884E+1	-1.000E-1
273	275	2.612E+1	-9.000E-2
276	277	-2.613E+1	1.000E-1
278	280	1.357E+1	-4.333E-2
281	282	7.284E+1	-2.550E-1
283	285	5.169E+1	-1.800E-1
286	290	2.091E+1	-7.200E-2
291	300	1.190E+0	-4.000E-3

2.2.6. Dose-response curve with MP-CB

To validate the effectiveness of the calculation using the new action spectrum for *Bacillus subtilis* spores for polychromatic sources, a comparison between LP-CB and MP-CB (refer to the emission spectra in Figure 23) was carried out using Batch 1. The comparison was performed on one day, and the results without any microbiological weighting are illustrated in Figure 22. Equation 8 was used for both regression calculations.

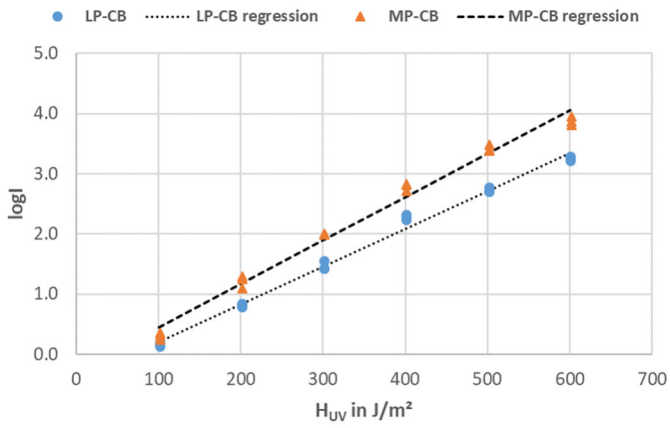

Figure 22: Dose-response curves of Bacillus subtilis *spores Batch 1 to 253.7 nm low pressure (blue circles and black dotted line) and medium pressure (orange triangles and black dashed line).*

As evident from the graph, the MP-CB dose-response curve exhibits a steeper slope compared to the LP-CB, indicating a higher efficacy of MP-lamps as a polychromatic source towards *Bacillus subtilis* spores. In numerical terms, this translates to a 20 % lower UV fluence requirement for achieving 2- and 3-log inactivation of *Bacillus subtilis* spores. The summarized data is presented in Table 15.

Table 15: UV dose-response results of Bacillus subtilis *spores Batch 1 with LP- and MP-CB for 2- and 3-log inactivation and the regression parameters A and B defining the dose-response curves using Equation 8.*

Wavelength in nm	**H_{UV} in J/m² needed for (± 95 % PI)**		**A**	**B in m²/J**
	2-logI	**3-logI**		
LP-CB	387 ± 33	546 ± 33	-4.305E-1	6.285E-3
MP-CB	315 ± 43	453 ± 43	-2.738E-1	7.220E-3

Using Equation 3 from chapter 1.6.5 to calculate the ASCF provides a means to quantify the increased efficacy of an MP-lamp in comparison to an LP-lamp. The emission spectrum of the MP-lamp within the MP-CB, coupled with the calculated action spectrum of *Bacillus subtilis* spores based on the data in Table 14, is depicted in Figure 23.

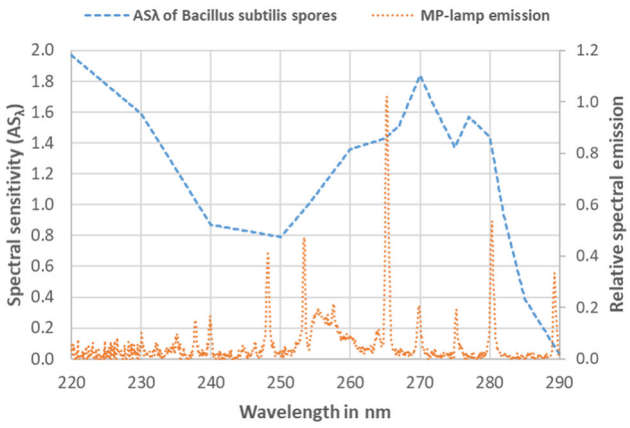

Figure 23: Calculated action spectrum of the Bacillus subtilis *spores (blue dashed line) and the emission spectrum of the MP-lamp (red dotted line).*

Figure 24 displays the dose-response curves for LP-CB (black dotted line) and MP with the action spectra from this thesis (orange dash-dot line) and weighted with the action spectrum from Cabaj et al. (2002) (green dashed line) using Equation 16.

$$H_{UV,weighted} = ASCF \cdot H_{UV} \tag{16}$$

With

$H_{UV,\ weighted}$	Weighted UV fluence of the MP-CB, in J/m²
ASCF	Action spectra correction factor calculated with Equation 3 based on the MP-lamp emission spectrum and the action spectrum from this thesis and Cabaj et al. (2002)
H_{UV}	Applied UV fluence in accordance to Equation 7

The ASCF calculated with the action spectrum from this thesis was 1.20 and with the action spectrum from Cabaj et al. (2002), it was 0.99. The weighted MP dose-response curve with the action spectrum data from this thesis aligns closely with the LP dose-response curve, showing differences in the UV fluence of < 2 % for 2- and 3-log inactivation. In comparison, when using the action spectrum from Cabaj et al. (2002), differences of 20 % in the UV fluence for 2- and 3-log inactivation are observed. This serves as further evidence of the reliability and accuracy of the action spectrum derived from this research.

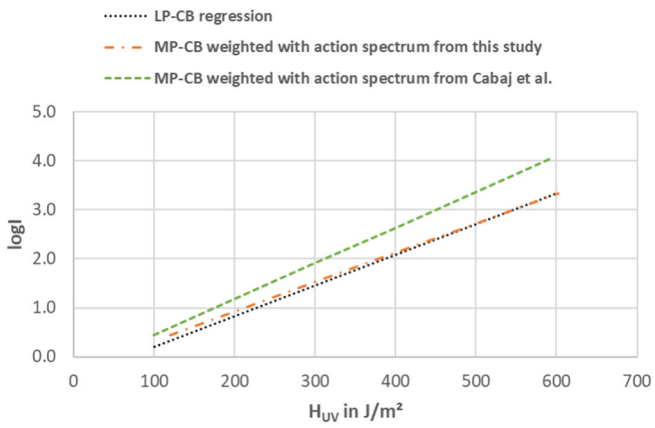

Figure 24: Dose-response curves of Bacillus subtilis *spores Batch 1 with LP-CB (black dotted line) and medium pressure weighted with the action spectrum from this study (orange dash-dot line) and weighted with the action spectrum from Cabaj et al. (2002) (green dashed line).*

2.3. Results and discussion MS2 phage irradiations

The following results refer to the scope listed in Table 6.

2.3.1. Comparison of 253.7 nm LP-CB and 254 nm laser-based setup

To showcase the comparability and repeatability of the laser-based setup at PTB with the LP-CB reference at TZW with MS2 phage, three dose-response curves were conducted, both at 254 nm and with the LP-CB, respectively.

The results are illustrated in Figure 25, where both dose-response curves exhibit a strong correlation within the combined dataset, with coefficient of determination (R^2) values of 0.986 and 0.991, respectively. Statistical significance (p-value < 0.05) was observed for the regression parameters, using Equation 12, of both dose-response curves.

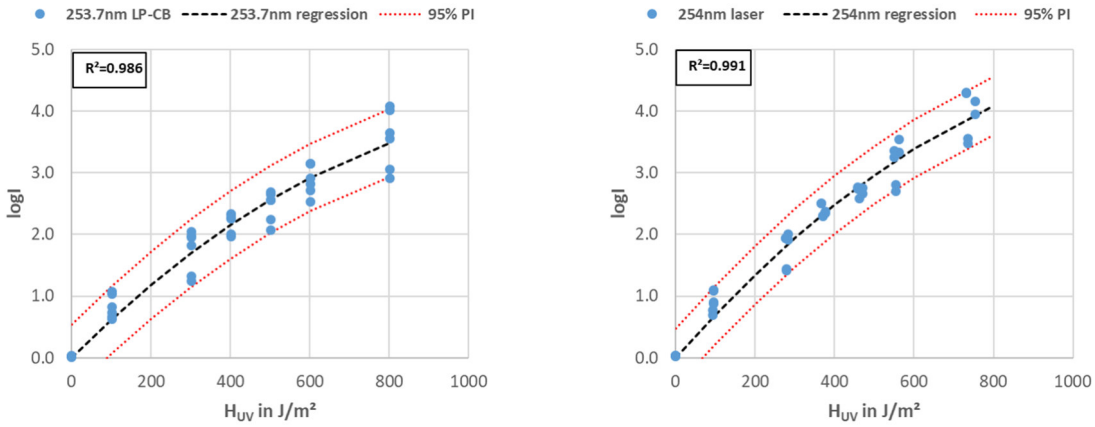

Figure 25: Dose-response curve of MS2 phage exposed to LP-CB (left figure) and to 254 nm using the laser-based setup (right figure). The curves are based on combined data from three individual repetitions each. The red dotted lines represent the 95th percentile prediction interval (≡U_{IN}).

In Figure 26, a comparison between the dose-response curves of the 254 nm laser-based setup and the 253.7 nm LP-CB is presented. The graph clearly demonstrates that the regression derived from the laser-based setup falls within the prediction interval (PI) of ± 0.55-logI of the conventional 253.7 nm LP-CB, which serves as the reference.

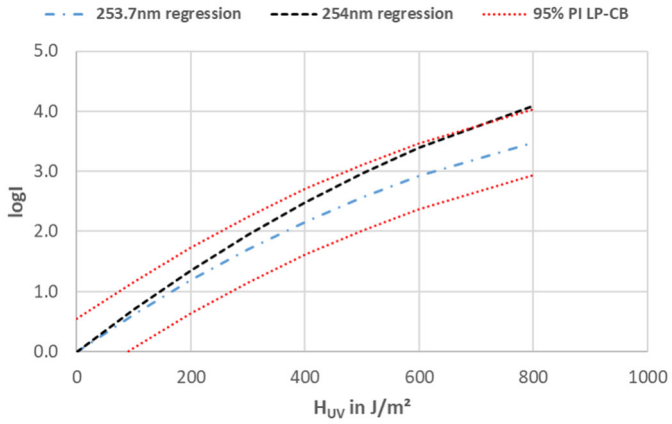

Figure 26: Dose-response curves MS2 phage to 254 nm from laser-based setup (black dashed line) and 253.7 nm from LP-CB (blue dash-dot line). The red dotted lines define the 95th percentile prediction from the LP-CB data.

Both curves exhibit comparable regression parameters, resulting in variations in the UV fluence for 2-logI and 3-logI between the laser-based and LB-CB irradiations of less than 20%, as detailed in Table 16. While these differences may seem higher compared to those presented in chapter 2.2.1 for *Bacillus subtilis* spores, the MS2 results meet the criteria within the measurement uncertainties. Thus two conclusions can be drawn: firstly, the laser-based system exhibited consistent stability throughout the experiments, and secondly, the outcomes were comparable to those obtained from the low-pressure collimated beam apparatus.

Table 16: UV dose-response results of MS2 phage for the wavelengths 254 nm with the laser-based setup and 253.7 nm with the LP CB for 2- and 3-log inactivation and the regression parameters A and B defining the dose-response curve using Equation 12.

Wavelength in nm	**H_{UV} in J/m² needed for (± 95 % PI*)**		**A in m²/J**	**B in m⁴/J²**
	2-logI	**3-logI**		
254 nm laser	310 ± 89	508 ± 112	7.285E-3	-2.719E-6
253.7 nm LP CB	365 ± 130	624 ± 206	6.426E-3	-2.590E-6

*highest values was taken

According to literature data for LP-CB at 253.7 nm [Malayeri, Mohensi, & Bolton, 2016], the dose-response curves of MS2 phage can exhibit significant variability, with an average UV fluence of 362 J/m² and a standard deviation of ± 84 J/m² for 2-log-inactivation, and an average UV fluence of

567 J/m² with a standard deviation of ± 134 J/m². The data from this thesis, both the 254 nm laser-based and LP-CB, demonstrated a good alignment with the literature data.

2.3.2. Dose-response curves with the different wavelengths from the laser-based setup

Figure 13 displays the results obtained at various wavelengths using the tunable laser. The R^2 values consistently exceed 0.980 except for the 280 nm data, and the interpolation uncertainty (according to Equation 10) varies between 0.31 and 0.85, averaging at 0.45. The 280 nm data exhibited the highest uncertainty of interpolation, primarily attributed to the variability in the results.

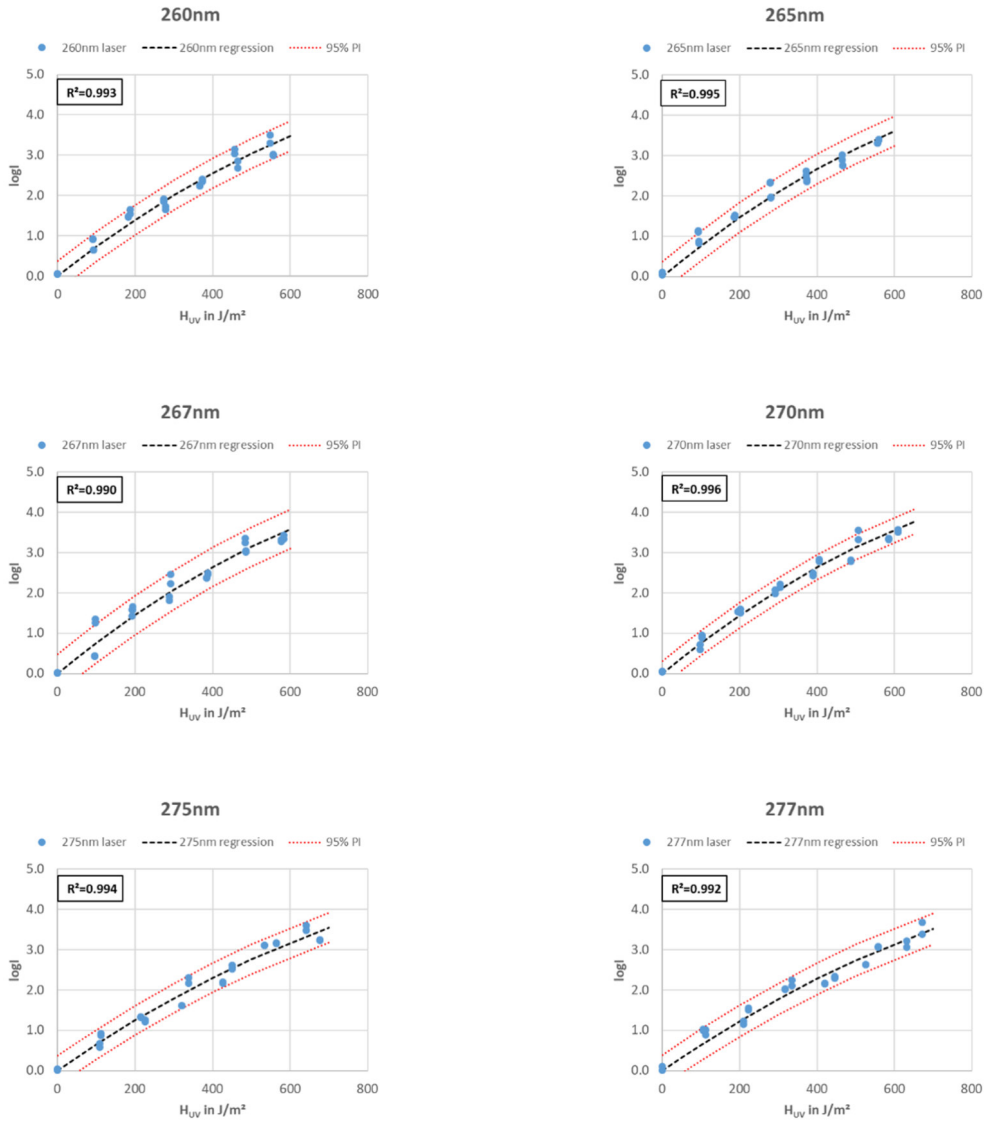

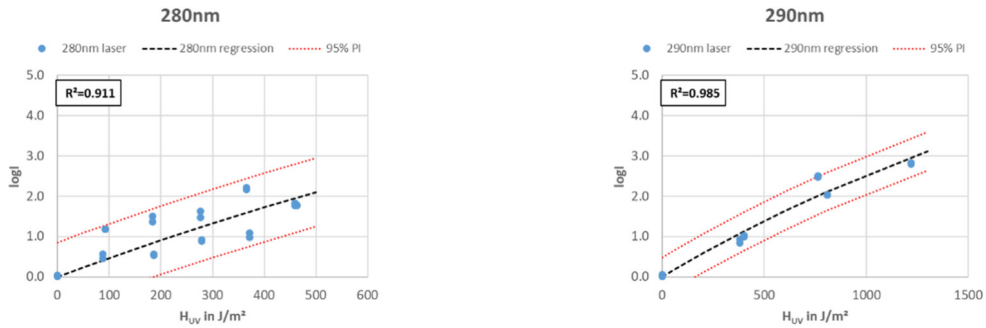

Figure 27: Dose-response curve of MS2 phage to wavelength specific UV light from tunable laser. The blue circles represent the combined data of the specific wavelength with the resulting regression curve (black dashed line). The red dotted lines define the 95th percentile prediction. Note different x-axis values.

The focus of the MS2 phage irradiation was on the comparison with literature data, namely the action spectrum determined by Beck et al. (2015). Figure 28 shows the data from Beck et al. (2015) and the action spectrum values from this thesis in one graph.

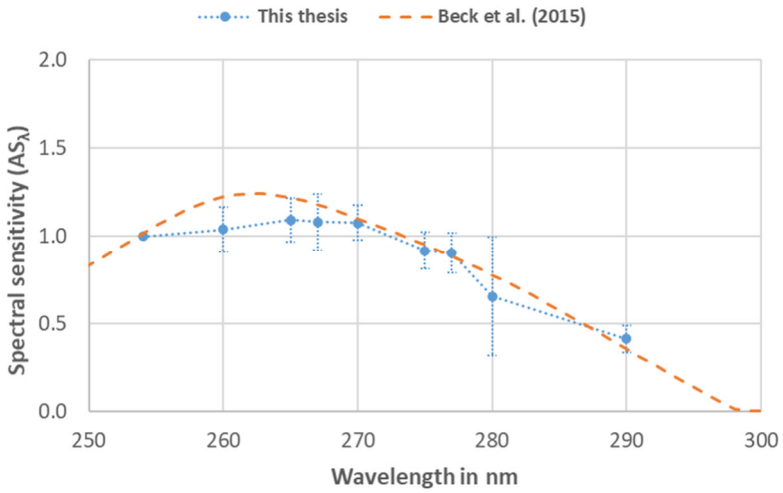

Figure 28: Action spectra values of MS2 phage from this thesis (blue circles with dotted line) compared to data from Beck et al. (2015) (orange dashed line).

Overall, the data from this thesis align well with the findings from Beck et al. (2015), providing additional evidence for the quality and reproducibility of this work. The detailed MS2 action spectrum values from this thesis, compared with Beck et al. (2015), are listed in Table 17. Apart from the 260 nm action spectrum value, which deviates by 0.19, all discrepancies fall within the measurement uncertainty of this thesis. Additionally, considering a reasonably estimated measurement uncertainty of the work from Beck et al. (2015) with U_{IN} = 0.15, the 260 nm value would already fall within the measurement uncertainties.

Table 17: Action spectra values (AS_λ) for MS2 from this thesis and from Beck et al. (2015) and verification if the differences of the action spectra values lie within the standard deviations (SD).

Wavelength in nm	**This study $AS_\lambda \pm SD$**	**Beck et al. (2015) AS_λ**	**Delta within SD?**
254	1.00	1.00	-
260	1.04 ± 0.13	1.22	No
265	1.09 ± 0.13	1.22	Yes
267	1.08 ± 0.16	1.18*	Yes
270	1.08 ± 0.10	1.10	Yes
275	0.92 ± 0.11	0.95*	Yes
277	0.90 ± 0.11	0.89*	Yes
280	0.66 ± 0.34	0.78	Yes
290	0.41 ±0.08	0.36	Yes

*data interpolated by Beck et al. 2015

3. Importance of a state-of-the-art *Bacillus subtilis* spores action spectrum on polychromatic UV system validation

To effectively validate polychromatic UV systems, an ideal surrogate should either demonstrate wavelength independence, ensuring consistent efficiency across the relevant wavelength spectrum, or exhibit the same wavelength dependence as the target pathogen. This characteristic minimizes measurement uncertainties during biodosimetry and enhances resilience against variations in UV source characteristics, particularly pertinent for LEDs. Recent findings have highlighted significant disparities between manufacturer specifications and actual measurements, as well as substantial variability among LEDs of the same type in terms of wavelength and UV output. For instance, recent data from the Ferdinand-Braun-Institut (FBH) [Einfeldt, 2022] vividly illustrate these challenges. In Figure 29, the various colors represent LED types from five distinct manufacturers, with hatched regions indicating the peak-wavelength and UV output specifications provided by the manufacturers. The circles of corresponding colors represent measured data from FBH.

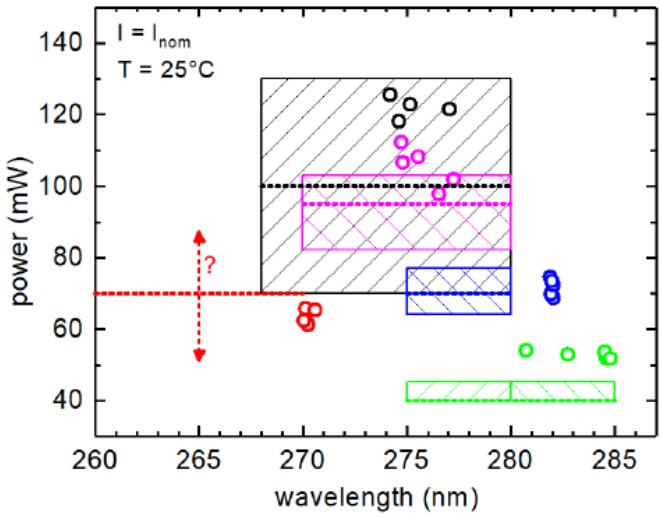

Figure 29: Wavelength and UV output (power) range for various LED types given in the data sheets from five different manufacturers (hatched areas with different colors) and measured data points from these LEDs (circles with different colors). The data was measured by Ferdinand-Braun-Institut [Einfeldt, 2022].

The graph also indicates that, according to the manufacturer's data sheets, LEDs with a specific peak wavelength can vary by ±5 nm. These tolerances can lead to a worst-case scenario that could compromise future safe operation. For instance, conducting biodosimetry of a LED UV system with a nominal LED peak wavelength of 275 nm, while operating the system with LEDs emitting at 280 nm where the germicidal efficacy is already decreasing for most microbes, could lead to an overestimation of the system's disinfection performance during operation.

To illustrate this effect, the ASCFs of MS2 phage and *Bacillus subtilis* spores were calculated based on LED emission spectra ranging from 250 nm to 290 nm. The LED spectra were simulated using data from a 270 nm LED measured at TZW, with a FWHM of 12 nm, and then adjusted to the corresponding

peak wavelength in 1 nm increments within the specified range. Some of these emission spectra are displayed in Figure 30 on the left graph. These emission spectra, along with the action spectra, were used to calculate ASCFs for MS2 and *Bacillus subtilis* spores using Equation 3, resulting in the data shown on the right graph in Figure 30.

It is observed that the FWHM of the LEDs flattens the curves compared to the original action spectra data. Consequently, the distinct efficacy of the 270 nm single wavelength for *Bacillus subtilis* is reduced, and the structure between 270 nm and 280 nm is eliminated. However, the steep dropping slope in the action spectrum above 270 nm for *Bacillus subtilis* spores cannot be averaged out with the FWHM of the LEDs. This is significant considering that UV LEDs above 270 nm are already available on the market, and the tolerances of LED peak wavelengths are not smaller than ±5 nm. In contrast, the MS2 spectrum appears smoother and less susceptible to variations in LED emission spectra.

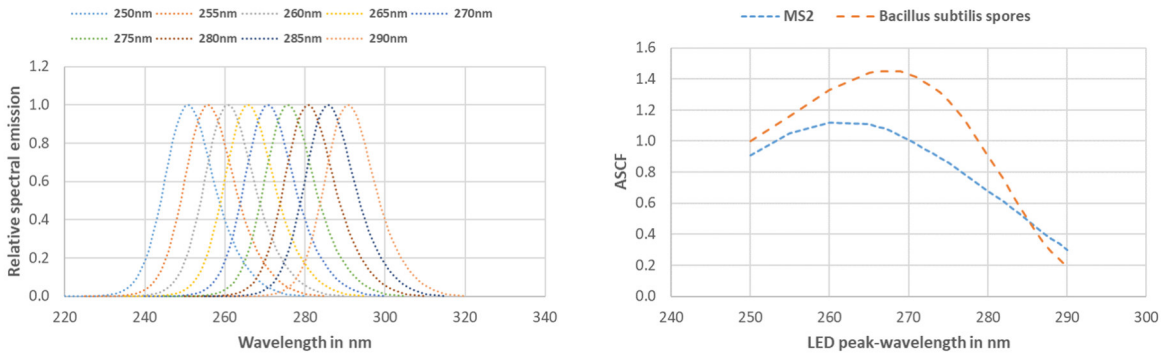

Figure 30: Left graph: Simulated LED emission spectra. Right graph: ASCFs for MS2 phage and Bacillus subtilis *spores depending on the peak-wavelength of the LEDs.*

However, the curves in the right graph of Figure 30 can be somewhat deceptive. Validating a system with 270 nm and then operating it with 280 nm would result in a significant decrease in the REF, without even considering the effects of hydraulics and fluence distribution. This decrease is similar for both MS2, at 23 %, and *Bacillus subtilis* spores, at 26 %. The situation becomes even more pronounced when a system is validated with 280 nm LEDs but then operated with 285 nm or 290 nm LEDs, leading to decreases in the REF of 28 % and 56 % for MS2, and 45 % and 79 % for Bacillus subtilis spores, respectively.

In conclusion, the action spectrum of *Bacillus subtilis* spores, determined in Chapter 2, displays a unique structure with exceptionally high resolution between 260 nm and 280 nm, featuring a significant peak at 270 nm. This unique feature contrasts sharply with other commonly used surrogates for UV system validation, such as MS2 phage, T1UV phage, and *Bacillus pumilus* spores. As shown in Figure 31, based on data from Beck et al. (2015), none of the other surrogates exhibit such a pronounced peak or steep slope above 280 nm. Given the use of LEDs with wavelengths of 280 nm or greater, it is not recommended to continue using *Bacillus subtilis* spores as surrogates in future DIN standards for UV system

validation with polychromatic UV sources, as this increases uncertainties beyond acceptable thresholds in the biodosimetric process. Overall, MS2 appears to be the most robust surrogate across a broad wavelength range. However, even when using MS2, it is advisable to include a factor to account for LED peak-wavelength tolerances with regards to the MS2 action spectrum.

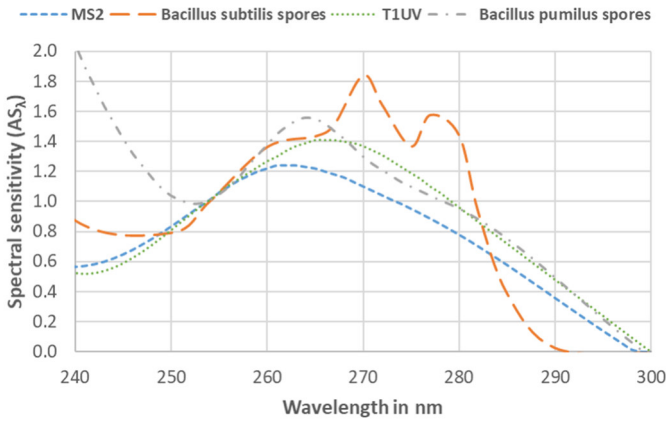

Figure 31: Action spectra values of Bacillus subtilis *spores (orange long dashed line) from this thesis and of MS2 (blue dashed line), T1UV (green dotted line) and* Bacillus pumilus *spores (grey dash-dot line) from Beck et al. (2015).*

4. Verification of the combined variable approach using COMSOL Multiphysics®

To demonstrate that the combined variable approach for full scale biodosimetry is theoretically viable and to show that simulated logI data can be fitted against the core equation of the combined variable approach (refer to Equation 4) a simplified sandbox model of a UV system was constructed in COMSOL Multiphysics® (version 5.4). COMSOL Multiphysics® is a versatile software platform designed for simulating and modeling physical phenomena across various engineering and scientific disciplines. It enables the creation of detailed and intricate multiphysics simulations by integrating modules for various physics domains, such as fluid dynamics, heat transfer, structural mechanics, electromagnetics, and more.

For this model the following physics were used:

- **"Turbulent flow"** for single-phase flow within the "fluid flow" module
- **"Geometrical optics"** within the "optics" module
- **"Particle tracing"** within the "fluid flow" module

The coupling of these three physics modules was carried out in the following sequence: First, the fluid velocity within the UV system was determined using the turbulent flow interface. Next, the volumetric fluence rate along rays emitted from the UV lamp's surface was calculated using the geometrical optics interface. Finally, particles were tracked along the fluid velocity streamlines, and the fluence rate along these particle trajectories was integrated. This process produced a fluence distribution file, which provided the physical fluence for each particle as it moved through the UV system. Afterwards, the fluence distribution files were exported to Excel to apply specific UV dose-response curves for various microbes in order to calculate microbe specific REFs.

4.1. Design of the UV system model

The model design is depicted in Figure 32. The UV system's vessel is 1 m long with a diameter of 0.1 m. Within the vessel, a UV source, 0.5 m in length and 0.02 m in diameter, is positioned at the center without any protective quartz sleeve for the sake of model simplicity.

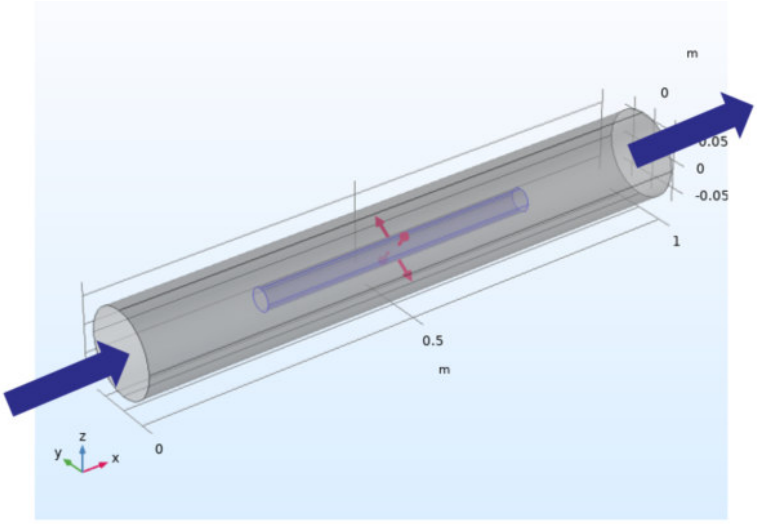

Figure 32: Model of the UV system used within COMSOL Multiphysics®. The blue arrows symbolize the direction of flow, the red arrows indicate the emission of the UV source.

4.1.1. Boundary conditions and input parameters of the model

As the **hydraulic model,** a Reynolds-Averaged Navier-Stokes (RANS) based realizable *k-ε* turbulence model was used, as applied by Ho et al. (2011) for the modeling of UV systems. The flow regime was defined by the Reynolds number, calculated using Equation 17. In fluid mechanics and hydrodynamics, the Reynolds number is utilized as a dimensionless quantity to characterize the transition between laminar and turbulent flow. The Reynolds number (Re) is defined as the ratio of inertial forces to viscous forces.

$$Re = \frac{v_m \cdot d}{\nu} \tag{17}$$

With:

Re	Reynolds number, unit less
v_m	Average velocity across the cross-section of the vessel, in m/s
d	Inner diameter of the vessel, in m
ν	Viscosity of the fluid, in m²/s

For UV systems, the Reynolds number typically falls within the turbulent regime, generally assumed to occur at Re > 2300 [Fox, McDonald, & Pritchard, 2011]. The flow rate was the primary input parameter for the hydraulic model, entered at the effluent side of the UV system, as shown in Figure 32. The solution was computed for stationary fluid flow, meaning that the simulated results at a specific time point are representative of the entire simulation period.

To model the turbulent flow within the UV system, the Reynolds-Averaged Navier-Stokes (RANS) equations were employed, using the realizable *k-ε* model [Shih, Liou, Shabbir, Yang, & Zhu, 1995]. The Navier-Stokes equations form the foundation of fluid dynamics, providing a comprehensive description of how the velocity field and pressure in a fluid evolve over time. These equations encompass the conservation laws for mass, momentum, and energy [Geiser, 2018]. In the case of incompressible fluids, such as water, the Navier-Stokes equations are simplified due to the absence of density variations along flow trajectories. Thus, the equations reduce to the continuity equation and the momentum equation, which are expressed as follows [Geiser, 2018]:

- **Continuity Equation:**

$$\nabla \cdot \mathbf{u} = 0 \tag{18}$$

This equation ensures mass conservation by stating that the divergence of the velocity field **u** is zero.

- **Momentum equation:**

$$\rho\left(\frac{\partial \mathbf{u}}{\partial t} + \mathbf{u} \cdot \nabla \mathbf{u}\right) = -\nabla p + \mu \nabla^2 \mathbf{u} + \mathbf{f} \tag{19}$$

This equation describes the conservation of momentum in a fluid. It accounts for forces acting towards the fluid, including pressure gradients, viscous forces, and external forces [White, 2011].

With:

$\nabla \cdot \mathbf{u}$	Divergence of the velocity field, in s^{-1}
ρ	Fluid density, in kg/m^3
$\partial \mathbf{u}/\partial \mathbf{t}$	Time derivative of the velocity field, in m/s^2
$\mathbf{u}\nabla \cdot \mathbf{u}$	Convective term, in m^2/s^3
∇p	Pressure gradient, in Pa/m
μ	Dynamic viscosity, in Pa·s
$\nabla^2 \mathbf{u}$	Laplacian of the velocity field, in $s^{-1} \cdot m^{-1}$
$\mathbf{f}$	Body forces such as gravity, in N/m^3

Directly solving the equations for turbulent flows is often impractical due to the complexity and scale of turbulence. Therefore, the Reynolds-Averaged Navier-Stokes (RANS) approach is employed to average the equations over time, focusing on mean flow characteristics while modeling the effects of turbulence through additional terms [Wilcox, 2006; Schwarze, 2013]. The standard *k-ε* model is the most commonly used turbulence model for Computational Fluid Dynamics (CFD) simulations [Schwarze, 2013]. The realizable *k-ε* model, however, provides improvements over the standard version, particularly in accurately modeling complex flow features such as rotational effects, flow separation, and recirculation. These enhancements lead to more accurate predictions in challenging flow conditions [Shih, Liou, Shabbir, Yang, & Zhu, 1995].

The standard *k-ε* model relies on two primary variables [Wilcox, 2006]:

1. **Turbulent kinetic energy (*k*):** This variable represents the energy generated by turbulence within the fluid, quantifying the intensity of the turbulence.
2. **Dissipation rate (ε):** This rate measures how quickly turbulent kinetic energy is converted into heat, indicating the rate at which turbulence dissipates.

The framework of the standard *k-ε* model is generally applicable to the realizable *k-ε* model as well, with some modifications. These include changes to certain model constants, which may be adjusted or replaced by functional relationships [Schwarze, 2013]. A detailed description of the equations and model constants used in COMSOL Multiphysics® can be found in Appendix D.

In the **optics model**, ray tracing was employed to delineate the UV intensity distribution within the UV system. The UV source emits radiation as a Lambertian source. The Lambertian radiation characteristic is an idealized model that describes the intensity of emitted radiation from a source as being proportional to the cosine of the angle between the emission direction and the surface normal [Smith W. J., 2000]. This relationship is mathematically represented as:

$$\mathrm{I}(\theta) = I_0 \cos(\theta) \tag{20}$$

With:

$\mathrm{I}(\theta)$	Radiation intensity at an angle θ from the normal, in a.u.
I_0	Maximum intensity

This equation indicates that the intensity decreases as the angle θ increases, resulting in a uniform distribution over a hemisphere.

To maintain simplicity in the calculations, the UV source was defined as monochromatic, with emission solely at 254 nm. The computation of the volumetric fluence rate within individual mesh elements results in a UV intensity distribution throughout the UV system, as illustrated in Figure 33. The UV intensity distribution within the UV system is influenced by the UVT of the water and the power of the UV lamp, both serving as input parameters. The UVT of the water is incorporated through the imaginary part of the refractive index, addressing absorption effects.

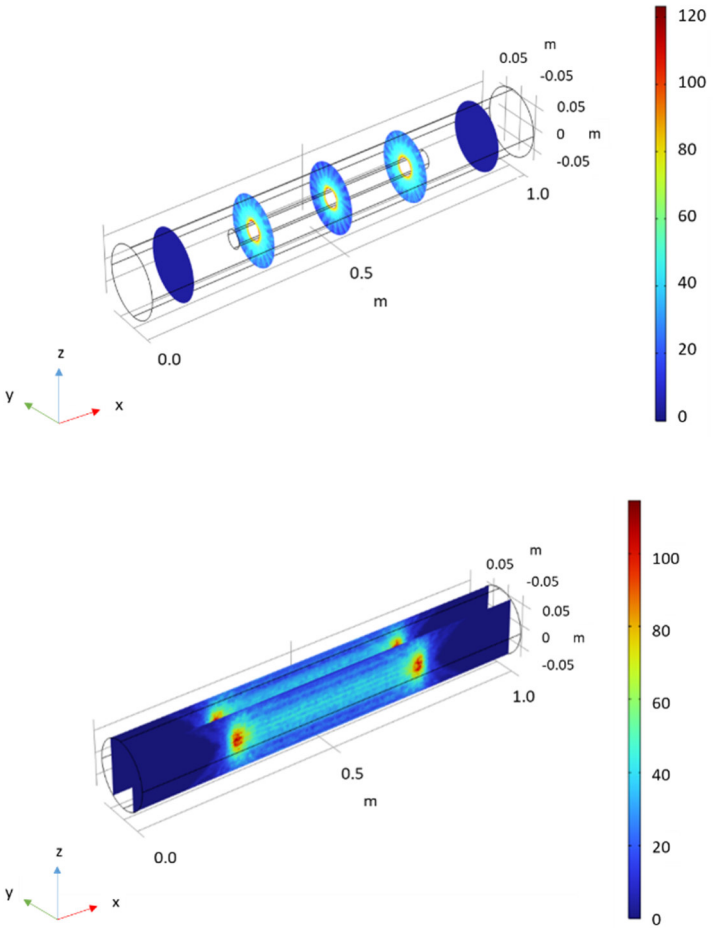

Figure 33: Exemplarily UV intensity distribution within the UV system model, in W/m², in y-z plane (top graph) and x-z plane (bottom graph).

COMSOL employs Lagrangian **particle tracing** as a numerical method to simulate the movement and behavior of discrete particles within a fluid flow. In this approach, particles are treated as Lagrangian entities, and their individual trajectories are tracked as they move through the fluid [Ferziger & Perić, 2002]. The equations of motion for each particle are solved based on the local fluid velocity field. These particles, representing microbes, are subjected to drag forces that account for flow resistance according to the velocity field, which is determined by the solution of the hydraulic model and governed by the same underlying equations. A total of 2000 microbes were introduced at the influent side. As they reached the effluent of the UV system model, the UV fluence for each microbe was recorded, resulting in the creation of a fluence distribution file.

4.1.2.Simulated data set

A total of 28 conditions were simulated, encompassing variations in the parameters UVT, flow rate, and UV lamp output power (P). Table 18 provides a summary of these 28 conditions, including the corresponding Reynolds number. It is noteworthy that the Reynolds number consistently falls within the

turbulent regime. For scenarios with identical water flow rates, flow simulations were conducted only once. However, for variations in UVT and UV lamp power, subsequent reruns were performed for both geometrical optics and particle tracing.

Table 18: UVT, water flow (Q), UV output (P) and corresponding Reynolds number for the 28 simulated conditions with the UV system model.

ID	UVT in %	Q in m^3/h	P in W	Re
1	98	10.0	100	23485
2	98	5.00	50.0	11742
3	98	5.00	10.0	11742
4	98	2.50	5.00	5871
5	98	250	500	587114
6	98	250	250	587114
7	98	250	350	587114
8	98	250	2500	587114
9	80	10.0	100	23485
10	80	5.00	50.0	11742
11	80	250	2500	587114
12	80	250	1000	587114
13	80	250	1750	587114
14	80	2.50	17.5	5871
15	90	2.50	17.5	5871
16	90	2.50	5.00	5871
17	90	25.0	50.0	58711
18	90	25.0	100	58711
19	90	250	1000	587114
20	60	100	1000	234846
21	60	100	5000	234846
22	60	10.0	500	23485
23	50	100	5000	234846
24	50	100	10000	234846
25	50	10.0	1000	23485
26	50	2.00	200	4697
27	50	250	25000	587114
28	40	100	10000	234846

Each condition produces a distinctive fluence distribution. Notably, conditions with the same UVT and an identical ratio of UV lamp power to water flow rate exhibit nearly identical fluence distributions leading to the same logI value as defined by Equation 4. The logI value remains unchanged, provided the ratio of the lamp power, typically represented by the S/S_0 term, to water flow rate remains constant within the combined variable term. This similarity is exemplified in Figure 34 for condition IDs 4 and 5, where the fluence distributions files are displayed graphically. This initial step serves as evidence supporting the theory of the combined variable, without yet incorporating the UV sensitivity of the microbes.

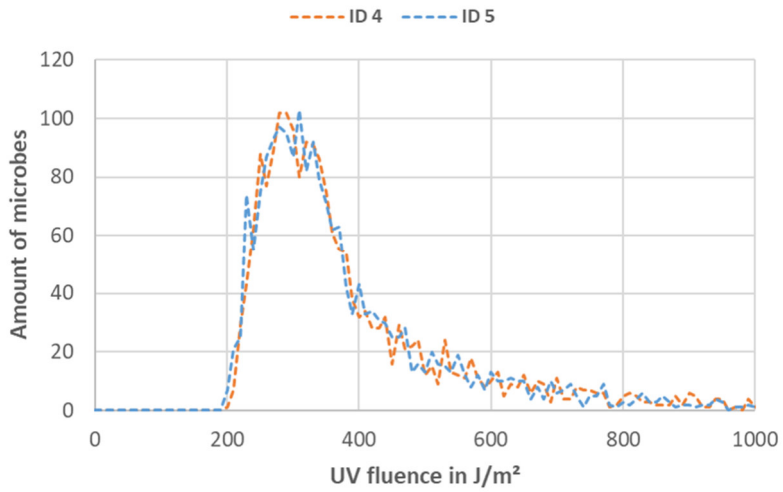

Figure 34: Fluence distributions for ID conditions 4 (UVT of 98 %, Q of 2.5 m³/h, P of 5.0 W) and 5 (UVT of 98 %, Q of 250 m³/h, P of 500 W).

From the 28 fluence distributions, a corresponding logI can be calculated for various microbes, provided that dose-response curves are available. In this demonstration of the combined variable approach, four commonly used surrogate microbes were employed for the calculations: *Bacillus subtilis* spores, MS2 phage, T1UV phage, and Qß phage. The LP-CB dose-response curves for these surrogates are depicted in Figure 35. These are unpublished data from past validations conducted at TZW. While *Bacillus subtilis* spores and MS2 phage exhibit a similar UV sensitivity of approximately 200 J/m² per logI, over a wide range of doses, the dose-response curve of *Bacillus subtilis* spores displays a notable distinction, specifically a shoulder behavior until UV fluences of around 100 J/m² (depending on the batch). T1UV phage shows the lowest DL-value with approximately 50 J/m² per logI, followed by Qß phage with an average DL-value of approximately 100 J/m². The three phage surrogates exhibit a polynomial (MS2- and Qß phage) or linear (T1UV phage) dose-response behavior.

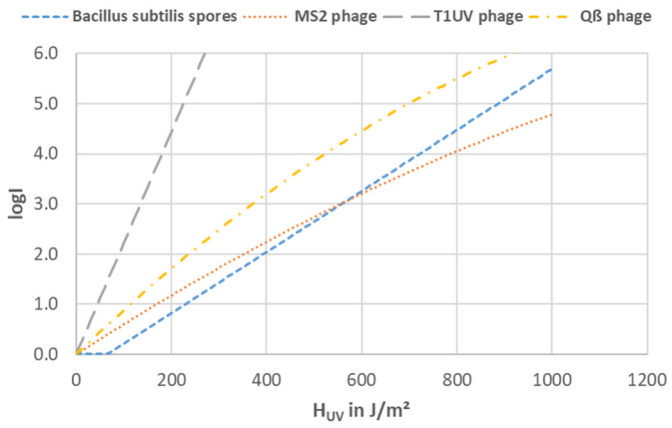

Figure 35: UV dose-response curves of Bacillus subtilis *spores (blue dashed line), MS2 phage (orange dotted line), T1UV phage (grey long dashed line) and Qß phage (yellow dash-dot line) [unpublished data from TZW].*

The parameters utilized for the calculation with these surrogates are outlined in Table 19 (unpublished data from past validations conducted at TZW). Equation 8 was applied for the calculation of *Bacillus subtilis* spores, while Equation 12 was employed for the phages.

Table 19: Parameters of the LP-CB dose-response curves for Bacillus subtilis *spores, MS2, T1UV and Qß phage used for modeling calculations [unpublished data from TZW].*

Parameter	***Bacillus subtilis* spores**	**MS2 phage**	**T1UV phage**	**Qß phage**
A*	-3.945E-1	6.157E-3	2.225E-2	9.139E-3
B**	6.088E-3	-1.363E-6	-	-2.834E-6

*in m^2/J for phage, without unit for *Bacillus subtilis* spores

**in m^4/J^2 for phage, in m^2/J for *Bacillus subtilis* spores

Utilizing four different microbes for every fluence distribution led to a total of 112 logI data points. The process to obtain specific logI values for each fluence distribution file involved the following steps:

- The 2000 ($N_{0,\,total}$) particle UV fluences were categorized in a total of 500 classes, ranging from 0 J/m² to 5000 J/m² in increments of 10 J/m², resulting in the amount of particles ($N_{0,\,i}$) per class, as partially shown in Table 20.
- Calculating the logI for each corresponding UV fluence class for each microbe. The logI calculation uses the higher UV fluence value in the interval. The logI values were calculated straight forward over the whole fluence range, without taking into account tailing at higher UV doses.
- Determination of the total amount of non-inactivated particles (N_{total}) with the following equation:

$$N_{total} = \sum_{i=1}^{500} 10^{(logN_{0,i} - logI_i)} \quad (21)$$

With:

N_{total}	Total amount of non-inactivated particles, unit less
$logN_{0,i}$	Log of the amount of particles per UV fluence class, unit less
$logI_i$	Log inactivation corresponding to the highest UV fluence values in the specific UV fluence class interval, unit less

- Calculating the overall $logI_{total}$ for the specific surrogate with the following Equation:

$$logI_{total} = \log\left(\frac{N_{0,total}}{N_{total}}\right) \quad (22)$$

With:

$logI_{total}$	Final logI value of the fluence distribution for the specific surrogate
N_{total}	Total amount of non-inactivated particles, unit less
$N_{0,total}$	Total amount of particles traversing through the UV system model

Table 20: Extract of a fluence distribution file categorized in: UV fluence classes, UV fluence range, corresponding amount of particles, Bacillus subtilis *spores logI for the specific UV fluence class, and resulting particle count after inactivation (N_i).*

UV fluence class	UV fluence range in J/m²	$N_{0,i}$	$\log N_{0,i}$	$\log I_i$	N_i
1	0	0	0.00	0.00	0.00
…	…	…			
18	161 - 170	0	0.00	0.64	0.00
19	171 - 180	0	0.00	0.70	0.00
20	181 - 190	0	0.00	0.76	0.00
21	191 - 200	1	0.00	0.82	0.00
22	201 - 210	7	0.85	0.88	0.91
23	211 - 220	29	1.46	0.94	3.29
24	221 - 230	43	1.63	1.01	4.24
25	231 - 240	62	1.79	1.07	5.32
26	241 - 250	88	1.94	1.13	6.56
27	251 - 260	77	1.89	1.19	4.99
28	261 - 270	89	1.95	1.25	5.01
29	271 - 280	102	2.01	1.31	5.00
30	281 - 290	102	2.01	1.37	4.34
31	291 - 300	96	1.98	1.43	3.55
32	301 - 310	80	1.90	1.49	2.57
33	311 - 320	92	1.96	1.55	2.57
34	321 - 330	91	1.96	1.61	2.21
35	331 - 340	86	1.93	1.68	1.82
36	341 - 350	75	1.88	1.74	1.38
37	351 - 360	61	1.79	1.80	0.97
…	…	…			
500	4991 – 5000	0	0.00	29.98	0.00

4.1.3. Analysis of the simulated data set

Because the simulated data lacked UV sensor values, adjustments to Equation 4 were made, which predicts logI based on UVT and the combined variable. In this modification, the S/S_0 term, representing UV output from irradiance values of a UV sensor, was substituted with P/P_0, where P/P_0 corresponds to

the actual UV output values entered into the model. The reference UV output, denoted as P_0, was standardized to 100 W, and the UV output values for the 28 conditions are detailed in Table 18. At this point an index for the coefficients A' and B' is introduced to enhance clarity within the following datasets. The objective of this analysis is to develop an equation based on Equation 4 that can predict the simulated logI values and allow for interpolation of the dataset without requiring additional simulated data.

$$logI_{sim} = A_1' \cdot {\vartheta_C}^{B_1'} = A_1' \cdot (\frac{\boldsymbol{P}/\boldsymbol{P_0} \cdot \omega}{Q \cdot D_L})^{B_1'} \quad (23)$$

With:

$logI_{sim}$	Simulated log inactivation of the surrogates, unitless
A_1' and B_1'	Empirical coefficients as a function of the UVT, unitless
ϑ_c	The combined variable
P	UV output entered into the model, in W
P_0	Reference UV output defined as 100 W
Q	Water flow through the UV system, in m^3/h
D_L	UV sensitivity of the surrogates, in J/m^2 per logI
ω	Unit correction factor, in m·J/h

To apply Equation 23 to the simulated data set, the only remaining parameter to be determined is D_L. The D_L of a microbe is the microbe-specific REF required to achieve a certain logI. This parameter can be described using Equation 24.

$$D_L = \frac{REF}{logI_{sim}} \quad (24)$$

With

REF	Reduction equivalent fluence of the surrogate, in J/m²

Prior to obtaining D_L, an intermediate step is essential, involving the computation of REF based on the simulated logI data for each surrogate, considering their specific dose-response parameters (refer to Table 19). For *Bacillus subtilis* spores, modifying and solving Equation 8 for REF yields Equation 25. In the case of MS2 and Qß phage, Equation 12 is modified and resolved using the quadratic formula, resulting in Equation 26. The linear dose-response curve of T1UV allows the calculation of REF through Equation 27.

$$REF = \frac{logI_{sim} - A_{B.sub.}}{B_{B.sub.}} \tag{25}$$

With:

$A_{B.sub.}$ and $B_{B.sub.}$	Regression parameters defining the UV dose-response of *Bacillus subtilis* spores as defined in Table 19, $A_{B.sub.}$ unit less and $B_{B.sub.}$ in m²/J

$$REF = \frac{-A_{MS2/Q\beta} + \sqrt{A_{MS2/Q\beta}^2 + 4 * B_{MS2/Q\beta} \cdot logI_{sim}}}{2 \cdot B_{MS2/Q\beta}} \tag{26}$$

With:

$A_{MS2/Q\beta}$ and $B_{MS2/Q\beta}$	Regression parameters defining the UV dose-response of MS2 and Qß as defined in Table 19, $A_{MS2/Q\beta}$ in m²/J and $B_{MS2/Q\beta}$ in m⁴/J²

$$REF = \frac{logI_{sim}}{A_{T1UV}} \tag{27}$$

With:

A_{T1UV}	Regression parameter defining the UV dose-response of T1UV as defined in Table 19, A_{T1UV} in m²/J

Finally the calculated REF values for each of the 112 conditions can be entered into Equation 24 to calculate D_L for the specific surrogate.

Utilizing Equation 23 with the entire simulation dataset comprising 112 conditions results in logI vs. combined variable values correlations for various UVTs, as illustrated in Figure 36. To enhance clarity, the data is divided into two graphs. Each UVT dataset exhibits a power function correlation, as defined by the combined variable in Equation 23, with an R^2 exceeding 0.992, demonstrating the robustness of this correlation.

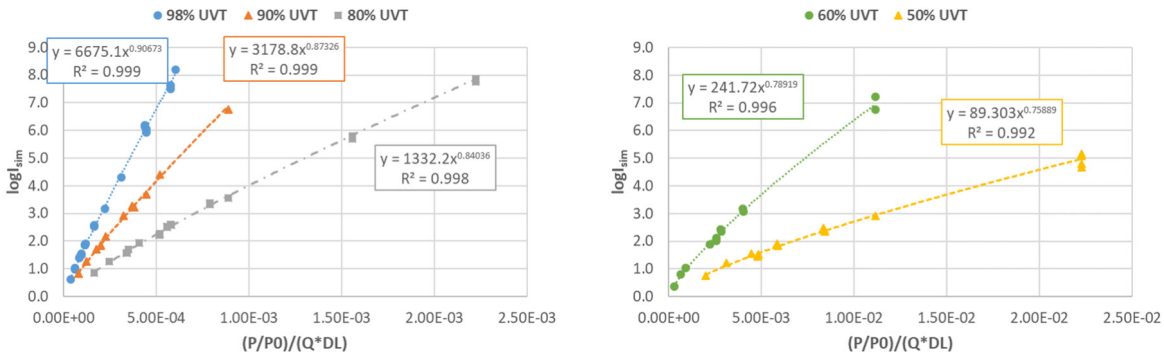

Figure 36: LogI of the simulated data depending on the combined variable. Left graph: UVTs of 98 % (blue circles and dotted line), 90 % (orange triangles and dashed line) and 80 % (grey squares and dash-dot line). Right graph: UVTs of 60 % (green circles and dotted line) and 50 % (yellow triangles and dashed line). Note different axis values.

The subsequent step involved establishing the correlation between A_1' and B_1' from Equation 23 with UVT. To enhance the fitting accuracy in the final analysis, it is advisable [EPA (United States Environmental Protection Agency), 2020] to convert the UVT values to UV absorption (UVA). This conversion can be achieved using Equation 28.

$$UVA = \log\left(\frac{UVT/_{100\%}}{-0.01m}\right) \tag{28}$$

With:

UVA	UV absorbance of the water, in m^{-1}
UVT	UV transmittance of the water for 1 cm, in %

Figure 37 depicts the relationship between A_1' and B_1' with respect to UVA. The values for A_1' and B_1' for each UVT can be extracted from the formulas presented in Figure 36.

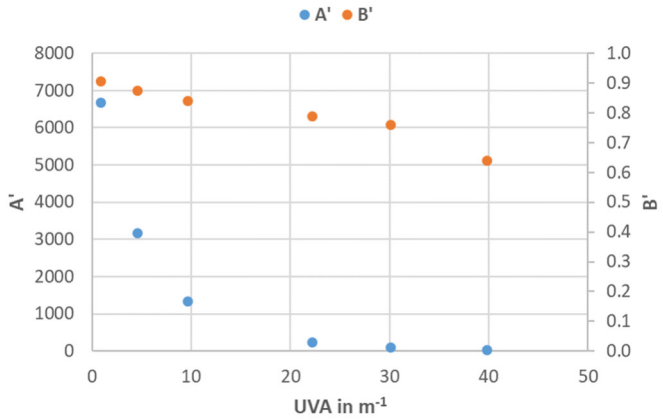

Figure 37: Dependence of the coefficients A' and B' based on the simulated data set for the UV system model.

The correlation for A_1' can be expressed by Equation 29, while Equation 30 describes the correlation for B_1'.

$$A_1' = a_1 \cdot b_1^{UVA} \cdot UVA^{c_1} \tag{29}$$

$$B_1' = d_1 + e_1 \cdot UVA + f_1 \cdot UVA^2 + g_1 \cdot UVA^3 \tag{30}$$

This results in the following algorithm (refer to Equation 31) for predicting logI using the combined variable approach, achieved by incorporating Equations 29 and 30 into Equation 23:

$$logI_{sim} = a_1 \cdot b_1^{UVA \cdot x_1} \cdot UVA^{c_1} \cdot x_1 \cdot \left(\frac{P/P_0 \cdot \omega}{Q \cdot D_L}\right)^{(d_1 + e_1 \cdot UVA \cdot x_1 + f_1 \cdot UVA^2 \cdot x_2 + g_1 \cdot UVA^3 \cdot x_3)} \tag{31}$$

With

a_1, b_1, c_1, d_1, e_1, f_1, g_1	Empirical coefficients
x_1	Unit correction factor, in m
x_2	Unit correction factor, in m²
x_3	Unit correction factor, in m³

The model data was fitted to Equation 31 through the following steps:

1. Using multivariate linear regression by fitting the model data to the linear form of Equation 31, yielding in Equation 32:

$$\log(logI_{sim}) = a_1 + UVA \cdot x_1 \cdot \log(b_1) + c_1 \cdot \log(UVA \cdot x_1) + d_1 \cdot \log(\frac{P/P_0 \cdot \omega}{Q \cdot D_L}) + e_1 \cdot UVA \cdot x_1 \cdot \log(\frac{P/P_0 \cdot \omega}{Q \cdot D_L}) + f_1 \cdot UVA^2 \cdot x_2 \cdot \log(\frac{P/P_0 \cdot \omega}{Q \cdot D_L}) + g_1 \cdot UVA^3 \cdot x_2 \cdot \log(\frac{P/P_0 \cdot \omega}{Q \cdot D_L}) \quad (32)$$

   The multivariate linear regression analysis revealed that the coefficients c_1 and f_1 in Equation 32 were not statistically significant at a 95th percent confidence level (p-value < 0.05). In the initial step, the term with the highest p-value (f_1) was excluded. After this adjustment, Step 1 was reiterated, and c_1 was found to be statistically insignificant at a 95th percent confidence level. Consequently, the term with c_1 was removed, and Step 1 was repeated once more. This time, all coefficients exhibited statistical significance at a 95th percent confidence level, resulting in the formulation of Equation 33, where $logI_{pred}$ is used in place of $logI_{sim}$ to predict the $logI_{sim}$ values.

$$logI_{pred} = a_1 \cdot b_1^{UVA \cdot x_1} \cdot (\frac{P/P_0 \cdot \omega}{Q \cdot D_L})^{d_1 + e_1 \cdot UVA \cdot x_1 + g_1 \cdot UVA^3 \cdot x_3} \quad (33)$$

2. Employing non-linear multivariate regression to fit the model data to Equation 33. The coefficients a_1, b_1, d_1, e_1, and g_1 from step 1 served as initial values. The non-linear multivariate regression was constrained to minimize the sum of the squares of the absolute residuals (the difference between simulated $logI_{sim}$ and predicted $logI_{pred}$ using Equation 33.

Table 21 provides the values and the statistical significance (p-value < 0.05) for the coefficients a_1, b_1, d_1, e_1, and g_1.

Table 21: Values for the algorithm coefficients a_1, b_1, d_1, e_1 and g_1 and corresponding p-values.

Empirical coefficients	Value	p-value
a_1	3.764E0	1.69E-120
b_1	-6.244E-2	6.55E-78
d_1	8.766E-1	1.26E-114
e_1	-2.428E-3	9.18E-13
g_1	-2.894E-6	1.27E-27

Figure 38 illustrates the strong correlation between the simulated logI data obtained from the COMSOL Multiphysics® fluence distribution files and the data calculated using the combined variable algorithm from Equation 33. The slope is very close to 1, and the R^2 value is 0.995.

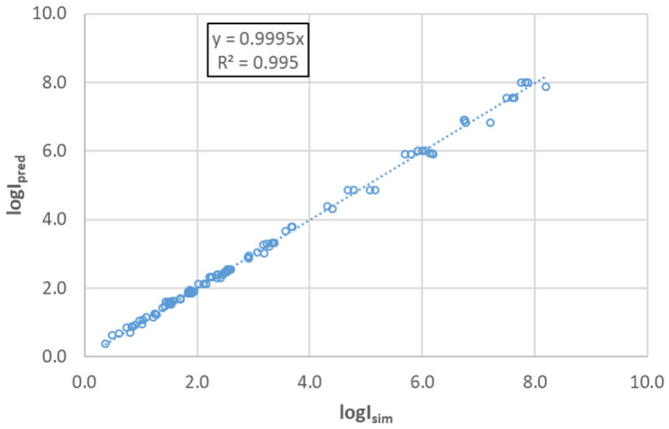

Figure 38: LogI data from the COMSOL Multiphysics® model ($logI_{sim}$) versus the logI data calculated with the combined variable algorithm ($logI_{pred}$).

This data demonstrates that the combined variable approach theoretically performs well with a straight-forward UV system model across a wide spectrum of water flow rates, UVT levels, UV outputs, and logI/REF values.

It is important to note that the modeled UV system assumes homogeneous dose distributions and lacks short-circuits, which could potentially affect the quality of the correlation. In real-life UV systems, short circuits may occur, and their impact is expected, particularly for microbes displaying shoulder behavior in their dose-response curves [Lawryshyn, 2018], as seen, for instance, in the case of *Bacillus subtilis* spores. To visualize this effect, two fluence distribution files from the simulated data were employed and 20 microbes traversing on short circuits were manually inputted. This is exemplified by fluence distribution ID 11 in Figure 39, where a red circle is visible on the right graph.

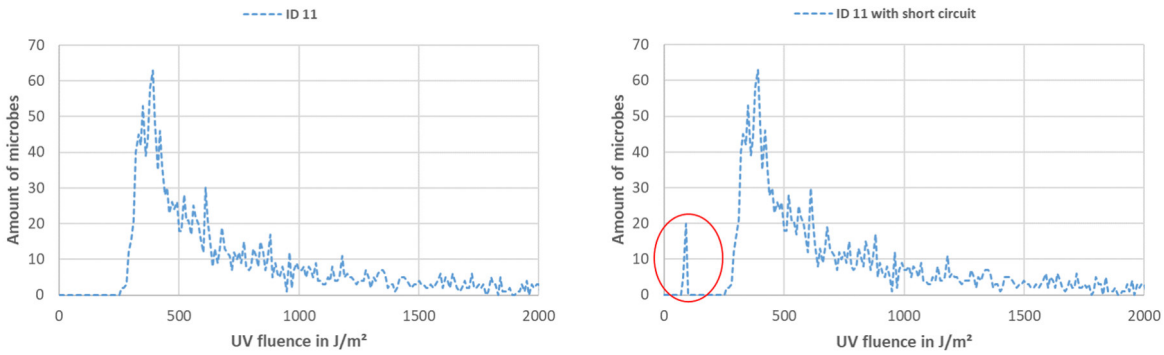

Figure 39: Fluence distribution of condition ID 11 from the simulated data (left graph) and fluence distribution of condition ID 11 with short circuit particles (right graph).

The left graph in Figure 40 shows the correlation of the simulated logI and the combined variable for the data corresponding to ID conditions 11 and 15 (refer to Table 18). This graph highlights the data points of the four surrogates used in the calculation. The results are derived from the original fluence distribution files generated by the COMSOL Multiphysics® model, which exhibit high R^2 values when correlated using a power fit.

In contrast, the right graph in Figure 40 includes data that incorporates manually added short circuit microbes. It is evident that the quality of the correlation diminishes significantly. As indicated by the arrows, this decline can be attributed to the data points of *Bacillus subtilis* spores, which show relatively low logI compared to the "phage curve." This discrepancy arises because the UV fluences of short circuit microbes fall directly into the shoulder range of the *Bacillus subtilis* spores' dose-response curve, resulting in no inactivation of these microbes.

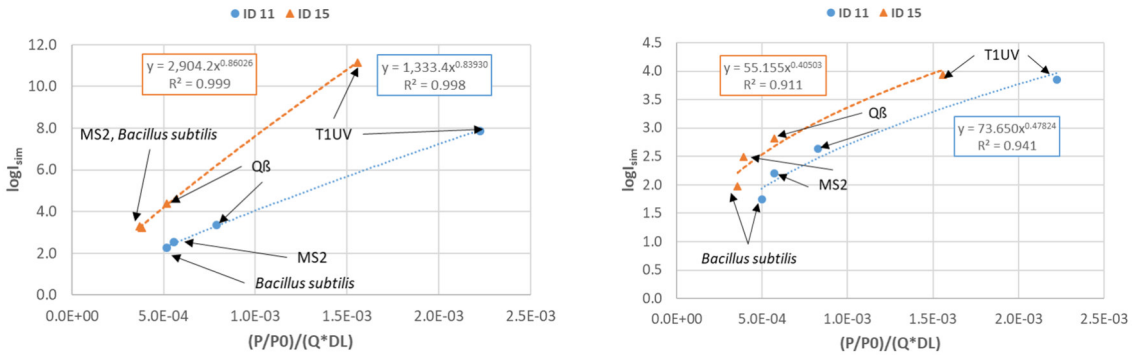

Figure 40: Left graph: $LogI_{sim}$ depending on the combined variable for simulated conditions ID 11 (blue circles and dotted line) and 15 (orange triangles and dashed line) indicating the data points of the four different surrogates. Right graph: $LogI_{sim}$ depending on the combined variable for modeled conditions ID 11 (blue circles and dotted line) and 15 (orange triangles and dashed line) including short circuit particles, indicating the data points of the four different surrogates. Note different y-axis values.

The above observations underscore the importance of considering non-ideal conditions, such as short circuits, in UV system modeling. While the combined variable approach shows promise under ideal

conditions, its applicability in practical scenarios may be limited by factors like short circuits and shoulder behavior of microbes, which are not captured in homogeneous models. Such non-ideal flow patterns can cause portions of the microbial population to receive sublethal doses, particularly for microbes with shoulder effects in their dose-response curves.

Moreover, the choice of microbes used for UV system validation can significantly influence the results. If a system is validated using a mix of microbes with and without shoulder effects, it can lead to greater measurement uncertainties. Microbes with shoulder effects might exhibit varying levels of resistance depending on the fluence distribution, while those without shoulders might respond more predictably. This variability can complicate the interpretation of validation data and ultimately affect the reliability of the UV system's performance assessment.

To provide further evidence supporting the combined variable approach in real-world scenarios, Appendix A includes additional experimental data from a full-scale validation of a medium-pressure UV system. This data demonstrates the practical implementation of the approach and offers guidance on data handling and analysis to ensure proper interpretation of results.

5. Optimized biodosimetric approach with regards to the German drinking water requirements

Unlike the combined variable approach discussed in previous chapter, the traditional method for validating UV systems in Germany has long been known as the UV intensity setpoint approach. This method involves validating the system's operating points using worst-case scenarios to ensure a minimum UV fluence of at least 400 J/m² referring to *Bacillus subtilis* spores [DVGW Deutsche Vereinigung de Gas- und Wasserfaches e.V., 2006; DIN (Deutsches Institut für Normung e.V.), 2020]. What sets this approach apart is its unique philosophy: rather than monitoring UVT during operation, changes in UVT are factored in through irradiance measurements from duty sensors. This directly ties UVT to irradiance measurements, akin to the sensor equations outlined in previous chapters.

The validation process may employ a single setpoint, where a minimum irradiance value corresponds to a maximum validated water flow rate, or multiple setpoints, typically a minimum of four, establishing an equation relating maximum validated water flows to minimum irradiance values. During validation testing, the combination of irradiance and water flow is determined to achieve a minimum REF of 400 J/m². For UV sensors to effectively ensure the minimum REF is maintained during operation, their placement is crucial. Ideally, sensors should be positioned to maintain a proportional relationship between UV irradiance and REF, regardless of fluctuations in UVT or UV output. This principle is illustrated in Figure 41: the top-left graph depicts an ideal sensor position where, for a given water flow rate, the correlation between UV irradiance and REF remains consistent across different UVT levels. Conversely, the top-right graph illustrates a scenario where the sensor is too close to the lamp, resulting in disparate ratios of flow to irradiance required to achieve the same REF for varying UVT levels. Similarly, if the sensor is too distant from the lamp, changes in UVT disproportionately affect the measured UV irradiance [EPA (United States Environmental Protection Agency), 2006].

In essence, optimal sensor placement is system-specific and requires careful consideration of the distance between the sensor and the lamp.

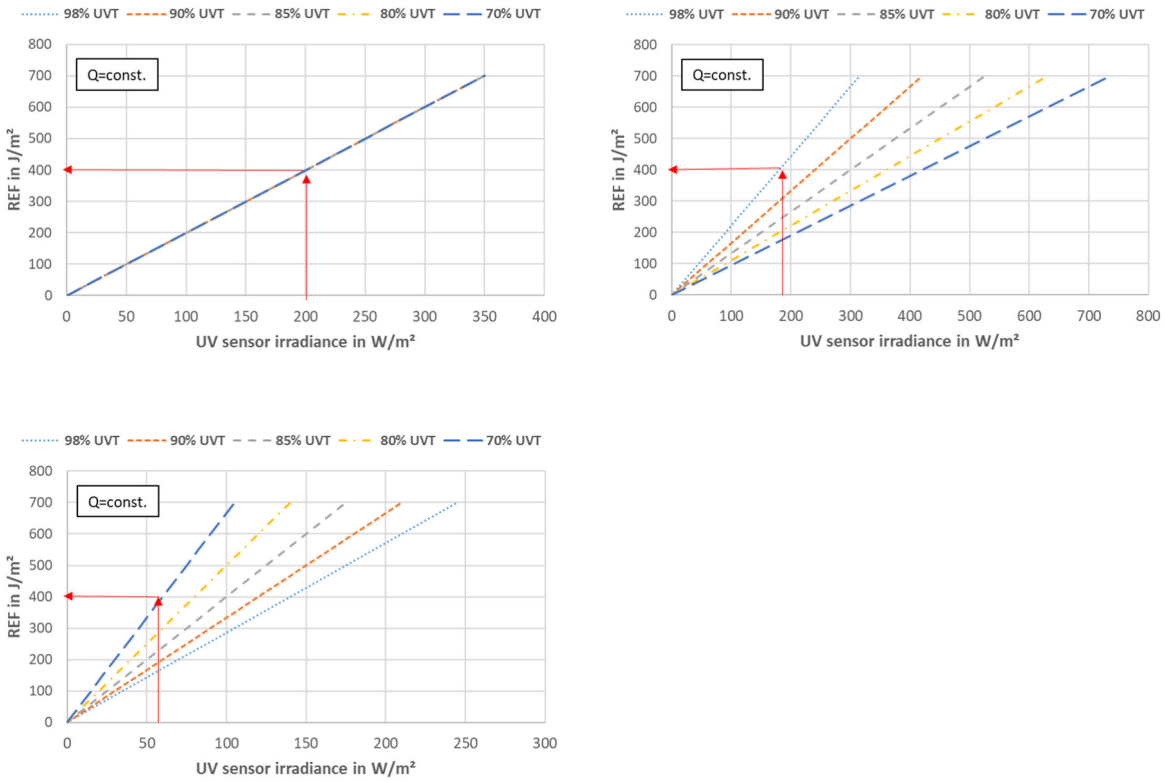

Figure 41: Exemplarily correlations between UV fluence and UV sensor irradiance for an ideal sensor position (left top graph), sensor close to the lamp (top right graph) and sensor far from the lamp (bottom left graph). [Adapted from EPA (United States Environmental Protection Agency), 2006].)

Given that not all systems may possess an optimal sensor position, ensuring safe operation without continuous monitoring of UVT entails adopting a UV intensity setpoint approach to test worst-case scenarios. The current DIN-19294-1 outlines three such scenarios:

- H-test scenario: Adjusts the minimum irradiance at 100 % BPL by using a UVT-reducing substance.
- L-test scenario: Adjusts the minimum irradiance at a high UVT (between 97.79 % and 98.95 %) by reducing the BPL.
- B-test scenario: Adjusts the minimum irradiance by using the nominal UVT provided by the manufacturer and reducing the BPL to 75 %.

These scenarios are conducted for each pair of water flow and UVT provided by the manufacturer, assuming a disinfection performance of REF ≥ 400 J/m². The minimum irradiances are determined based on the sensor equation at 75 % BPL, accounting for a safety factor for aging and fouling effects.

While these worst-case scenarios aim to mitigate the impact of non-ideal sensor positions in most cases, they have some inherent weaknesses. Firstly, they may not always cover the actual worst-case scenarios in operational settings, as confirmed by real validation data and CFD data from TZW. For instance, CFD data of one specific UV system [unpublished data from TZW] provided four pairs of water flow and

UVT, each resulting in a specific setpoint defined by the minimum irradiance (minimum S), as illustrated in Table 22.

Table 22: Example of test points of a UV intensity setpoint approach with given setpoint ID, water flow, nominal UVT and minimum irradiance.

Setpoint ID	Q in m³/h	Nominal UVT in %	Minimum S in W/m²
1	110	97.7	479
2	85	93.5	359
3	58	87.0	228
4	35	80.0	138

The graphs depicted in Figure 42 illustrate the relationship between REF and UVT for each of the four setpoints outlined in Table 22, each representing a different flow-to-irradiance ratio. Additionally, the graph highlights the positions of the H-, B-, and L-test scenarios in terms of UVT.

For setpoints 1 and 2, the three scenarios adequately determine the worst-case UVT for the specific sensor position. However, for setpoints 3 and 4, these scenarios fail to cover the worst-case scenario comprehensively. This discrepancy reveals a significant weakness of this approach: as the nominal UVT of the UV system decreases, the gap between the B-test and L-test UVT's widens, making this UVT range more challenging to assess accurately.

This example underscores how the REF for a fixed ratio of flow and irradiance can vary depending on UVT, with some cases exhibiting multiple minima and/or maxima in these dependencies.

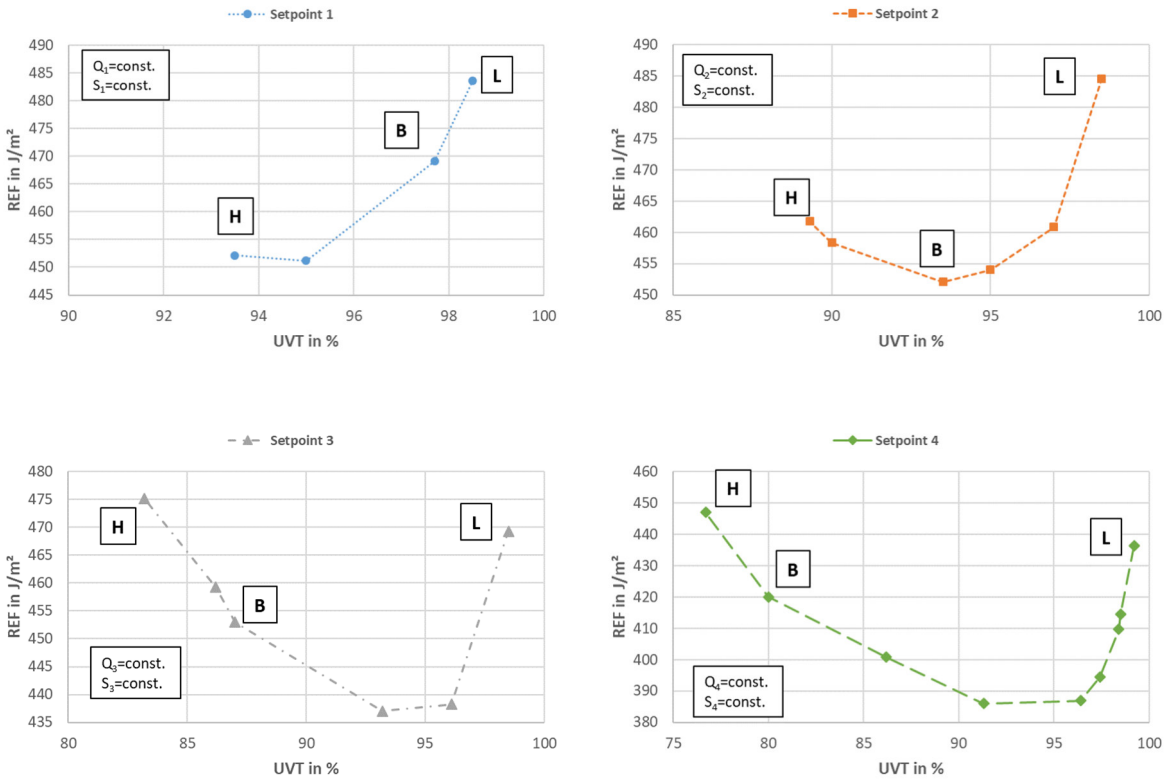

Figure 42: H-, B-, and L-test scenario for the exemplary setpoints based on CFD data [unpublished data from TZW]. Note different axis values.

To directly compare this approach with the combined variable method, the REFs of the H-, B-, and L-tests for the setpoints from Figure 42 are depicted based on the combined variable in Figure 43. In the top-left graph, as the UVT of the setpoints decreases from left to right, the L-tests are represented as a cloud of four points on the left side, while the single point on the far right corresponds to the H-test of setpoint 4. In the top-right graph, biodosimetric data was simulated for the same UV system using the combined variable approach, testing the REF range from 300 J/m² to 600 J/m² for four UVT levels. The flow and UVT range used corresponded to the setpoints (refer to Table 22). The bottom-left graph compares these two data sets. With an equal number of total test points (n = 12), the combined variable data set defines a broader range in terms of UVT, flow, and REF/logI, resulting in a more efficient characterization of the UV system. In contrast, the UV intensity setpoint approach is limited to test points only within a narrow disinfection range, with data points not equally distributed over the UVT range.

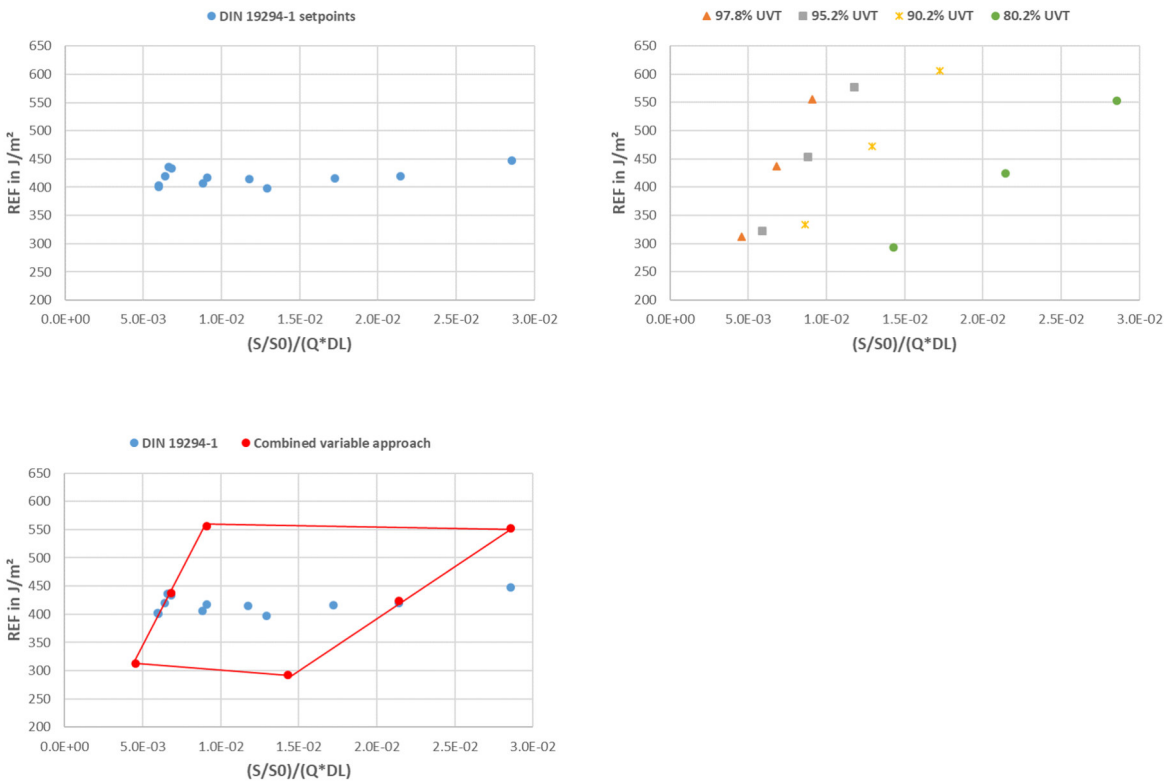

Figure 43: Left top graph: REF depending on the combined variable of the H-, B- and L-test for the UV intensity setpoint approach example. Right top graph: REF depending on the combined variable testing with the combined variable approach. Left bottom graph: Comparison of the test envelope from UV intensity setpoint approach and combined variable approach example.

The advantages of using the combined variable approach over the UV intensity setpoint approach can be summarized as follows:

- Robust data for equation interpolation: The combined variable approach provides robust data to establish equations for interpolating disinfection performance across the tested UVT range. This allows for the calculation of worst-case UVTs for each flow-to-irradiance ratio, enhancing safety during operation.
- Determination of ideal sensor position: During the validation process, the combined variable approach enables the determination of the ideal sensor position. This enhances the efficacy of UV systems during operation by ensuring optimal sensor placement.
- No test point failures: Unlike the UV intensity setpoint approach, which may encounter failures at certain test points, the combined variable approach tests over a broader range of REF, allowing all data to be utilized for calculation purposes.
- Avoidance of unrealistic scenarios: In some instances, the L-test in the UV intensity setpoint approach can result in "unrealistic" scenarios where lamps need to dim significantly below a reasonable operating point to meet minimum irradiance values. This may involve the use of

meshes or other methods to reduce lamp output, leading to increased measurement uncertainties during biodosimetry due to non-uniform lamp emission.

- Realistic number of test points: The combined variable approach maintains the same number of test points as the UV intensity approach, ensuring a realistic and comparable testing framework.

6. Conclusion

This dissertation has systematically investigated the validation of UV disinfection systems, primarily focusing on the enhanced biodosimetric approaches that incorporate the variations observed in microbial response to different UV wavelengths. This thesis provides an in-depth analysis of the validation methodologies for UV disinfection systems, critically assessing the use of *Bacillus subtilis* spores and introducing the combined variable approach as an optimized method.

A major outcome of this thesis has been the validation of the "combined variable" approach. The theoretical presented here not only support the efficacy of this approach but also suggest its preference over the traditional UV intensity setpoint method, particularly in its ability to account for variations in UV system design and operating conditions.

The findings related to the action spectrum of *Bacillus subtilis* spores underscore the limitations of this microbe as a surrogate for polychromatic UV systems. However, this research goes further by providing a higher resolution action spectrum, identifying higher UV sensitivity in specific wavelength ranges. This insight is crucial for the validation of modern UV systems, particularly those using medium-pressure lamps or LEDs, which have more complex emission spectra than traditional low-pressure systems

The adoption of the "combined variable" approach allows for a more nuanced understanding and implementation of UV disinfection systems, accommodating the spectral sensitivity variations of different microbes. This approach ensures a higher degree of disinfection assurance and operational safety, which is critical for public health protection. Furthermore, the findings advocate for the revision of international standards concerning UV disinfection to incorporate these more detailed and accurate biodosimetric methods, promoting their widespread adoption in UV system validations globally.

While this research has provided significant insights, it also acknowledges certain limitations. The experiments' dependence on specific surrogate microbes and the variability in their response across different UV wavelengths suggest the need for a broader spectrum of surrogates and pathogens to fully understand and simulate the dynamics of microbial inactivation. Additionally, the experimental setup was constrained to laboratory conditions, which might not fully replicate the complexities encountered in real-world UV system operations. Additionally, the focus on *Bacillus subtilis* and MS2 phage, while relevant, limits the generalization of the findings to other potential surrogate organisms that might be considered in the future.

Moreover, the combined variable approach, although validated through simulations, may require further refinement when applied to different types of UV systems, particularly new LED systems with unconventional designs.

Future research should aim to broaden the spectrum of surrogate microbes used in biodosimetry to better accommodate the evolving range of applications and disinfection requirements. This expansion would

support the development of more comprehensive and universally applicable UV disinfection strategies. Furthermore, there is a critical need for long-term field studies to validate laboratory findings under real-world conditions typical of municipal water treatment facilities. As UV disinfection technology advances, particularly with the increasing adoption of LED systems, validation methods must be continually adapted and optimized to maintain their relevance and suitability. Moreover, careful attention must be given to the 400 J/m² threshold to ensure it remains sufficient for achieving 4-log inactivation. There is also a significant gap in the literature regarding the action spectra of most pathogenic microbes, which requires further investigation

In conclusion, this dissertation not only advances the scientific understanding of UV disinfection but also contributes practical solutions to enhance the efficacy and reliability of water treatment systems. The introduction of optimized biodosimetric methods aligned with the "combined variable" approach marks a significant step forward in the field of environmental engineering and public health protection. The continued exploration and adoption of these innovations is essential for ensuring the safety and sustainability of water resources worldwide.

References

American Public Health Association (APHA), Water Environmental Federation. (2023). *Standard Methods for the Examination of Water and Wastewater*. 24th ed. Washington DC: APHA Press.

American Public Health Association (APHA), (2017). *9224 detection of coliphages in: Standard Methods For the Examination of Water and Wastewater 24th edition*. Washington DC: APHA Press.

Barrow, G. (1964). *The structure of molecles*. New York: W. A. Benjamin Inc.

Beck, S., Wright, H., Hargy, T., Larason, T., & Linden, K. (2015). Action spectra for validation of pathogen disinfection in medium-pressure ultraviolet (UV) systems. *Water Research*, S. 27-37.

Bernhardt, H., Hoyer, O., Nick, K., Schoenen, D., Gebel, J., Hengesbach, B., Schöler, H.-F. (1994). Desinfektion aufbereiteter Oberflächenwässer mit UV-Strahlen. *gwf Wasser/Abwasser*, S. 677-689.

Blatchley, E. R., & Hunt, B. A. (1994). Bioassay for full-scale UV disinfection plants. *Wat. Sci. Tech. Vol. 39*, S. 115-123.

Bolton, J. R., & Linden, K. G. (2003). Standardization of Methods for Fluence (UV Dose) Determination in Bench-Scale UV Experiments. *Journal of Environmental Engineering*, S. 209-215.

Bolton, J. R., & Cotton, C. A. (2008). *The Ultraviolet Disinfection Handbook. 1st ed.* American Waterworks Association.

Bolton, J. R. (2010). *Ultraviolet Applications Handbook*. ICC Lifelong Learn Inc.

Bolton, J. R., Beck, S., & Linden, K. G. (2015). Protocol for the determination of fluence (UV dose) using a low-pressure or low-pressure high-output UV lamp in bench-scale collimated beam ultraviolet experiments. *IUVA News 17 (1)*, S. 11-17.

Cabaj, A., Sommer, R., & Schoenen, D. (1996). Biodosimetry: Model Calculations for UV Water Disinfection Devices with regard to Dose Distribution. *Water Research Vol. 30, No. 4*, S. 1003-1009.

Cabaj, A., Sommer, R., Pribil, W., & Haider, T. (2002). The spectral UV sensitivity of microbes used in biodosimetry. *Water Sci. Tech.: Water Supply 2 (3)*, S. 175-181.

Calgua, B., Carratalà, A., Guerrero-Latorre, L., de Abreu Corrêa, A., Kohn, T., Sommer, R., & Girones, R. (2014). UVC inactivation of dsDNA and ssRNA viruses in water: UV fluences and a qPCR-based approach to evaluate decay on viral infectivity. *Food Environ. Virol. 6(4)*, S. 260-268.

Campell, I. S., Tzipori, S., G., H., & Angus, K. W. (1982). Effect of disinfectants on survival of *Cryptosporidium*. *Vet. Rec. 111*, S. 414-415.

Chen, J., Loeb, S., & Kim, J.-H. (2017). LED revolution: fundamentals and prospects for UV disinfection applications. *Environ. Sci.: Water Res. Technol. (3)*, S. 188-202.

Chevremont, A., Boudenne, J., Coulomb, B., & Farnet, A. (2013a). Fate of carbamazepine and anthracene in soils watered with UV-LED treated wastewaters. *Water Research 43 (20)*, S. 6574-6584.

Chick, H. (1908). An investigation of the laws of disinfections. *J. Hyg. 8*, S. 92-158.

Clancy, J. L., Hargy, T. M., Marshall, M. M., & Dyksen, J. E. (1998). UV light inactivation of Cryptosporidium oocysts. *J. Am. Water Works Assoc. 90 (9)*, S. 92-102.

Davidson, J. (1965). *The biochemistry of the nucleic acids*, 5th edition. London: Cox and wyman.

DIN (Deutsches Institut für Normung e.V.). (2020). DIN 19294-1. *Geräte zur Desinfektion von Wasser mittels Ultravioletttstrahlung - Teil 1: Geräte mit UV-Niederdrucklampen - Anforderungen und Prüfung*. Berlin: Beuth Verlag GmbH.

DIN (Deutsches Institut für Normung e.V.). (2020). DIN 19294-3. *Geräte zur Desinfektion von Wasser mittels Ultravioletttstrahlung - Teil 3: Referenzradiometer für Geräte mit UV-Niederdrucklampen - Anforderungen und Prüfung*. Berlin: Beuth Verlag GmbH.

DVGW Deutsche Vereinigung des Gas- und Wasserfaches e.V. (2023). DVGW Arbeitsblatt W 294-1. *Planung, Betrieb und Überwachung von UV-Desinfektionsanlagen in der Wasserversorgung*. Wirtschafts- und Verlagsgesellschaft Gas und Wasser mbH, Bonn.

DVGW Deutsche Vereinigung des Gas- und Wasserfaches e.V. (2006). DVGW Arbeitsblatt W 294-2. *UV-Geräte zur Desinfektion in der Wasserversorgung; Teil 2: Prüfung von Beschaffenheit, Funktion und Desinfektionswirksamkeit*. Wirtschafts- und Verlagsgesellschaft Gas und Wasser mbH, Bonn.

DVGW Deutsche Vereinigung des Gas- und Wasserfaches e.V. (2006). DVGW Arbeitsblatt W 294-3. *UV-Geräte zur Desinfektion in der Wasserversorgung; Teil 3: Messfenster und Sensoren zur radiometrischen Überwachung von UV-Desinfektionsgeräten; Andorderungen, Prüfung und Kalibrierung*. Wirtschafts- und Verlagsgesellschaft Gas und Wasser mbH, Bonn.

Einfeldt, S. (17. Mai 2022). Technischer Vortrag LEDs. *DVGW-Workshop LED-Prüfnorm Tag 1*. online.

EPA (United States Environmental Protection Agency). (2006). Ultraviolet Disinfection Guidance Manual for the Final Long Term 2 Enhanced Surface Water Treatment Rule. *Pirnie, M. Inc., Carollo Engineers, The Cadmus Group, Linden, K. G., Malley, J. P.*

EPA (United States Environmental Protection Agency). (2020). Innovative Approaches for Validation of Ultraviolet Disinfection Reactors For Drinkig Water Systems.

Ferziger, J., & Perić, M. (2002). *Computational Methods for Fluid Dynamics. 3rd ed*. Springer.

Fox, R. W., McDonald, A. T., & Pritchard, P. J. (2011 (7th edition)). *Introduction to Fluid Mechanics.* John Wiley & Sons.

Grubbs, F. E. (1950). Sample Criteria for Testing Outlying Observations. *The Annals of Mathematical Statistics*, S. 27-58.

Harm, W. (1980). *Biologial effects of ultraviolet radiation.* Cambridge university press.

Harris, T. R., Pagan, J., & Batoni, P. (2013). Optical and Fluidic Co-Designs of a UV-LED Water Disinfection Chamber. *ESC Transactions 45(17)*, S. 11-18.

Havelaar, A., Nieuwstad, T. J., Meulemans, C. C., & van Olphen, M. (1991). F-specific RNA bacteriophages as model viruses in UV disinfection of wastewater. *Wat. Sci. Tech. Vol. 24 (2)*, S. 347-352.

Henriques, A. O., & Moran, C. P. (2007). Structure, assembly, and function of the spore surface layers. *Annual Review of Microbiology 61*, S. 555-588

Ho, C. K., Khalsa, S. S., Wright, H. B., & Wicklein, E. (2011). *Computational Fluid Dynamics Based Models for Assessing UV Reactor Design and Installation.* Water Research Foundation.

Hoyer, O. (1998). Testing performance and monitoring of UV systems for drinking water disinfection. *Water Supply, Vol. 16*, S. 424-429.

International Union of Pure and Applied Chemistry. (2006). *IUPAC Compendium of Chemical Terminology, 3rd ed.* Online version 3.0.1, 2019. https://doi.org/10.1351/goldbook.F02448.

International Union of Pure and Applied Chemistry. (2006). *IUPAC Compendium of Chemical Terminology, 3rd ed.* Online version 3.0.1, 2019. https://doi.org/10.1351/goldbook.DT07361.

Jagger, J. (1967). *Introduction to research in ultraviolet photobiol*ogy. New Jersey: Prentice Hall.

Kennedy, M. J., Reader, S. L., & Swierczynski, L. M. (1994). Presevation records of micro-organisms: evidence of the tenacity of life. *Microbiology 140*, S. 2513-2529.

Korich, D. G., Mead, J. R., Madore, M. S., Sinclair, N. A., & Sterling, C. (1990). Effects of Ozone , Chlorine Dioxide, Chlorine, and Monochloramine on *Cryptosporidium parvum* Oocyst Viability. *Appl. Environ. Microbiol. Vol. 56 (5)*, S. 1423-1428.

Kowalski, W. J., Bahnfleth, W. P., & Hernandez, M. T. (2009). A Genomic Model for Predicting the Ultraviolet Susceptibility of Viruses. *IUVA News Vol. 11 No. 2*, S. 15-28.

Kowalski, W. J., Bahnfleth, W. P., Raguse, M., & Moeller, R. (2020). The cluster model of ultraviolet disinfection explains tailing kinetics. *Journal of Applied Microbiology 128 (4)*, S. 1003-1014.

Kuo, J., Chen, C.-I., & Nellor, M. (2003). Standardized Collimated Beam Testing Protocol for Water/Wastewater Ultraviolet Disinfection. *Journal of Environmental Engineering*, S. 774-779.

Lawryshyn, Y. (26-28. February 2018). An Assessment of the Combined Variable Approach with Second Order Disinfection Kinetics. *IUVA Americas Conference*. Redondo Beach, CA:

Linden, K., Wright, H., Collins, J., Cotton, C., & Beck, S. (2015). *Guidance for Implementing Action Spectra Correction With Medium Pressure UV Disinfection.* Denver: Water Research Foundation.

Lindenauer, K. G., & Darby, J. L. (1994). Ultraviolet disinfection of wasterwater: effect of dose on subsequent photoreactivation. *Water Research 28(4)*, S. 805-817.

Lister, G. G., Lawler, J. E., Lapatovich, W. P., & Godyak, V. A. (April 2004). The physics of discharge lamps. *Review of Modern Physics, Volume 76, S. 541-598.*

Malayeri, A. H., Mohensi, M. C., & Bolton, J. R. (2016). Fluence (UV Dose) Required to Achieve Incremental Log Inactivation of Bacteria, Protozoa, Viruses and Algae. *IUVA News Vol. 18, Issue 3 Fall 2016*, S. 4-6.

Mamane-Gravetz, H., Linden, K. G., Cabaj, A., & Sommer, R. (2005). Spectral sensitivity of *Bacillus subtilis* spores and MS2 Coliphage for validation testing of ultraviolet reactors for water disinfection. *Environ. Sci. Technol. 39 (20)*, S. 7845-7852.

Mayor-Smith, I. (2014). *Polychromatic Fluence: Calculation and Application in Ultraviolet Reactors for Water Treatment.*

Meulemans, C. (1987). The basic principles of UV-Disinfection of water. *Ozone science and engineering, vol. 9*, S. 299-314.

NATIONAL WATER RESEARCH INSTITUTE. (2012). Ultraviolet Disinfection: Guidelines for Drinking Water and Water Reuse.

Nicholson, W. L., Munakata, N., Horneck, G., Melosh, H. J., & Setlow, P. (2000). Resistance of Bacillus endospore to extreme terrestrial and extraterrestrial environments. *Microbiology and Molecular Biology Reviews 64*, S. 548-572.

NSF International. (2020). NSF / ANSI 55 -2020. *Ultraviolet Microbiological Water Treatment Systems*. Michigan: NSF International.

Nyangaresi, P. O., Rathnayake, T., & Beck, S. E. (2023). Evaluation of disinfection efficacy of single UV-C, and UV-A followed by UV-C LED irradiation on *Escherichia coli*, *B. spizizenii* and MS2 bacteriophage, in water. *Science of the Total Environment 859*, S. 1-11.

ÖNORM M 5873-1. (2020). *Geräte zu Desinfektion von Wasser mittels Ultraviolettstrahlung. Teil 1: Geräte mit UV-Niederdrucklampen. Anforderungen und Prüfung* . Wien: Austrian Standards International.

Parker, J. A., & Darby, J. L. (1995). Particle-associated coliform in secondary effluents: Shielding from ultraviolet light disinfection. *Water Environment Research 67*, S. 1065-1075.

Pfeifer, G. (1997). Formation and processing of UV photoproducts: Effects of DNA sequence and chromatin environment. *Photochemistry & Photobiology 65*, S. 270-283

Piggot, P. J., & Hilbert, D. W. (2004). Sporulation of Bacillus subtilis. *Current Opinion in Microbiology 7*, S. 579-586.

Qualls, R., & Johnson, J. (1983). Bioassay and Dose Measurement in UV Disinfection. *Appl. Environ. Microbiol. Vol. 45*, S. 872-877.

Schwarze, R. (2013). *CFD-Modellierung: Grundlagen und Anwendungen bei Strömungsprozessen*. Springer Vieweg.

Setlow, J. (1967). The Effects of Ultraviolet Radiation and Photoreactivation. *Comprehensive Biochemistry, Vol. 27*, S. 157-209.

Setlow, P. (2006). Spores of Bacillus subtilis: their resistance to and killing by radiation, heat and chemicals. *Journal of Applied Microbiology 101*, S. 514-525.

Simons, R., Lawal, O., & Pagán, J. (2022). 2022 State of the industry: UV-C LEDs and their applications. https://uvsolutionsmag.com/articles/2022/2022-state-of-the-industry-uv-c-leds-and-their-applications/.

Smith, K. C., & Hanawalt, P. C. (1969). *Molecular Photobiology: Inactivation and Recovery.* New York: Academic Press.

Smith, W. J. (2000). *Modern Optical Engineering: The Design of Optical Systems. 3rd ed*. McGraw-Hill.

Snowball, M., & Hornsey, I. (1988). Purification of water supplies using ultraviolet light. *Developments in food microbiology (3),* S. 171-191.

Sommer, R., & Cabaj, A. (1993). Evaluation of the efficiency of a UV plant for drinking water disinfection. *Wat. Sci. Tech. Vol. 27*, S. 357-362.

Sommer, R., Pribil, W., Appelt, S., Gehringer, P., Eschweiler, H., Leth, H., Haider, T. (2001). Inactivation of bacteriophages in water by means of non-ionizing (UV-253.7 nm) and ionizing (gamma) radiation: a comparative approach. *Water Research Vol. 35(13)*, S. 3109-3116.

Sommer, R., Cabaj, A., & Haider, T. (1996). Microbicidal effect of reflected UV radiation in devices for water desinfection. *Wat. Sci. Tech. Vol. 34*, S. 173-177.

Sommer, R., Haider, T., Cabaj, A., Pribil, W., & Lhotsky, M. (1998). Time dose reciprocity in UV disinfection of water. *Wat. Sci. Tech. Vol. 38 (12)*, S. 145-150.

Song, K., Mohensi, M., & Taghipour, F. (2016). Application of ultraviolet light-emitting diodes (UV-LEDs) for water disinfection: A review. *Water Research 94*, S. 341-349.

Sutherland, J. C. (2002). Biological Effects of Polychromatic Light. *Photochemistry and Photobiology 76 (2)*, S. 164-170.

U.S. Department of Health and Human Services. (2013). Grade "A" Pasteurized Mild Ordinance.

U.S. Department of Health and Human Services. (2014). The Model Aquatic Health Code: 1st Edition.

Union, E. (2011). Directive 2011/65/EU.

Valegård, K., Fridborg, K., & Unge, T. (1990). The three-dimensional structure of the bacterial virus MS2. *Nature 345*, S. 36-41.

Vreeland, R. H., Rosenzweig, W. D., & Powers, D. W. (2000). Isolation of a 250 million-year old halotolerant bacterium from a primary salt crystal. *Nature 407*, S. 897-900.

Watson, H. E. (1908). A note on variation of the rate of disinfection with change in the concentration of the disinfectant. *J. Hyg. 8*, S. 536-542.

White, F. M. (2011). *Fluid Mechanics. 7th ed*. McGraw-Hill.

Wilcox, D. (2006). *Turbulence Modeling for CFD. 3rd ed*. California: DCW Industries, Inc.

ATCC database

https://www.atcc.org/products/6633

Appendix A: Verification of the combined variable approach using a full scale example

This appendix will present experimental data from a full scale MP UV system (spectral emission as per Figure A-49) test employing the combined variable approach, with data incorporating *Bacillus subtilis* spores, MS2 phage, and T1UV phage. The aim is to demonstrate the general applicability of the combined variable approach for UV systems in full scale experiments. Additionally, it will substantiate that accounting for the specific action spectra of surrogates for polychromatic UV sources increases accuracy.

A.1. Material and Methods

A.1.1. Test facility

The biodosimetric tests for the MP UV system were conducted at the TZW test facility, adhering to the DVGW worksheet W294-2. This facility is specifically equipped to carry out detailed evaluations of UV disinfection systems under controlled conditions. The test train was designed to simulate realistic operational scenarios while maintaining strict control over variables that could affect the outcome of the tests.

A.1.2. Test setup

The MP UV system was installed within a test train to evaluate its performance across different flow rates, UVT levels, UV outputs of the lamps and microbial loads. The layout of the test track, along with the placement of measurement devices, sampling points and bypass injection of microbes and UVT reducing substances was designed to ensure that data collected was both accurate and representative of actual operating conditions.

A.1.3. Test water

The TZW test facility in Meindorf is connected to the groundwater pump station of the WTV (Wahnbachtalsperrenverband). The test water is not treated before validation testing. The local water quality is typically characterized by the following parameters:

- UVT: 98.5 % on average, with maximum fluctuations between 97.9 % and 99.5 %
- Temperature: 11.5 ± 0.5°C
- Turbidity: < 0.1 FNU
- Conductivity 40 ± 5 mS/m
- Biology: Colony forming units at 22°C and 36°C typically 0/ml and always under 5/ml; E. coli and coliform bacteria in 100 ml not detectable

A.1.4. Flow measurement

For flow measurements a calibrated magnetic-inductive device (WATERFLUX 3000 from Krohne) was utilized, ensuring that the flow conditions remained consistent across all test scenarios.

A.1.5. Irradiance measurement

The measurement and analysis of irradiances are based on the readings from the duty sensors of the UV system. The MP UV system, equipped with six lamps, utilized six duty sensors, each with a 40° opening angle. All duty sensors underwent calibration by their manufacturer.

A.1.6. Transmission measurements

Two measurement devices operated concurrently: a laboratory photometer, LAMBDA25 from Perkin-Elmer LAS, and a handheld photometer, RealTec UV254 P300 from Real Tech Inc. Both instruments underwent daily calibration and comparison using potassium dichromate standards from Starna Scientific Ltd. The handheld device was utilized for adjusting transmission during testing (with this data incorporated into the analysis). The laboratory photometer was employed for spot-check comparison measurements with samples taken on the test day and to generate transmission spectra of the water. Measurements were executed using a 40 mm path length cuvette for the RealTec and a 50 mm or 10 mm path length cuvette for the LAMBDA25. For final analysis all UVT values were calculated to 10 mm path lengths.

A.1.7. UVT reducing substance

To modulate the UVT of the water across a wide spectrum, SuperHume® by Cropmaster®, a highly concentrated form of liquefied organic carbon extracted from a humate source, Leonardite, mined in the

USA, was employed. SuperHume® did not impact the UV sensitivity of the surrogates during the biodosimetric testing. To validate this, dose-response curves of the surrogates were determined using the matrix water spiked with SuperHume® throughout the entirety of the full scale testing.

A.1.8. Gear pumps

To ensure a pulsation-free injection of surrogates and the UVT-reducing substance MCP-Z, process gear pumps from ISMATEC were used. Both surrogates and the UVT-reducing substance were injected separately via bypasses into the piping of the mainstream.

A.1.9. Surrogates

The stock preparation, enumeration, and statistical analysis of *Bacillus subtilis* spores and MS2 phage are comprehensively outlined in Chapter 2.1. The only deviation from that chapter is that all samples were plated in triplicate, contrasting with the duplicate plating used for MS2 phage in the action spectra experiments. The procedures for T1UV phage will be expounded upon in the following section.

The T1UV phage was obtained from GAP. Detection of T1UV phage involved the single-layer method, wherein the sample was placed into an empty Petri dish, and agar mixed with the host bacteria (*Escherichia coli*, WG5) was poured over the sample. For the assay, bacterial host cultures were incubated for approximately 3 hours at 37 °C to achieve an optical density at 600 nm (OD600) of 0.45. The bacteria were stored on ice until usage. The media in the bottles were dissolved with a steamer and kept fluid at 42 °C in a water bath. Additional media compounds (CaCl or CaGlucose) as well as bacteria were added to a media bottle directly before use.

The samples were plated in triplicate and incubated at 37 °C for 18 hours. Dilutions and aliquots of the samples were adjusted to count 10 to 300 plaque-forming units (pfu) per Petri dish. Negative controls and positive controls (to ensure the assay's effectiveness) were plated each day.

The statistical analysis of T1UV dose-response curves is identical to the MS2 ones, described with Equation 12, except that sometimes the dose-response curve tends to be more linear than quadratic, causing the second term of the equation with the parameter "B" to be excluded.

A.2. MP UV system results

A comprehensive set of 51 test conditions (excluding blanks) involving MS2, T1UV, and *Bacillus subtilis* spores was executed to derive an equation predicting the logI of a microbe based on flow, UVT, and UV output. The initial test plan aimed to cover a UVT range from 70.0 % to 98.5 % (measured at 254 nm) and a logI range from 0 to 5, utilizing MS2 and T1UV phage surrogates.

While the *Bacillus subtilis* spores conditions were originally designed to meet the requirements of the DVGW worksheet W 294-2 [DVGW Deutsche Vereinigung des Gas- und Wasserfaches e.V., 2006], additional test conditions were conducted to complement the MS2/T1UV envelope by expanding the

UVT and logI range for *Bacillus subtilis* spores conditions. Typically, DVGW worksheet validations aim for ≈ 2-logI (equivalent to a REF of ≈ 400 J/m²). It is important to note that aiming for > 3-logI with *Bacillus subtilis* spores at these high flows would incur exceptionally high costs compared to testing with phage surrogates. The price difference lies in the substantial costs associated with acquiring the required amounts of spore surrogates, which differ by three orders of magnitude.

The total of 51 test conditions can be categorized into 18 with MS2, 12 with T1UV, and 21 with *Bacillus subtilis* spores. An overview of the total test conditions is depicted in Figure A-44, illustrating the logI of the three surrogates as a function of UVT in the left graph and the UVT and flow range in the right graph. These graphs showcase the replicate pairs of the actual measured biodosimetric data after removing outliers and test conditions with insufficient pfu/cfu counts in the effluent.

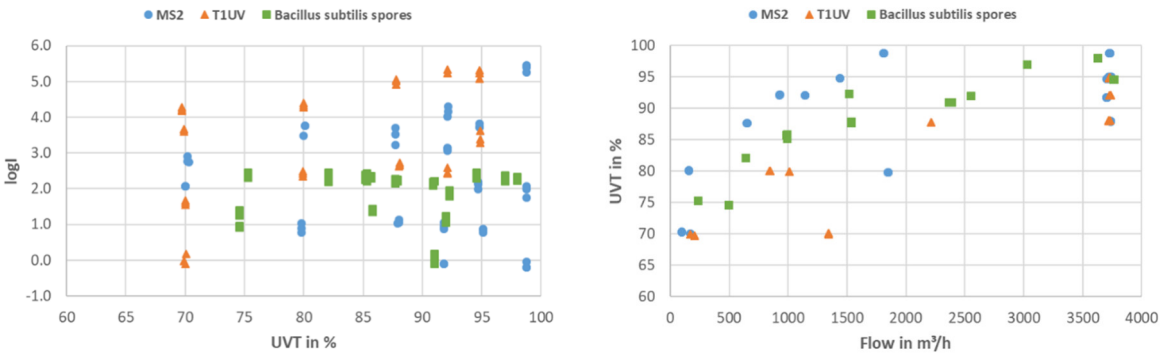

Figure A-44: Left graph: LogI depending on UVT for MS2 (blue circles), T1UV (orange triangles) and Bacillus subtilis *spores (green squares. Right graph: Flow and UVT range for MS2 (blue circles), T1UV (orange triangles) and* Bacillus subtilis *spores (green squares.*

A.2.1. Sensor equation

Before conducting biodosimetric testing, sensor equations were established to calculate the S_0 values for each of the test conditions. This equation enables the prediction of duty sensor readings based on UVT and ballast power level (BPL). Importantly, these equations account for aging and fouling effects that may occur during the full scale testing, which is crucial for the accurate analysis and interpretation of results using an equation derived from the combined variable theory (refer to Equation 4).

For the MP UV system, separate sensor equations were derived for each of the six duty sensors. However, these six duty sensors could be categorized into two optical systems. Duty sensor IDs 1, 2, 4, and 5 shared the same position within the reactor, leading to similar irradiances dependent on UVT and BPL. On the other hand, duty sensor IDs 3 and 6 were part of a second optical system and were positioned closer to the lamp. The correlation between irradiance (measured with the duty sensors) and UVT was examined across a range from approximately 66.5 % to about 99.5 % (equivalent to the background UVT of the test water) and with four different BPL. The measured data is illustrated exemplarily for duty sensor #1 in Figure A-45.

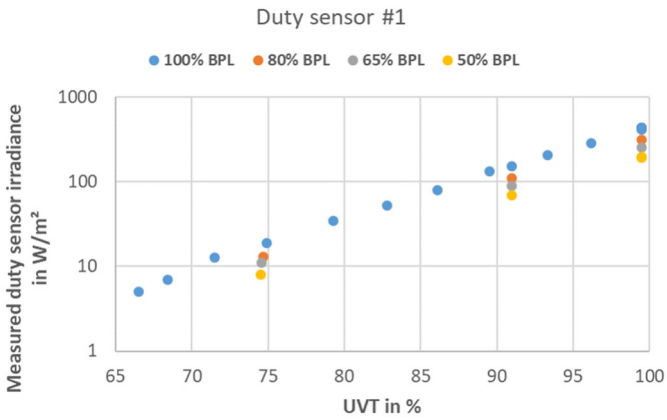

Figure A-45: Irradiance as a function of UVT, conducted with four different BPL, measured with duty sensor #1.

Based on the measured irradiance data, the sensor equations were developed using multivariate linear regression in the first step and non-linear multivariate regression in the second step. Equation 34 describes this equation for all six duty sensors, each having different empirical coefficients. Due to the empirical nature of this equation, unit correction factors are introduced.

$$S = 10^{i_2} \cdot (10^{j_2})^{UVA \cdot x_1} \cdot x_1 \cdot UVA^{k_2} \cdot (10^{l_2})^{BPL \cdot y_1} \cdot y_1 \cdot BPL^{m_2} \cdot z_1 \quad (34)$$

With:

S	Predicted irradiance, in W/m²
BPL	Ballast power level, in %
i_2, j_2, k_2, l_2, m_2	Empirical coefficients
x_1	Unit correction factor, in m
y_1	Unit correction factor, in $\%^{-1}$
z_1	Unit correction factor, in W/m²

To calculate S_0, the BPL value is to set to 100 % which defines the 100 % UV output of the lamp.

The empirical coefficients i_2, j_2, k_2, l_2, and m_2 for the six duty sensors are provided in Table 26. All these coefficients exhibited statistical significance (p-value < 0.05), with the exception of duty sensor #4, where k_2 was omitted from the equation.

Table A-23: Values for the sensor equation; empirical coefficients i_2, j_2, k_2, l_2, and m_2 for the six duty sensors.

Duty sensor	i_2	j_2	k_2	l_2	m_2
#1	1.086E0	-1.061E-1	-3.002E-2	3.297E-3	6.109E-1
#2	8.848E-1	-1.031E-1	-2.352E-2	3.322E-3	7.067E-1
#3	1.021E0	-7.886E-2	-2.353E-2	3.463E-3	6.931E-1
#4	7.557E-1	-1.102E-1	-	2.174E-3	8.386E-1
#5	1.203E0	-1.076E-1	-2.198E-2	4.205E-3	5.015E-1
#6	1.158E0	-7.766E-2	-1.834E-2	2.348E-3	6.714E-1

The left graph in Figure A-46 demonstrates the correlation between the measured duty sensor readings and the predicted irradiances of the six duty sensors using Equation 34. The slope of 1.007 and R^2 of 0.999 confirm the high-quality fit between the measured and predicted values, covering the complete sensor dataset. The right graph in Figure A-46 displays the relative residuals, calculated as the difference between measured duty sensor reading and predicted irradiance divided by the predicted irradiance. The residuals showed an average of -0.1 % with a standard deviation of 3.1 % and ranged from -10.5 % to 10.9 %. The highest discrepancies were observed between 5 W/m² and 30 W/m². This might be attributed to the resolution of the duty sensors, which lacked digits and thereby increased the relative uncertainty of the prediction within this irradiance range. However, the residuals were generally well within ± 5 %.

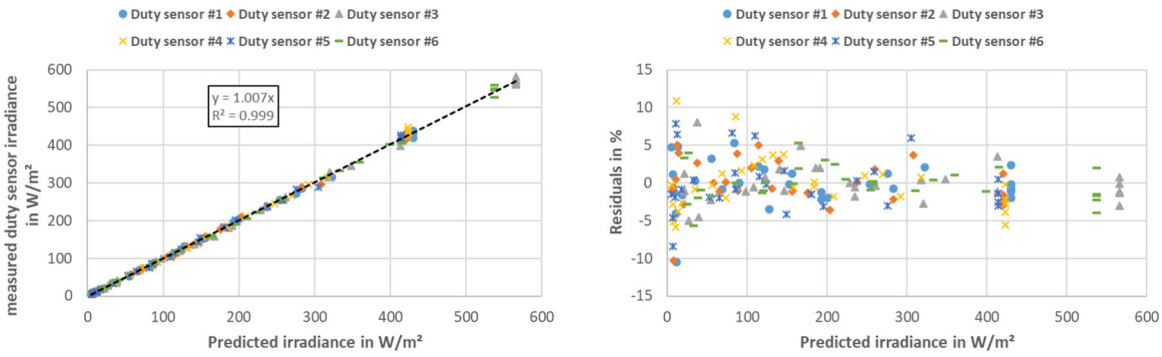

Figure A-46: Left graph: Correlation between predicted and measured irradiance for duty sensors #1 (blue circles), #2 (orange diamonds), #3 (grey triangles), #4 (yellow crosses), #5 (dark blue stars) and #6 (green dashes). Right graph: Residuals for measured irradiances and predicted irradiances for duty sensors #1 (blue circles), #2 (orange diamonds), #3 (grey triangles), #4 (yellow crosses), #5 (dark blue stars) and #6 (green dashes).

The accuracy of the sensor equation is a crucial first step in reducing measurement uncertainty during full scale testing. By establishing a reliable control value for each test condition, the uncertainty in the interpolation phase during the analysis of the full biodosimetric data set is also minimized (refer to Chapter A.2.4)

A.2.2. CB data of the surrogates

Throughout the testing period, LP-CB dose-response curves were generated for the surrogates using water samples obtained on the day of testing. Replicate dose-response curves were conducted for each testing day to improve statistical robustness. The dose-response curve parameters for MS2 are based on 27 fluences (including four fluences with zero J/m² as $\log N_0$) spanning a fluence range from 0 J/m² to 1500 J/m². For T1UV, a total of 14 fluences (including two fluences with zero J/m² as $\log N_0$) ranging from 0 J/m² to 300 J/m² were utilized. The *Bacillus subtilis* spores dose-response was based on 40 fluences (including 12 fluences with zero J/m² as $\log N_0$) within a range from 0 J/m² to 700 J/m². Equation 12 was applied for both phage surrogates, and Equation 8 for the spores' dose-response analysis. The three dose-response curves are depicted in Figure A-47, with the parameters detailed in Table A-24.

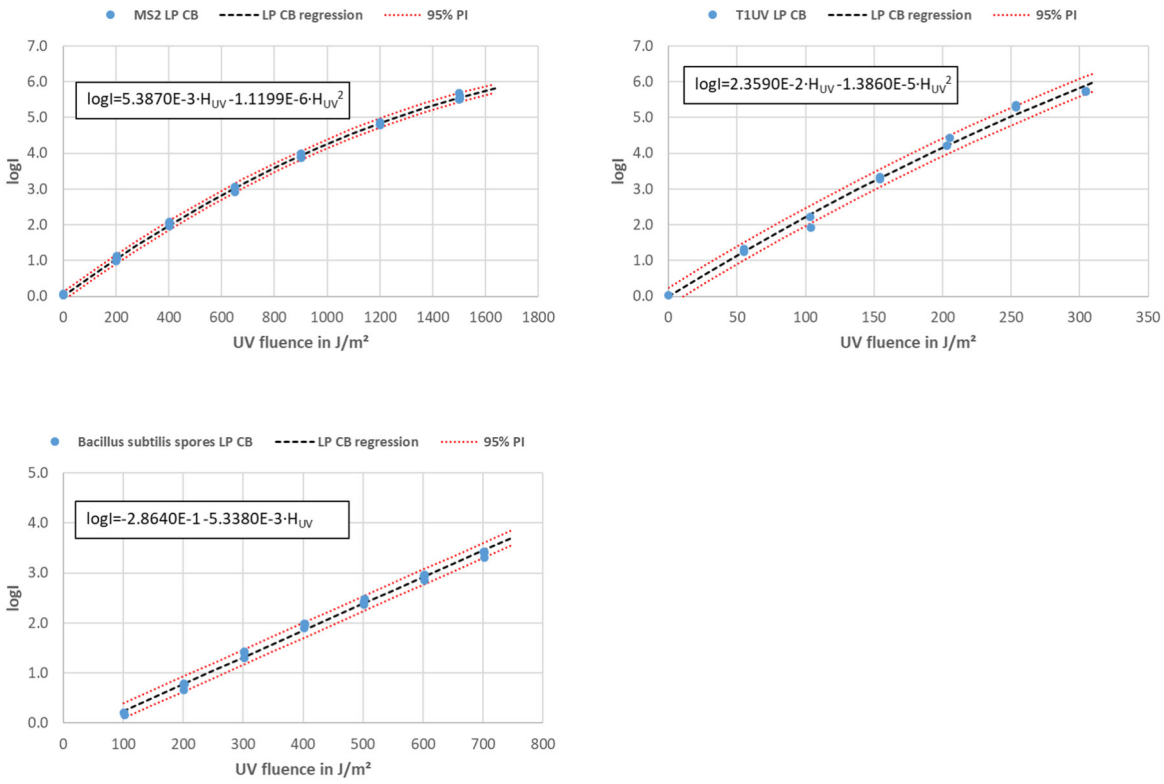

Figure A-47: Dose-response curves of MS2 phage (left graph on top), T1UV phage (right graph on top) and Bacillus subtilis *spores (left graph on bottom) with related equations used for the analysis of the MP UV system. Note different axis.*

Table A-24: Parameters of the LP-CB dose-response curves for MS2 and T1UV phage and Bacillus subtilis *spores used for analysis of the MP UV system.*

Parameter	*Bacillus subtilis* spores	MS2 phage	T1UV phage
A*	-2.8640E-1	5.3870E-3	2.3590E-2
B**	-5.3380E-3	-1.1199E-6	-1.3860E-5

*in m^2/J for phage, without unit for *Bacillus subtilis* spores

**in m^4/J^2 for phage, in m^2/J for *Bacillus subtilis* spores

A.2.3. Implementation of the action spectra correction factor (ASCF)

Given that the MP-lamp has a polychromatic spectrum, it is crucial to consider the distinct action spectra of the surrogates. To address this, Equation 3 is employed, incorporating the action spectra for MS2 and T1UV from Beck et al. (2015), and for *Bacillus subtilis* spores based on the results presented in this thesis in Chapter 2.2.5. The action spectra for the three surrogates are depicted in Figure A-48.

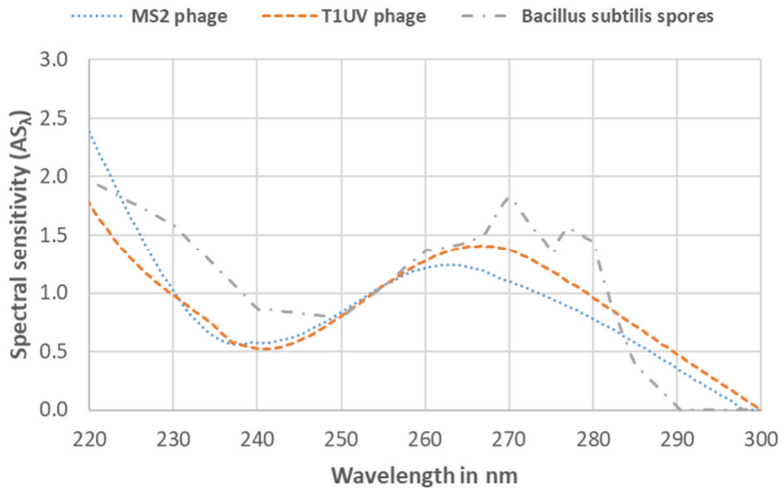

Figure A-48: Action spectrum relative to 254 nm of MS2 phage (blue dotted line), T1UV phage (orange dashed line), adapted from Beck, et al. (2015), and Bacillus subtilis *spores (grey dash-dot line) from this thesis.*

The MP-lamp's emission characteristics were provided by the manufacturer. Additionally, the transmission spectra of the quartz sleeve, also supplied by the manufacturer, were factored in to consider only the emitted spectrum that penetrates the water within the UV system. The left graph of Figure A-49 illustrates the relative emission spectrum of the MP-lamp and the UVT of the quartz sleeve with a thickness of 2 mm. In the right graph of Figure A-49, the MP-lamp emission is shown, considering the absorption of lamp emission within the quartz sleeve. The quartz sleeve is designed to minimize wavelengths below 240 nm as much as possible, leading to noticeable differences in the two emission spectra, especially in this wavelength range. Henceforth, when referring to the MP-lamp emission in subsequent calculations, it implies the emission adjusted for the UVT of the quartz sleeve.

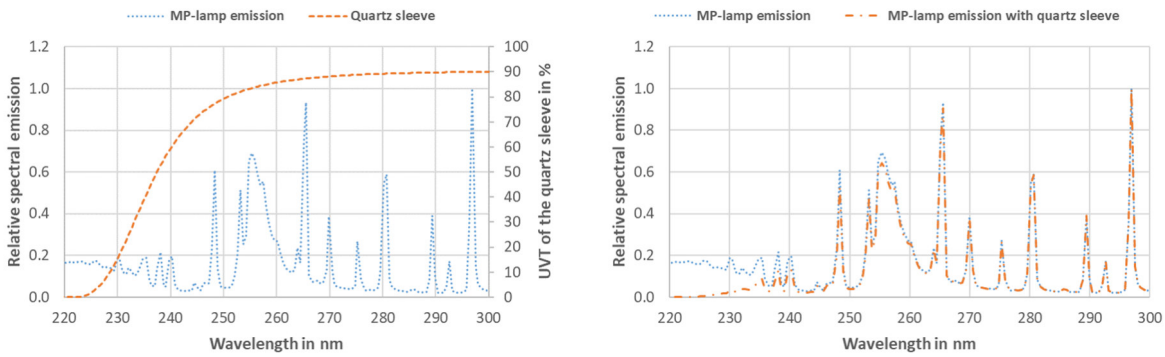

Figure A-49: Left graph: Relative spectral emission of the MP-lamp (blue dotted line) and the UVT of the quartz sleeve (orange dashed line). Right graph: Relative spectral emission of the MP-lamp (blue dotted line) and relative spectral emission of the MP-lamp considering the UVT of the quartz sleeve (orange dash-dot line).

The integration limits from Equation 3 were refined to 220 nm to 300 nm for more precise calculations. Utilizing the MP-lamp emission and applying the action spectrum for each surrogate with Equation 3, the corresponding ASCFs can be determined (refer to Table 25). Figure A-50 presents an example of the germicidal spectral emission, equivalent to P_G in Equation 3, based on the action spectrum for *Bacillus subtilis* spores.

Table 25: Action spectra correction factors for Bacillus subtilis *spores, MS2 and T1UV phage using the MP-lamp emission considering the quartz sleeve transmission.*

	***Bacillus subtilis* spores**	**MS2 phage**	**T1UV phage**
ASCF	1.04	0.88	0.96

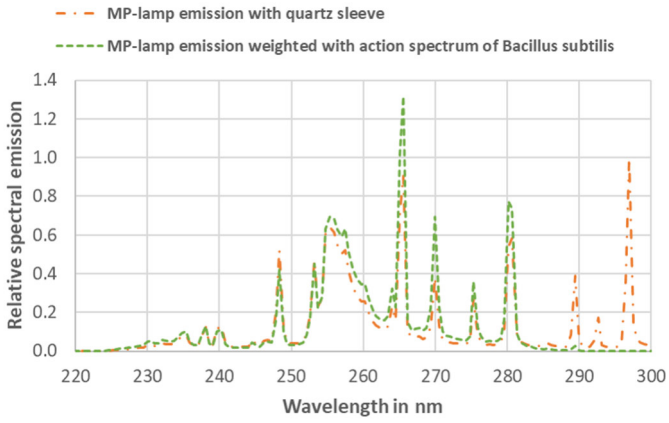

Figure A-50: Relative spectral emission of the MP-lamp considering the UVT of the quartz sleeve (orange dash-dot line) and relative spectral emission weighted with the action spectra of Bacillus subtilis *spores (green dashed line).*

During validation testing and subsequently in operation, the UVT measurement consistently refers to 254 nm. While this may not pose significant challenges for a LP UV system, it can be critical for polychromatic UV systems. In theory, two waters could have the same UVT at 254 nm but vastly different transmissions at higher or lower wavelengths, leading to potential under- or overestimations of the UV system's performance in operation. Throughout the biodosimetric testing of the MP UV system, this issue was explored using the UVT-reducing substance SuperHume® and the background UVT of the test water. The following pages will also provide guidance on calculating the impact of the combination of UV source emission spectrum and UVT spectrum of the water.

Figure A-51 illustrates some of the transmission spectra of water with SuperHume® at various UVT levels (measured at 254 nm) and one with the background UVT of the test water (dark blue dashed line). In the following graphs, the UVT will always be accompanied by an additional description when referring to the UVT measured at 254 nm to prevent any confusion.

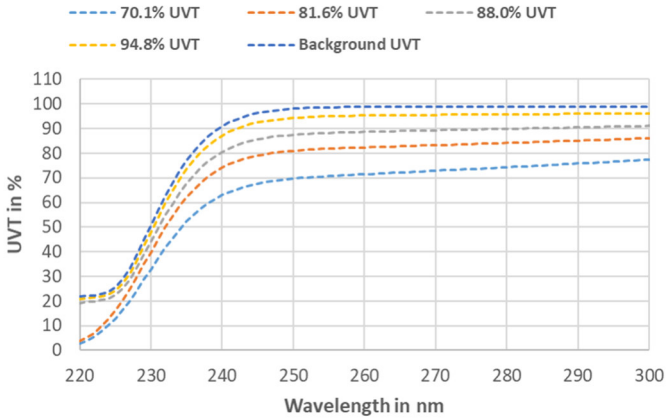

Figure A-51: Transmission spectra of the test water for different UVT levels and for the background UVT of the test water.

The spectra of the water with SuperHume® appear quite consistent, without noticeable intermediate peaks or valleys that could complicate ASCF calculations during biodosimetric testing. However, the precise impact was determined through the following steps, utilizing a total of 12 transmission spectra measured during biodosimetric testing covering the UVT range from 70.1 % to 98.4 %, measured at 254 nm:

1. The wavelength range of 220 nm to 300 nm of the water's transmission spectra was divided into 10 nm intervals (220 nm to 229 nm, 230 nm to 239 nm, etc.), and the average UVT value was calculated for each interval to simplify data handling and reduce computational effort.
2. For each 10 nm interval, a regression analysis of the average UVT values as a function of the UVT measured at 254 nm was conducted, as demonstrated in Figure A-52 for selected intervals.

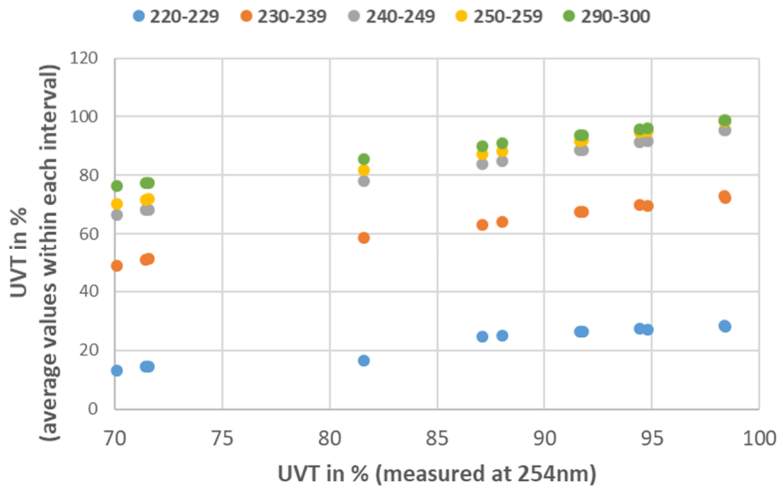

Figure A-52: The average UVT value within a wavelength interval as a function of the UVT measured at 254 nm.

3. The wavelength range of 220 nm to 300 nm of the MP-lamp emission and the germicidal MP-lamp emission for all three surrogates was divided into 10 nm intervals, and the integral of the relative spectral emission was calculated for each interval.
4. The residual relative spectral emission, accounting for the absorption of UV radiation by the water, was calculated for each wavelength interval and over the complete UVT range from 70.1 % to 98.4 % (measured at 254 nm) in 1 nm increments. This calculation utilized the relative spectral emissions from step 3 and the UVT regressions from step 2. The process was carried out separately for the MP-lamp emission and the three germicidal MP lamp-emissions.
5. The 10 nm intervals of the residual relative spectral emission for each 1 nm UVT interval, measured at 254 nm, from step 4 were summed up. Subsequently, the sum of the germicidal relative spectral emission was divided by the sum of the relative spectral MP lamp emission for all three surrogates, resulting in the ASCFs depending on the UVT measured at 254 nm while considering the overall wavelength range of the water transmission (refer to Figure A-53).

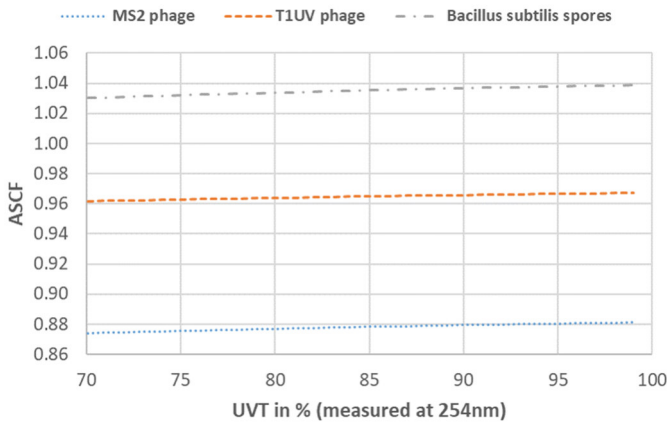

Figure A-53: Dependence of the ASCF for MS2 phage (blue dotted line), T1UV phage (orange dashed line) and Bacillus subtilis *spores (grey dash-dot line) on the UVT of the test water measured at 254 nm.*

6. To calculate the final ASCFs for biodosimetric data analysis, the values of each surrogate were averaged across the UVT range, as illustrated in Figure A-53. This results in a minor adjustment from Table 25, where the ASCF for *Bacillus subtilis* spores is now 1.03 instead of 1.04

The ASCFs of the surrogates, as depicted in Figure A-53, exhibit minimal variation, typically within ±1 %, based on the UVT measured at 254 nm. This consistency underscores SuperHume® as a suitable substance for UV system testing. While the biodosimetric testing revealed no significant impact, it is crucial to conduct these calculations for each combination of polychromatic UV source, test water, and UVT reducing substance during validation testing. Additionally, understanding the water characteristics and spectra over an extended period at the operational site is recommended, as outlined in the DVGW worksheet W 294-1 [DVGW Deutsche Vereinigung des Gas- und Wasserfaches e.V., 2006].

A.2.4. Biodosimetric data analysis

Figure 53 depicts the logI results corresponding to the combined variable values. For every UVT (e.g., represented by blue circles denoting UVT 98.5% in Figure 53), a power function trend line can be plotted based on Equation 4. This function consistently yields a reasonable coefficient of determination (> 0.960), except for the highest UVT. In this instance, limited data were available for this UVT. However, this generally confirms the efficacy of the combined variable approach, employing ASCF for the biodosimetric dataset of the MP UV system. The graph showcases the average measured UVTs. Although some individual UVT data points are not depicted in this graph, they were included in the final data analysis.

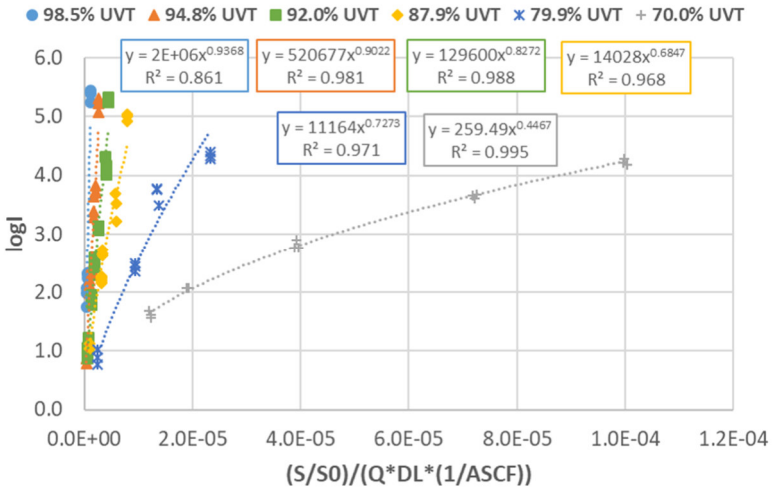

Figure A-54: LogI of the MP UV system biodosimetric data depending on the combined variable for the average UVTs 98.5 % (blue circles), 94.8 % (orange triangles), 92.0 % (green squares), 87.9 % (yellow diamonds), 79.9 % (dark blue stars) and 70.0 % (grey crosses).

Using the biodosimetric data set the empirical coefficients A2' and B2' can be derived based on the UVT-dependent equations: Equation 35 for A2' and Equation 36 for B2'. Utilizing UVA for analysis ensures greater precision.

$$A_2' = 10^{a_2} \cdot (10^{b_2})^{UVA/100} \cdot (\frac{UVA}{100})^{c_2} \quad (35)$$

$$B_2' = d_2 + e_2 \cdot UVA/100 + f_2 \cdot (UVA/100)^2 \quad (36)$$

This results in the development of the following algorithm (refer to Equation 37) for predicting logI utilizing the combined variable approach. This is accomplished by integrating Equations 35 and 36 into Equation 5:

$$logI_{pred} = 10^{a_2} \cdot (10^{b_2})^{UVA/100 \cdot x_1} \cdot (\frac{UVA \cdot x_1}{100})^{c_2} \cdot (\frac{S/S0 \cdot \omega}{Q \cdot D_L \cdot 1/ASCF})^{(d_2 + e_2 \cdot UVA/100 \cdot x_1 + f_2 \cdot (UVA/100)^2 \cdot x_2)} \quad (37)$$

With

a_2, b_2, c_2, d_2, e_2, f_2 Empirical coefficients

The biodosimetric data was fitted to Equation 37. Table 29 presents the values and the statistical significance (p-value < 0.05) for the coefficients a_2, b_2,c_2, d_2, e_2 and f_2.

Table A-26: Values for the algorithm coefficients a_2, b_2, c_2, d_2, e_2 and f_2 and corresponding p-values.

Empirical coefficients	Value	p-value
a_2	5.863E0	3.31E-59
b_2	-2.285E1	3.29E-24
c_2	-3.183E-1	6.12E-6
d_2	9.722E-1	1.65E-66
e_2	-1.818E0	5.82E-8
f_2	-8.482E0	2.26E-11

The efficacy of the algorithm for predicting logI (refer to Equation 37 and Table 29) is showcased in the left panel of Figure A55, demonstrating the correlation between predicted logI using the algorithm and the actual logI measured from biodosimetric data. A slope of 1.000 and an R^2 of 0.976 attest to the algorithm's high predictive accuracy. In the right panel of Figure A55, the residuals between measured and predicted logI are depicted against the predicted logI. The U_{IN} value is 0.42 log units, which falls

within a reasonable and realistic range. Notably, these U_{IN} values are derived from experience and data accumulated over the past decade of UV system validation at TZW.

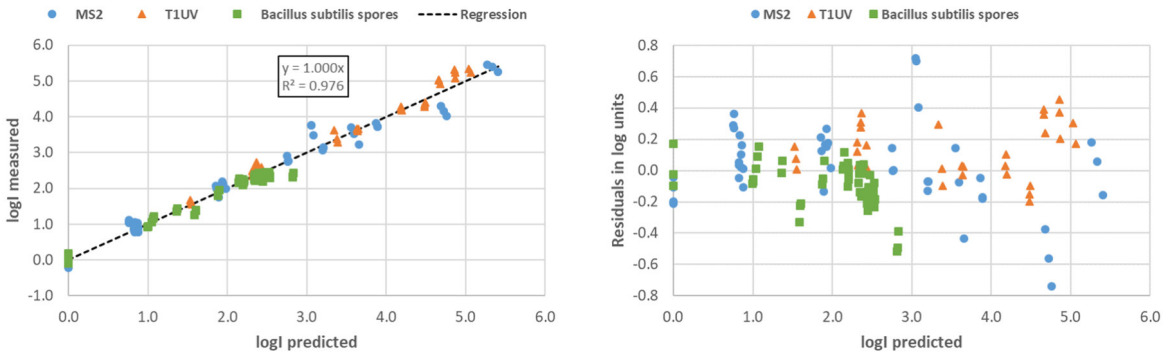

Figure A55: Left graph: Correlation of the predicted and measured logI for MS2 (blue circles), T1UV (orange triangles) and Bacillus subtilis *spores (green squares).Right graph: Residuals for measured logI minus predicted logI MS2 (blue circles), T1UV (orange triangles) and Bacillus subtilis spores (green squares).*

The results from the extensive biodosimetric dataset for an MP UV system not only confirm the effectiveness of the combined variable approach but also shed light on the robustness of using three surrogates with different ASCFs: MS2 and T1UV phage, and Bacillus subtilis spores. This comprehensive analysis did not uncover any inconsistencies in the application of the ASCFs across the dataset, nor did it reveal any discernible impact stemming from the Bacillus subtilis spores' CB shoulder behavior with this particular MP UV system. However, it is worth noting that further investigations, particularly with additional Bacillus subtilis spores data at higher logI levels, could provide more conclusive insights into the potential impact of the shoulder effect. This approach would be particularly informative as the manifestation of the shoulder effect is anticipated to be more pronounced at elevated logI values, offering a more comprehensive understanding of its implications in practical UV system applications.

Appendix B: Final action spectrum of *Bacillus subtilis* spores

Wavelength in nm	α_λ		Wavelength in nm	α_λ
220	1.97		261	1.37
221	1.93		262	1.39
222	1.89		263	1.40
223	1.86		264	1.42
224	1.82		265	1.43
225	1.78		266	1.47
226	1.74		267	1.51
227	1.70		268	1.62
228	1.67		269	1.73
229	1.63		270	1.84
230	1.59		271	1.74
231	1.52		272	1.64
232	1.45		273	1.55
233	1.37		274	1.46
234	1.30		275	1.37
235	1.23		276	1.47
236	1.16		277	1.57
237	1.09		278	1.53
238	1.01		279	1.48
239	0.94		280	1.44
240	0.87		281	1.19
241	0.86		282	0.93
242	0.85		283	0.75
243	0.85		284	0.57
244	0.84		285	0.39
245	0.83		286	0.32
246	0.82		287	0.25
247	0.81		288	0.17
248	0.81		289	0.10
249	0.80		290	0.03
250	0.79		291	0.00
251	0.84		292	0.00
252	0.89		293	0.00
253	0.95		294	0.00
254	1.00		295	0.00
255	1.06		296	0.00
256	1.12		297	0.00
257	1.18		298	0.00
258	1.24		299	0.00
259	1.30		300	0.00
260	1.36			

Appendix C: Raw data Chapter 2

Bacillus subtilis spores: logN0-values: Batch 1

Irradiation day 1: 26th November 2021

Sampling at the start of the irradiation day												
Dilution	Aliquot	Count a	Dilution	Aliquot	Count b	Dilution	Aliquot	Count c	loga	logb	logc	Average
-4	1	141	-4	1	143	-4	1	114	6.15	6.16	6.06	6.12
-4	1	123	-4	1	113	-4	1	126	6.09	6.05	6.10	6.08
-4	1	129	-4	1	122	-4	1	127	6.11	6.09	6.10	6.10
Sampling in the middle of the irradiation day												
Dilution	Aliquot	Count a	Dilution	Aliquot	Count b	Dilution	Aliquot	Count c	loga	logb	logc	Ave
-4	1	162	-4	1	119	-4	1	123	6.21	6.08	6.09	6.12
-4	1	138	-4	1	101	-4	1	114	6.14	6.00	6.06	6.07
-4	1	139	-4	1	106	-4	1	95	6.14	6.03	5.98	6.05
Sampling at the end of the irradiation day												
Dilution	Aliquot	Count a	Dilution	Aliquot	Count b	Dilution	Aliquot	Count c	loga	logb	logc	Ave
-4	1	162	-4	1	99	-4	1	125	6.21	6.00	6.10	6.10
-4	1	149	-4	1	107	-4	1	133	6.17	6.03	6.12	6.11
-4	1	147	-4	1	107	-4	1	120	6.17	6.03	6.08	6.09
										Daily average $logN_0$		6.09
										SD $logN_0$		0.06

Bacillus subtilis spores: logN0-values: Batch 1

Irradiation day 2: 30th November 2021

Sampling at the start of the irradiation day												
Dilution	Aliquot	Count a	Dilution	Aliquot	Count b	Dilution	Aliquot	Count c	loga	logb	logc	Average
-4	1	100	-4	1	88	-4	1	79	6.00	5.94	5.90	5.95
-4	1	86	-4	1	68	-4	1	83	5.93	5.83	5.92	5.90
-4	1	98	-4	1	89	-4	1	104	5.99	5.95	6.02	5.99
Sampling in the middle of the irradiation day												
Dilution	Aliquot	Count a	Dilution	Aliquot	Count b	Dilution	Aliquot	Count c	loga	logb	logc	Ave
-4	1	107	-4	1	91	-4	1	87	6.03	5.96	5.94	5.98
-4	1	88	-4	1	101	-4	1	91	5.94	6.00	5.96	5.97
-4	1	113	-4	1	91	-4	1	107	6.05	5.96	6.03	6.01
Sampling at the end of the irradiation day												
Dilution	Aliquot	Count a	Dilution	Aliquot	Count b	Dilution	Aliquot	Count c	loga	logb	logc	Ave
-4	1	91	-4	1	107	-4	1	119	5.96	6.03	6.08	6.02
-4	1	129	-4	1	114	-4	1	111	6.11	6.06	6.05	6.07
-4	1	111	-4	1	130	-4	1	127	6.05	6.11	6.10	6.09
										Daily average $logN_0$		6.00
										SD $logN_0$		0.07

Bacillus subtilis spores: logN0-values: Batch 1

Irradiation day 3: 1st December 2021

Sampling at the start of the irradiation day												
Dilution	Aliquot	Count a	Dilution	Aliquot	Count b	Dilution	Aliquot	Count c	loga	logb	logc	Average
-4	1	110	-4	1	129	-4	1	106	6.04	6.11	6.03	6.06
-4	1	128	-4	1	125	-4	1	110	6.11	6.10	6.04	6.08
-4	1	114	-4	1	89	-4	1	123	6.06	5.95	6.09	6.03
Sampling in the middle of the irradiation day												
Dilution	Aliquot	Count a	Dilution	Aliquot	Count b	Dilution	Aliquot	Count c	loga	logb	logc	Ave
-4	1	140	-4	1	149	-4	1	117	6.15	6.17	6.07	6.13
-4	1	97	-4	1	153	-4	1	141	5.99	6.18	6.15	6.11
-4	1	108	-4	1	134	-4	1	140	6.03	6.13	6.15	6.10
Sampling at the end of the irradiation day												
Dilution	Aliquot	Count a	Dilution	Aliquot	Count b	Dilution	Aliquot	Count c	loga	logb	logc	Ave
-4	1	116	-4	1	102	-4	1	121	6.06	6.01	6.08	6.05
-4	1	130	-4	1	97	-4	1	129	6.11	5.99	6.11	6.07
-4	1	122	-4	1	91	-4	1	95	6.09	5.96	5.98	6.01
										Daily average $logN_0$		6.07
										SD $logN_0$		0.06

Bacillus subtilis spores: logN0-values: Batch 1

Irradiation day 4: 1st February 2022

Sampling in the middle of the irradiation day												
Dilution	Aliquot	Count a	Dilution	Aliquot	Count b	Dilution	Aliquot	Count c	loga	logb	logc	Average
-4	1	122	-4	1	156	-4	1	149	6.09	6.19	6.17	6.15
-4	1	126	-4	1	129	-4	1	123	6.10	6.11	6.09	6.10
-4	1	141	-4	1	123	-4	1	135	6.15	6.09	6.13	6.12
										Daily average $logN_0$		6.12
										SD $logN_0$		0.04

Bacillus subtilis spores: logN0-values: Batch 1

Irradiation day 5: 2nd February 2022

Sampling at the start of the irradiation day												
Dilution	Aliquot	Count a	Dilution	Aliquot	Count b	Dilution	Aliquot	Count c	loga	Dilution	Aliquot	Average
-4	1	122	-4	1	100	-4	1	89	6.09	6.00	5.95	6.01
-4	1	100	-4	1	102	-4	1	89	6.00	6.01	5.95	5.99
-4	1	105	-4	1	94	-4	1	83	6.02	5.97	5.92	5.97
Sampling in the middle of the irradiation day												
Dilution	Aliquot	Count a	Dilution	Aliquot	Count b	Dilution	Aliquot	Count c	loga	Dilution	Aliquot	Average
-4	1	98	-4	1	139	-4	1	102	5.99	6.14	6.01	6.05
-4	1	108	-4	1	136	-4	1	91	6.03	6.13	5.96	6.04
-4	1	103	-4	1	127	-4	1	88	6.01	6.10	5.94	6.02
Sampling at the end of the irradiation day												
Dilution	Aliquot	Count a	Dilution	Aliquot	Count b	Dilution	Aliquot	Count c	loga	Dilution	Aliquot	Average
-4	1	94	-4	1	88	-4	1	101	5.97	5.94	6.00	5.97
-4	1	83	-4	1	86	-4	1	80	5.92	5.93	5.90	5.92
-4	1	80	-4	1	91	-4	1	65	5.90	5.96	5.81	5.89
										Daily average $logN_0$		5.98
										SD $logN_0$		0.07

Bacillus subtilis spores: logN0-values: Batch 1

Irradiation day 6: 12th April 2022

Sampling at the start of the irradiation day												
Dilution	Aliquot	Count a	Dilution	Aliquot	Count b	Dilution	Aliquot	Count c	loga	Dilution	Aliquot	Average
-4	1	125	-4	1	112	-4	1	165	6.10	6.05	6.22	6.12
-4	1	153	-4	1	125	-4	1	160	6.18	6.10	6.20	6.16
-4	1	172	-4	1	168	-4	1	136	6.24	6.23	6.13	6.20
Sampling in the middle of the irradiation day												
Dilution	Aliquot	Count a	Dilution	Aliquot	Count b	Dilution	Aliquot	Count c	loga	Dilution	Aliquot	Average
-4	1	169	-4	1	111	-4	1	125	6.23	6.05	6.10	6.12
-4	1	163	-4	1	124	-4	1	133	6.21	6.09	6.12	6.14
-4	1	105	-4	1	113	-4	1	127	6.02	6.05	6.10	6.06
Sampling at the end of the irradiation day												
Dilution	Aliquot	Count a	Dilution	Aliquot	Count b	Dilution	Aliquot	Count c	loga	Dilution	Aliquot	Average
-4	1	150	-4	1	143	-4	1	101	6.18	6.16	6.00	6.11
-4	1	144	-4	1	128	-4	1	141	6.16	6.11	6.15	6.14
-4	1	147	-4	1	143	-4	1	129	6.17	6.16	6.11	6.14
										Daily average $logN_0$		6.13
										SD $logN_0$		0.07

Bacillus subtilis spores: logN0-values: Batch 2

Irradiation day 1: 1st Februrary 2022

Sampling at the start of the irradiation day												
Dilution	Aliquot	Count a	Dilution	Aliquot	Count b	Dilution	Aliquot	Count c	loga	Dilution	Aliquot	Average
-4	1	258	-4	1	163	-4	1	141	6.41	6.21	6.15	6.26
-4	1	89	-4	1	100	-4	1	68	5.95	6.00	5.83	5.93
-4	1	64	-4	1	79	-4	1	98	5.81	5.90	5.99	5.90
Sampling at the end of the irradiation day												
Dilution	Aliquot	Count a	Dilution	Aliquot	Count b	Dilution	Aliquot	Count c	loga	Dilution	Aliquot	Average
-4	1	84	-4	1	96	-4	1	140	5.92	5.98	6.15	6.02
-4	1	97	-4	1	82	-4	1	107	5.99	5.91	6.03	5.98
-4	1	201	-4	1	131	-4	1	68	6.30	6.12	5.83	6.08
										Daily average $logN_0$		6.03
										SD $logN_0$		0.17

Bacillus subtilis spores: Batch 1

Laser-based setup with wavelength 220 nm, #1

Date	01.02.2022				
Volume Petri dish in ml	4		These parameters were the same for all laser-based irradiations		
Volume Stirrer in ml	0.226				
Diameter Petri dishin cm	3.5				
Pathlength suspension	0.43924166				
Distance Microlense array	24.5				
PF	0.9800				
WF	0.9900				
RF	0.9750				
DF	0.9824				
λ in nm	220				
UVT in %	95.5				
S in W/m²	S_{ave} in W/m²	t in s	Fluence in J/m²		
0.28	0.27	101.6	27		
0.28	0.27	169.4	45		
0.28	0.27	254.1	68		
0.28	0.27	338.7	92		
0.28	0.27	440.4	119		
$logN_0$	6.12	irradiation day 4			
Fluence in J/m²	Dilution	Aliquot	Count	logN	logI
27	-4	1	95	5.98	0.15
27	-4	1	64	5.81	0.32
27	-4	1	61	5.79	0.34
45	-4	1	48	5.68	0.44
45	-4	1	43	5.63	0.49
45	-4	1	54	5.73	0.39
68	-4	1	22	5.34	0.78
68	-4	1	30	5.48	0.65
68	-4	1	25	5.40	0.73
92	-3	1	226	5.35	0.77
92	-3	1	217	5.34	0.79
92	-3	1	187	5.27	0.85

Bacillus subtilis spores: Batch 1

Laser-based setup with wavelength 220 nm, #2

Date	14.04.2022				
PF	0.9800				
WF	0.9976				
RF	0.9750				
DF	0.9824				
λ in nm	220				
UVT in %	95.5				
S in W/m²	S_{ave} in W/m²	t in s	Fluence in J/m²		
0.26	0.25	383.5	94		
0.27	0.25	768.1	192		
0.27	0.25	1155.3	290		
0.27	0.25	1343.2	338		
$logN_0$	6.13	irradiation day 6			
Fluence in J/m²	Dilution	Aliquot	Count	logN	logI
94	-3	1	131	5.12	1.02
94	-3	1	126	5.10	1.03
94	-3	1	131	5.12	1.02
192	-2	1	126	4.10	2.03
192	-2	1	97	3.99	2.15
192	-2	1	122	4.09	2.05
290	-1	1	131	3.12	3.02
290	-1	1	117	3.07	3.07
290	-1	1	120	3.08	3.05
338	-1	1	28	2.45	3.69
338	-1	1	52	2.72	3.42
338	-1	1	34	2.53	3.60

Bacillus subtilis spores: Batch 1

Laser-based setup with wavelength 230 nm, #1

Date	01.02.2022				
PF	0.9800				
WF	0.9929				
RF	0.9750				
DF	0.9824				
λ in nm	230				
UVT in %	96.8				
S in W/m²	S_{ave} in W/m²	t in s	Fluence in J/m²		
1.12	1.04	45.3	47		
1.11	1.03	90.6	93		
1.12	1.04	135.9	141		
1.11	1.03	226.5	234		
$logN_0$	6.12	irradiation day 4			
Fluence in J/m²	Dilution	Aliquot	Count	logN	logI
47	-4	1	102	6.01	0.12
47	-4	1	68	5.83	0.29
47	-4	1	88	5.94	0.18
93	-4	1	35	5.54	0.58
93	-4	1	29	5.46	0.66
93	-4	1	42	5.62	0.50
141	-3	1	104	5.02	1.11
141	-3	1	104	5.02	1.11
141	-3	1	88	4.94	1.18
234	-2	1	150	4.18	1.95
234	-2	1	143	4.16	1.97
234	-2	1	150	4.18	1.95

Bacillus subtilis spores: Batch 1

Laser-based setup with wavelength 230 nm, #2

Date	12.04.2022				
PF	0.9800				
WF	0.9973				
RF	0.9750				
DF	0.9824				
λ in nm	230				
UVT in %	98.8				
S in W/m²	S_{ave} in W/m²	t in s	Fluence in J/m²		
1.04	0.98	100.6	98		
1.04	0.98	200.9	196		
1.04	0.97	301.3	294		
1.04	0.98	351.5	343		
logN0	6.13	irradiation day 6			
Fluence in J/m²	Dilution	Aliquot	Count	logN	logI
98	-4	1	39	5.59	0.54
98	-4	1	46	5.66	0.47
98	-4	1	39	5.59	0.54
196	-3	1	42	4.62	1.51
196	-3	1	40	4.60	1.53
196	-3	1	36	4.56	1.58
294	-2	1	39	3.59	2.54
294	-2	1	46	3.66	2.47
294	-2	1	37	3.57	2.57
343	-1	1	141	3.15	2.98
343	-1	1	146	3.16	2.97
343	-1	1	144	3.16	2.98

Bacillus subtilis spores: Batch 1

Laser-based setup with wavelength 230 nm, #2

Date	12.04.2022				
PF	0.9800				
WF	0.9973				
RF	0.9750				
DF	0.9824				
λ in nm	230				
UVT in %	98.8				
S in W/m²	S_{ave} in W/m²	t in s	Fluence in J/m²		
1.04	0.98	100.6	98		
1.04	0.98	200.9	196		
1.04	0.97	301.3	294		
1.04	0.98	351.5	343		
logN0	6.13	irradiation day 6			
Fluence in J/m²	Dilution	Aliquot	Count	logN	logI
98	-4	1	39	5.59	0.54
98	-4	1	46	5.66	0.47
98	-4	1	39	5.59	0.54
196	-3	1	42	4.62	1.51
196	-3	1	40	4.60	1.53
196	-3	1	36	4.56	1.58
294	-2	1	39	3.59	2.54
294	-2	1	46	3.66	2.47
294	-2	1	37	3.57	2.57
343	-1	1	141	3.15	2.98
343	-1	1	146	3.16	2.97
343	-1	1	144	3.16	2.98

Bacillus subtilis spores: Batch 1

Laser-based setup with wavelength 240 nm, #1

Date	02.02.2022				
PF	0.9800				
WF	0.9940				
RF	0.9750				
DF	0.9824				
λ in nm	240				
UVT in %	97.3				
S in W/m²	S_{ave} in W/m²	t in s	Fluence in J/m²		
1.43	1.34	74.3	99		
1.41	1.31	148.6	195		
1.40	1.31	222.9	292		
1.40	1.30	297.2	387		
1.40	1.30	371.5	484		
logN0	5.98	irradiation day 5			
Fluence in J/m²	Dilution	Aliquot	Count	logN	logI
99	-4	1	59	5.77	0.21
99	-4	1	59	5.77	0.21
99	-4	1	36	5.56	0.43
195	-3	1	215	5.33	0.65
195	-3	1	190	5.28	0.71
195	-3	1	169	5.23	0.76
292	-3	1	58	4.76	1.22
292	-3	1	59	4.77	1.21
292	-3	1	50	4.70	1.29
387	-2	1	215	4.33	1.65
387	-2	1	218	4.34	1.65
387	-2	1	234	4.37	1.62
484	-2	1	51	3.71	2.28
484	-2	1	30	3.48	2.51
484	-2	1	25	3.40	2.59

Bacillus subtilis spores: Batch 1

Laser-based setup with wavelength 240 nm, #2

Date	12.04.2022				
PF	0.9800				
WF	0.9976				
RF	0.9750				
DF	0.9824				
λ in nm	240				
UVT in %	98.9				
S in W/m²	S_{ave} in W/m²	t in s	Fluence in J/m²		
1.30	1.21	165.2	201		
1.30	1.22	331.0	404		
1.30	1.22	412.6	503		
1.31	1.22	536.3	656		
logN0	6.13	irradiation day 6			
Fluence in J/m²	Dilution	Aliquot	Count	logN	logI
201	-4	1	24	5.38	0.75
201	-4	1	31	5.49	0.64
201	-4	1	27	5.43	0.70
404	-3	1	40	4.60	1.53
404	-3	1	31	4.49	1.64
404	-3	1	71	4.85	1.28
503	-2	1	71	3.85	2.28
503	-2	1	57	3.76	2.38
503	-2	1	48	3.68	2.45
656	-1	1	107	3.03	3.10
656	-1	1	104	3.02	3.12
656	-1	1	99	3.00	3.14

Bacillus subtilis spores: Batch 1

Laser-based setup with wavelength 250 nm, #1

Date	01.12.2021				
PF	0.9800				
WF	0.9892				
RF	0.9750				
DF	0.9824				
λ in nm	250				
UVT in %	95.2				
S in W/m²	S_{ave} in W/m²	t in s	Fluence in J/m²		
2.00	1.86	107.3	200		
2.01	1.86	214.6	400		
2.00	1.86	321.9	598		
2.01	1.87	429.2	802		
logN0	6.07	irradiation day 3			
Fluence in J/m²	Dilution	Aliquot	Count	logN	logI
200	-4	1	37	5.57	0.50
200	-4	1	29	5.46	0.61
200	-4	1	36	5.56	0.51
400	-2	1	224	4.35	1.72
400	-2	1	217	4.34	1.73
400	-2	1	215	4.33	1.74
598	-1	1	203	3.31	2.76
598	-1	1	215	3.33	2.74
598	-1	1	227	3.36	2.72
802	-1	1	25	2.40	3.67
802	-1	1	13	2.11	3.96
802	-1	1	22	2.34	3.73

Bacillus subtilis spores: Batch 1

Laser-based setup with wavelength 250 nm, #2

Date	02.02.2022				
PF	0.9800				
WF	0.98943				
RF	0.9750				
DF	0.9824				
λ in nm	250				
UVT in %	97.4				
S in W/m²	S_{ave} in W/m²	t in s	Fluence in J/m²		
1.77	1.66	114.7	190		
1.79	1.67	229.3	382		
1.80	1.68	344.0	577		
1.79	1.67	401.3	670		
logN0	5.98	irradiation day 5			
Fluence in J/m²	Dilution	Aliquot	Count	logN	logI
190	-4	1	40	5.60	0.38
190	-4	1	46	5.66	0.32
190	-4	1	40	5.60	0.38
382	-3	1	24	4.38	1.60
382	-3	1	36	4.56	1.43
382	-3	1	43	4.63	1.35
577	-1	1	551	3.74	2.24
577	-1	1	582	3.76	2.22
577	-1	1	410	3.61	2.37
670	-1	1	265	3.42	2.56
670	-1	1	230	3.36	2.62
670	-1	1	248	3.39	2.59

Bacillus subtilis spores: Batch 1

Laser-based setup with wavelength 250 nm, #2

Date	02.02.2022				
PF	0.9800				
WF	0.98943				
RF	0.9750				
DF	0.9824				
λ in nm	250				
UVT in %	97.4				
S in W/m²	S_{ave} in W/m²	t in s	Fluence in J/m²		
1.77	1.66	114.7	190		
1.79	1.67	229.3	382		
1.80	1.68	344.0	577		
1.79	1.67	401.3	670		
logN0	5.98	irradiation day 5			
Fluence in J/m²	Dilution	Aliquot	Count	logN	logI
190	-4	1	40	5.60	0.38
190	-4	1	46	5.66	0.32
190	-4	1	40	5.60	0.38
382	-3	1	24	4.38	1.60
382	-3	1	36	4.56	1.43
382	-3	1	43	4.63	1.35
577	-1	1	551	3.74	2.24
577	-1	1	582	3.76	2.22
577	-1	1	410	3.61	2.37
670	-1	1	265	3.42	2.56
670	-1	1	230	3.36	2.62
670	-1	1	248	3.39	2.59

Bacillus subtilis spores: Batch 1

Laser-based setup with wavelength 254 nm, #1

Date	28.01.2021				
PF	0.9800				
WF	0.9967				
RF	0.9750				
DF	0.9824				
λ in nm	254				
UVT in %	98.5				
S in W/m²	S_{ave} in W/m²	t in s	Fluence in J/m²		
1.89	1.77	51.3	91		
1.89	1.77	102.6	181		
1.89	1.77	153.8	272		
1.89	1.77	205.1	363		
1.85	1.73	256.4	445		
1.85	1.73	307.7	532		
logN0	6.09	irradiation day 1			
Fluence in J/m²	Dilution	Aliquot	Count	logN	logI
91	-4	1	46	5.66	0.43
91	-4	1	51	5.71	0.39
91	-4	1	59	5.77	0.32
181	-3	1	224	5.35	0.74
181	-3	1	229	5.36	0.73
181	-3	1	215	5.33	0.76
272	-3	1	80	4.90	1.19
272	-3	1	56	4.75	1.35
272	-3	1	59	4.77	1.32
363	-2	1	221	4.34	1.75
363	-2	1	203	4.31	1.79
363	-2	1	193	4.29	1.81
445	-2	1	54	3.73	2.36
445	-2	1	33	3.52	2.58
445	-2	1	48	3.68	2.41
532	-1	1	175	3.24	2.85
532	-1	1	129	3.11	2.98
532	-1	1	220	3.34	2.75

Bacillus subtilis spores: Batch 1

Laser-based setup with wavelength 254 nm, #2

Date	28.01.2021				
PF	0.9800				
WF	0.9967				
RF	0.9750				
DF	0.9824				
λ in nm	254				
UVT in %	98.5				
S in W/m²	S_{ave} in W/m²	t in s	Fluence in J/m²		
1.81	1.70	51.3	87		
1.80	1.69	102.6	173		
1.80	1.68	153.8	259		
1.82	1.70	205.1	349		
1.82	1.70	256.4	436		
1.81	1.69	307.7	520		
logN0	6.09	irradiation day 1			
Fluence in J/m²	Dilution	Aliquot	Count	logN	logI
87	-4	1	55	5.74	0.35
87	-4	1	49	5.69	0.40
87	-4	1	73	5.86	0.23
173	-3	1	129	5.11	0.98
173	-3	1	153	5.18	0.91
173	-3	1	186	5.27	0.82
259	-3	1	52	4.72	1.38
259	-3	1	62	4.79	1.30
259	-3	1	51	4.71	1.39
349	-2	1	175	4.24	1.85
349	-2	1	138	4.14	1.95
349	-2	1	154	4.19	1.91
436	-2	1	58	3.76	2.33
436	-2	1	45	3.65	2.44
436	-2	1	33	3.52	2.58
520	-1	1	147	3.17	2.93
520	-1	1	171	3.23	2.86
520	-1	1	128	3.11	2.99

Bacillus subtilis spores: Batch 1

Laser-based setup with wavelength 254 nm, #3

Date	28.01.2021				
PF	0.9800				
WF	0.9967				
RF	0.9750				
DF	0.9824				
λ in nm	254				
UVT in %	98.5				
S in W/m²	S_{ave} in W/m²	t in s	Fluence in J/m²		
1.74	1.62	51.3	83		
1.77	1.65	102.6	169		
1.76	1.65	153.8	254		
1.77	1.65	205.1	339		
1.78	1.66	256.4	426		
1.79	1.68	307.7	516		
logN0	6.09	irradiation day 1			
Fluence in J/m²	Dilution	Aliquot	Count	logN	logI
83	-4	1	95	5.98	0.12
83	-4	1	121	6.08	0.01
83	-4	1	83	5.92	0.17
169	-4	1	36	5.56	0.54
169	-4	1	27	5.43	0.66
169	-4	1	16	5.20	0.89
254	-3	1	64	4.81	1.29
254	-3	1	49	4.69	1.40
254	-3	1	58	4.76	1.33
339	-2	1	146	4.16	1.93
339	-2	1	123	4.09	2.00
339	-2	1	128	4.11	1.99
426	-2	1	52	3.72	2.38
426	-2	1	39	3.59	2.50
426	-2	1	43	3.63	2.46
516	-1	1	105	3.02	3.07
516	-1	1	131	3.12	2.98
516	-1	1	114	3.06	3.04

Bacillus subtilis spores: Batch 1

Laser-based setup with wavelength 254 nm, #4

Date	30.11.2021				
PF	0.9800				
WF	0.9884				
RF	0.9750				
DF	0.9824				
λ in nm	254				
UVT in %	94.8				
S in W/m²	S_{ave} in W/m²	t in s	Fluence in J/m²		
2.09	1.94	46.3	90		
2.07	1.92	92.6	178		
2.06	1.92	138.9	266		
2.03	1.89	185.2	350		
2.02	1.87	231.5	433		
1.99	1.85	277.8	513		
logN0	6.00	irradiation day 2			
Fluence in J/m²	Dilution	Aliquot	Count	logN	logI
90	-4	1	79	5.90	0.10
90	-4	1	42	5.62	0.37
90	-4	1	68	5.83	0.16
178	-3	1	165	5.22	0.78
178	-3	1	205	5.31	0.68
178	-3	1	175	5.24	0.75
266	-3	1	48	4.68	1.32
266	-3	1	45	4.65	1.34
266	-3	1	31	4.49	1.51
350	-2	1	91	3.96	2.04
350	-2	1	86	3.93	2.06
350	-2	1	85	3.93	2.07
433	-2	1	42	3.62	2.37
433	-2	1	37	3.57	2.43
433	-2	1	27	3.43	2.57
513	-1	1	122	3.09	2.91
513	-1	1	116	3.06	2.93
513	-1	1	126	3.10	2.90

Bacillus subtilis spores: Batch 1

Laser-based setup with wavelength 254 nm, #5

Date	02.02.2022				
PF	0.9800				
WF	0.9943				
RF	0.9750				
DF	0.9824				
λ in nm	254				
UVT in %	97.4				
S in W/m²	S_{ave} in W/m²	t in s	Fluence in J/m²		
1.67	1.56	56.3	88		
1.66	1.55	112.5	174		
1.66	1.55	168.8	262		
1.67	1.56	225.0	351		
1.68	1.57	281.3	442		
1.69	1.58	337.5	533		
logN0	5.98	irradiation day 5			
Fluence in J/m²	Dilution	Aliquot	Count	logN	logI
88	-4	1	62	5.79	0.19
88	-4	1	56	5.75	0.24
88	-4	1	62	5.79	0.19
174	-4	1	21	5.32	0.66
174	-4	1	30	5.48	0.51
174	-4	1	21	5.32	0.66
262	-3	1	110	5.04	0.94
262	-3	1	64	4.81	1.18
262	-3	1	61	4.79	1.20
351	-3	1	19	4.28	1.71
351	-3	1	18	4.26	1.73
351	-3	1	18	4.26	1.73
442	-2	1	53	3.72	2.26
442	-2	1	51	3.71	2.28
442	-2	1	42	3.62	2.36
533	-2	1	24	3.38	2.60
533	-2	1	24	3.38	2.60
533	-2	1	24	3.38	2.60

Bacillus subtilis spores: Batch 1

Laser-based setup with wavelength 254 nm, #6

Date	12.04.2022				
PF	0.9800				
WF	0.9978				
RF	0.9750				
DF	0.9824				
λ in nm	254				
UVT in %	99.0				
S in W/m²	S_{ave} in W/m²	t in s	Fluence in J/m²		
1.73	1.62	62.5	102		
1.69	1.59	124.8	198		
1.68	1.58	187.3	295		
1.67	1.56	249.3	389		
1.66	1.55	311.6	483		
1.66	1.55	374.5	582		
logN0	6.13	irradiation day 6			
Fluence in J/m²	Dilution	Aliquot	Count	logN	logI
102	-4	1	67	5.83	0.31
102	-4	1	89	5.95	0.18
102	-4	1	64	5.81	0.33
198	-4	1	31	5.49	0.64
198	-4	1	35	5.54	0.59
198	-4	1	34	5.53	0.60
295	-3	1	40	4.60	1.53
295	-3	1	47	4.67	1.46
295	-3	1	43	4.63	1.50
389	-2	1	193	4.29	1.85
389	-2	1	165	4.22	1.92
389	-2	1	178	4.25	1.88
483	-2	1	77	3.89	2.25
483	-2	1	56	3.75	2.39
483	-2	1	73	3.86	2.27
582	-1	1	310	3.49	2.64
582	-1	1	269	3.43	2.70
582	-1	1	165	3.22	2.92

Bacillus subtilis spores: Batch 1

Laser-based setup with wavelength 260 nm, #1

Date	28.10.2021				
PF	0.9800				
WF	0.9965				
RF	0.9750				
DF	0.9824				
λ in nm	260				
UVT in %	98.4				
S in W/m²	S_{ave} in W/m²	t in s	Fluence in J/m²		
1.89	1.77	52.9	93		
1.89	1.77	79.4	140		
1.90	1.78	105.8	188		
1.89	1.77	158.7	281		
1.89	1.77	211.6	374		
logN0	6.09	irradiation day 1			
Fluence in J/m²	Dilution	Aliquot	Count	logN	logI
93	-4	1	79	5.90	0.20
93	-4	1	54	5.73	0.36
93	-4	1	59	5.77	0.32
140	-3	1	192	5.28	0.81
140	-3	1	153	5.18	0.91
140	-3	1	144	5.16	0.94
188	-3	1	64	4.81	1.29
188	-3	1	59	4.77	1.32
188	-3	1	59	4.77	1.32
281	-2	1	122	4.09	2.01
281	-2	1	113	4.05	2.04
281	-2	1	111	4.05	2.05
374	-1	1	181	3.26	2.84
374	-1	1	242	3.38	2.71
374	-1	1	215	3.33	2.76

Bacillus subtilis spores: Batch 1

Laser-based setup with wavelength 260 nm, #2

Date	30.11.2021				
PF	0.9800				
WF	0.9879				
RF	0.9750				
DF	0.9824				
λ in nm	260				
UVT in %	94.6				
S in W/m²	S_{ave} in W/m²	t in s	Fluence in J/m²		
1.97	1.82	52.2	95		
1.98	1.84	78.3	144		
1.98	1.84	104.4	192		
2.00	1.86	156.6	291		
1.98	1.84	182.7	336		
1.99	1.84	208.8	385		
logN0	6.00	irradiation day 2			
Fluence in J/m²	Dilution	Aliquot	Count	logN	logI
95	-4	1	40	5.60	0.39
95	-4	1	40	5.60	0.39
95	-4	1	42	5.62	0.37
144	-3	1	150	5.18	0.82
144	-3	1	123	5.09	0.91
144	-3	1	140	5.15	0.85
192	-3	1	40	4.60	1.39
192	-3	1	54	4.73	1.26
192	-3	1	39	4.59	1.41
291	-2	1	66	3.82	2.18
291	-2	1	77	3.89	2.11
291	-2	1	71	3.85	2.15
336	-2	1	46	3.66	2.33
336	-2	1	27	3.43	2.57
336	-2	1	36	3.56	2.44
385	-1	1	159	3.20	2.80
385	-1	1	187	3.27	2.72
385	-1	1	168	3.23	2.77

Bacillus subtilis spores: Batch 1

Laser-based setup with wavelength 265 nm, #1

Date	30.11.2021				
PF	0.9800				
WF	0.9884				
RF	0.9750				
DF	0.9824				
λ in nm	265				
UVT in %	94.8				
S in W/m²	S_{ave} in W/m²	t in s	Fluence in J/m²		
1.30	1.21	45.8	55		
1.31	1.21	91.6	111		
1.31	1.22	137.5	168		
1.32	1.23	183.3	225		
1.34	1.24	274.9	341		
1.34	1.24	320.8	397		
logN0	6.00	irradiation day 2			
Fluence in J/m²	Dilution	Aliquot	Count	logN	logI
55	-4	1	65	5.81	0.18
55	-4	1	76	5.88	0.12
55	-4	1	64	5.81	0.19
111	-3	1	209	5.32	0.68
111	-3	1	205	5.31	0.68
111	-3	1	187	5.27	0.72
168	-3	1	45	4.65	1.34
168	-3	1	49	4.69	1.31
168	-3	1	46	4.66	1.33
225	-2	1	157	4.20	1.80
225	-2	1	175	4.24	1.75
225	-2	1	134	4.13	1.87
341	-2	1	21	3.32	2.67
341	-2	1	19	3.28	2.72
341	-2	1	31	3.49	2.51
397	-1	1	82	2.91	3.08
397	-1	1	83	2.92	3.08
397	-1	1	73	2.86	3.13

Bacillus subtilis spores: Batch 1

Laser-based setup with wavelength 265 nm, #2

Date	1.12.2021				
PF	0.9800				
WF	0.9884				
RF	0.9750				
DF	0.9824				
λ in nm	265				
UVT in %	94.8				
S in W/m²	S_{ave} in W/m²	t in s	Fluence in J/m²		
1.09	1.01	45.8	47		
1.09	1.01	91.6	92		
1.08	1.00	137.5	138		
1.10	1.02	183.3	187		
1.12	1.04	274.9	285		
1.13	1.05	320.8	337		
logN0	6.07	irradiation day 4			
Fluence in J/m²	Dilution	Aliquot	Count	logN	logI
47	-4	1	70	5.85	0.23
47	-4	1	94	5.97	0.10
47	-4	1	105	6.02	0.05
92	-4	1	36	5.56	0.51
92	-4	1	38	5.58	0.49
92	-4	1	37	5.57	0.50
138	-3	1	186	5.27	0.80
138	-3	1	131	5.12	0.95
138	-3	1	125	5.10	0.97
187	-3	1	52	4.72	1.36
187	-3	1	46	4.66	1.41
187	-3	1	54	4.73	1.34
285	-2	1	89	3.95	2.12
285	-2	1	82	3.91	2.16
285	-2	1	92	3.96	2.11
337	-1	1	376	3.58	2.50
337	-1	1	380	3.58	2.49
337	-1	1	383	3.58	2.49

Bacillus subtilis spores: Batch 1

Laser-based setup with wavelength 265 nm, #3

Date	02.02.2022				
PF	0.9800				
WF	0.9943				
RF	0.9750				
DF	0.9824				
λ in nm	265				
UVT in %	97.4				
S in W/m²	S_{ave} in W/m²	t in s	Fluence in J/m²		
1.06	0.99	94.6	93		
1.04	0.97	141.9	138		
1.04	0.97	189.2	184		
1.06	0.98	236.4	233		
1.05	0.98	283.7	278		
1.05	0.98	378.3	369		
logN0	5.98	irradiation day 5			
Fluence in J/m²	Dilution	Aliquot	Count	logN	logI
93	-4	1	30	5.48	0.51
93	-4	1	51	5.71	0.28
93	-4	1	47	5.67	0.31
138	-3	1	149	5.17	0.81
138	-3	1	149	5.17	0.81
138	-3	1	128	5.11	0.88
184	-3	1	60	4.78	1.21
184	-3	1	46	4.66	1.32
184	-3	1	58	4.76	1.22
233	-2	1	135	4.13	1.85
233	-2	1	140	4.15	1.84
233	-2	1	123	4.09	1.89
278	-2	1	63	3.80	2.19
278	-2	1	75	3.88	2.11
278	-2	1	41	3.61	2.37
369	-1	1	95	2.98	3.01
369	-1	1	133	3.12	2.86
369	-1	1	114	3.06	2.93

Bacillus subtilis spores: Batch 1

Laser-based setup with wavelength 265 nm, #4

Date	12.04.2022				
PF	0.9800				
WF	0.9972				
RF	0.9750				
DF	0.9824				
λ in nm	265				
UVT in %	98.7				
S in W/m²	S_{ave} in W/m²	t in s	Fluence in J/m²		
0.88	0.83	115.3	95		
0.88	0.83	172.8	143		
0.88	0.82	230.4	189		
0.89	0.83	288.8	240		
0.89	0.83	345.4	287		
0.90	0.84	460.5	388		
logN0	6.13	irradiation day 6			
Fluence in J/m²	Dilution	Aliquot	Count	logN	logI
95	-4	1	58	5.76	0.37
95	-4	1	46	5.66	0.47
95	-4	1	59	5.77	0.36
143	-3	1	139	5.14	0.99
143	-3	1	199	5.30	0.83
143	-3	1	175	5.24	0.89
189	-3	1	56	4.75	1.39
189	-3	1	67	4.83	1.31
189	-3	1	56	4.75	1.39
240	-3	1	28	4.45	1.69
240	-3	1	37	4.57	1.57
240	-3	1	17	4.23	1.90
287	-2	1	107	4.03	2.10
287	-2	1	83	3.92	2.21
287	-2	1	85	3.93	2.20
388	-1	1	133	3.12	3.01
388	-1	1	215	3.33	2.80
388	-1	1	235	3.37	2.76

Bacillus subtilis spores: Batch 1

Laser-based setup with wavelength 267 nm, #1

Date	02.02.2022				
PF	0.9800				
WF	0.9944				
RF	0.9750				
DF	0.9824				
λ in nm	267				
UVT in %	97.5				
S in W/m²	S_{ave} in W/m²	t in s	Fluence in J/m²		
1.57	1.47	31.0	46		
1.57	1.47	62.0	91		
1.58	1.47	93.1	137		
1.57	1.47	124.1	182		
1.59	1.48	186.1	275		
1.58	1.48	217.2	321		
logN0	5.98	irradiation day 5			
Fluence in J/m²	Dilution	Aliquot	Count	logN	logI
46	-4	1	103	6.01	-0.03
46	-4	1	86	5.93	0.05
46	-4	1	101	6.00	-0.02
91	-3	1	232	5.37	0.62
91	-3	1	216	5.33	0.65
91	-3	1	208	5.32	0.67
137	-3	1	102	5.01	0.98
137	-3	1	79	4.90	1.09
137	-3	1	77	4.89	1.10
182	-3	1	25	4.40	1.59
182	-3	1	33	4.52	1.47
182	-3	1	48	4.68	1.30
275	-2	1	55	3.74	2.24
275	-2	1	59	3.77	2.21
275	-2	1	54	3.73	2.25
321	-1	1	168	3.23	2.76
321	-1	1	172	3.24	2.75
321	-1	1	187	3.27	2.71

Bacillus subtilis spores: Batch 1

Laser-based setup with wavelength 267 nm, #2

Date	12.04.2022				
PF	0.9800				
WF	0.9964				
RF	0.9750				
DF	0.9824				
λ in nm	267				
UVT in %	98.4				
S in W/m²	S_{ave} in W/m²	t in s	Fluence in J/m²		
1.43	1.34	36.6	49		
1.44	1.35	73.0	98		
1.43	1.34	109.4	146		
1.44	1.34	145.8	196		
1.44	1.35	218.6	294		
1.43	1.33	255.0	340		
logN0	6.13	irradiation day 6			
Fluence in J/m²	Dilution	Aliquot	Count	logN	logI
49	-4	1	117	6.07	0.07
49	-4	1	102	6.01	0.12
49	-4	1	97	5.99	0.15
98	-4	1	64	5.81	0.33
98	-4	1	48	5.68	0.45
98	-4	1	57	5.76	0.38
146	-3	1	138	5.14	0.99
146	-3	1	111	5.05	1.09
146	-3	1	162	5.21	0.92
196	-3	1	27	4.43	1.70
196	-3	1	43	4.63	1.50
196	-3	1	40	4.60	1.53
294	-2	1	46	3.66	2.47
294	-2	1	48	3.68	2.45
294	-2	1	52	3.72	2.42
340	-1	1	410	3.61	2.52
340	-1	1	430	3.63	2.50
340	-1	1	424	3.63	2.51

Bacillus subtilis spores: Batch 1

Laser-based setup with wavelength 270 nm, #1

Date	28.10.2021				
PF	0.9800				
WF	0.9927				
RF	0.9750				
DF	0.9824				
λ in nm	270				
UVT in %	96.7				
S in W/m²	S_{ave} in W/m²	t in s	Fluence in J/m²		
1.95	1.81	52.9	96		
1.95	1.81	79.4	144		
1.95	1.81	105.8	192		
1.95	1.82	158.7	289		
logN0	6.09	irradiation day 1			
Fluence in J/m²	Dilution	Aliquot	Count	logN	logI
96	-4	1	34	5.53	0.56
96	-4	1	36	5.56	0.54
96	-4	1	31	5.49	0.60
144	-3	1	56	4.75	1.35
144	-3	1	64	4.81	1.29
144	-3	1	46	4.66	1.43
192	-2	1	168	4.23	1.87
192	-2	1	177	4.25	1.85
192	-2	1	174	4.24	1.85
289	-1	1	131	3.12	2.98
289	-1	1	119	3.08	3.02
289	-1	1	141	3.15	2.94

Bacillus subtilis spores: Batch 1

Laser-based setup with wavelength 270 nm, #2

Date	30.11.2021				
PF	0.9800				
WF	0.9898				
RF	0.9750				
DF	0.9824				
λ in nm	270				
UVT in %	95.4				
S in W/m²	S_{ave} in W/m²	t in s	Fluence in J/m²		
2.04	1.89	50.7	96		
2.04	1.89	76.1	144		
2.05	1.90	101.4	193		
2.05	1.90	126.8	241		
2.04	1.89	152.2	288		
2.04	1.90	177.5	337		
logN0	6.00	irradiation day 2			
Fluence in J/m²	Dilution	Aliquot	Count	logN	logI
96	-3	1	177	5.25	0.75
96	-3	1	144	5.16	0.84
96	-3	1	162	5.21	0.79
144	-3	1	48	4.68	1.32
144	-3	1	56	4.75	1.25
144	-3	1	34	4.53	1.46
193	-2	1	116	4.06	1.93
193	-2	1	100	4.00	2.00
193	-2	1	134	4.13	1.87
241	-2	1	27	3.43	2.57
241	-2	1	40	3.60	2.39
241	-2	1	46	3.66	2.33
288	-1	1	166	3.22	2.78
288	-1	1	156	3.19	2.80
288	-1	1	146	3.16	2.83
337	-1	1	37	2.57	3.43
337	-1	1	58	2.76	3.23
337	-1	1	39	2.59	3.41

Bacillus subtilis spores: Batch 1

Laser-based setup with wavelength 270 nm, #3

Date	02.02.2022				
PF	0.9800				
WF	0.9944				
RF	0.9750				
DF	0.9824				
λ in nm	270				
UVT in %	97.5				
S in W/m²	S_{ave} in W/m²	t in s	Fluence in J/m²		
1.75	1.63	55.8	91		
1.75	1.63	83.6	136		
1.74	1.62	111.5	181		
1.74	1.62	139.4	226		
1.75	1.64	167.3	273		
1.75	1.63	195.1	319		
logN0	5.98	irradiation day 5			
Fluence in J/m²	Dilution	Aliquot	Count	logN	logI
91	-4	1	30	5.48	0.51
91	-4	1	24	5.38	0.60
91	-4	1	27	5.43	0.55
136	-3	1	67	4.83	1.16
136	-3	1	72	4.86	1.13
136	-3	1	65	4.81	1.17
181	-2	1	181	4.26	1.73
181	-2	1	153	4.18	1.80
181	-2	1	146	4.16	1.82
226	-2	1	40	3.60	2.38
226	-2	1	52	3.72	2.27
226	-2	1	55	3.74	2.24
273	-1	1	150	3.18	2.81
273	-1	1	199	3.30	2.69
273	-1	1	194	3.29	2.70
319	-1	1	76	2.88	3.10
319	-1	1	61	2.79	3.20
319	-1	1	46	2.66	3.32

Bacillus subtilis spores: Batch 1

Laser-based setup with wavelength 270 nm, #4

Date	12.04.2022				
PF	0.9800				
WF	0.9965				
RF	0.9750				
DF	0.9824				
λ in nm	270				
UVT in %	98.4				
S in W/m²	S_{ave} in W/m²	t in s	Fluence in J/m²		
1.57	1.47	67.5	99		
1.56	1.46	101.1	147		
1.55	1.45	134.8	196		
1.56	1.46	169.0	247		
1.54	1.44	202.0	292		
1.55	1.45	235.7	341		
logN0	6.13	irradiation day 6			
Fluence in J/m²	Dilution	Aliquot	Count	logN	logI
99	-4	1	25	5.40	0.74
99	-4	1	33	5.52	0.62
99	-4	1	42	5.62	0.51
147	-3	1	58	4.76	1.37
147	-3	1	62	4.79	1.34
147	-3	1	48	4.68	1.45
196	-2	1	134	4.13	2.01
196	-2	1	140	4.15	1.99
196	-2	1	125	4.10	2.04
247	-2	1	31	3.49	2.64
247	-2	1	42	3.62	2.51
247	-2	1	30	3.48	2.66
292	-1	1	214	3.33	2.80
292	-1	1	201	3.30	2.83
292	-1	1	190	3.28	2.85
341	-1	1	101	3.00	3.13
341	-1	1	69	2.84	3.29
341	-1	1	67	2.83	3.31

Bacillus subtilis spores: Batch 1

Laser-based setup with wavelength 272 nm, #1

Date	12.04.2022				
PF	0.9800				
WF	0.9962				
RF	0.9750				
DF	0.9824				
λ in nm	272				
UVT in %	98.3				
S in W/m²	S_{ave} in W/m²	t in s	Fluence in J/m²		
1.49	1.39	35.0	49		
1.50	1.40	69.7	98		
1.49	1.39	104.4	146		
1.49	1.40	139.2	194	Sample tube was broken	
1.49	1.39	208.6	291		
1.49	1.39	243.4	339		
logN0	6.13	irradiation day 6			
Fluence in J/m²	Dilution	Aliquot	Count	logN	logI
49	-4	1	99	6.00	0.14
49	-4	1	110	6.04	0.09
49	-4	1	105	6.02	0.11
98	-4	1	40	5.60	0.53
98	-4	1	43	5.63	0.50
98	-4	1	51	5.71	0.43
146	-3	1	140	5.15	0.99
146	-3	1	123	5.09	1.04
146	-3	1	111	5.05	1.09
291	-2	1	46	3.66	2.47
291	-2	1	33	3.52	2.62
291	-2	1	27	3.43	2.70
339	-1	1	110	3.04	3.09
339	-1	1	104	3.02	3.12
339	-1	1	98	2.99	3.14

Bacillus subtilis spores: Batch 1

Laser-based setup with wavelength 275 nm, #1

Date	30.11.2021				
PF	0.9800				
WF	0.9913				
RF	0.9750				
DF	0.9824				
λ in nm	275				
UVT in %	96.1				
S in W/m²	S_{ave} in W/m²	t in s	Fluence in J/m²		
1.46	1.36	42.0	57		
1.45	1.35	83.9	113		
1.46	1.36	125.9	171		
1.47	1.36	167.8	229		
1.46	1.36	251.7	342		
1.47	1.37	293.7	402		
logN0	6.00	irradiation day 2			
Fluence in J/m²	Dilution	Aliquot	Count	logN	logI
57	-4	1	62	5.79	0.20
57	-4	1	79	5.90	0.10
57	-4	1	88	5.94	0.05
113	-4	1	31	5.49	0.51
113	-4	1	34	5.53	0.46
113	-4	1	24	5.38	0.62
171	-3	1	83	4.92	1.08
171	-3	1	68	4.83	1.16
171	-3	1	55	4.74	1.26
229	-2	1	202	4.31	1.69
229	-2	1	144	4.16	1.84
229	-2	1	174	4.24	1.76
342	-2	1	19	3.28	2.72
342	-2	1	30	3.48	2.52
342	-2	1	39	3.59	2.41
402	-1	1	72	2.86	3.14
402	-1	1	91	2.96	3.04
402	-1	1	110	3.04	2.96

Bacillus subtilis spores: Batch 1

Laser-based setup with wavelength 275 nm, #2

Date	01.12.2021				
PF	0.9800				
WF	0.9913				
RF	0.9750				
DF	0.9824				
λ in nm	275				
UVT in %	96.1				
S in W/m²	S_{ave} in W/m²	t in s	Fluence in J/m²		
1.26	1.17	42.0	49		
1.28	1.19	83.9	100		
1.28	1.19	125.9	150		
1.29	1.20	167.8	201		
1.30	1.21	251.7	304		
1.31	1.21	293.7	357		
logN0	6.07	irradiation day 3			
Fluence in J/m²	Dilution	Aliquot	Count	logN	logI
49	-4	1	122	6.09	-0.02
49	-4	1	88	5.94	0.13
49	-4	1	79	5.90	0.17
100	-4	1	55	5.74	0.33
100	-4	1	48	5.68	0.39
100	-4	1	46	5.66	0.41
150	-3	1	183	5.26	0.81
150	-3	1	157	5.20	0.88
150	-3	1	171	5.23	0.84
201	-3	1	56	4.75	1.32
201	-3	1	71	4.85	1.22
201	-3	1	61	4.79	1.29
304	-2	1	114	4.06	2.01
304	-2	1	89	3.95	2.12
304	-2	1	97	3.99	2.08
357	-1	1	388	3.59	2.48
357	-1	1	408	3.61	2.46
357	-1	1	378	3.58	2.49

Bacillus subtilis spores: Batch 1

Laser-based setup with wavelength 275 nm, #3

Date	02.02.2022				
PF	0.9800				
WF	0.9946				
RF	0.9750				
DF	0.9824				
λ in nm	275				
UVT in %	97.6				
S in W/m²	S_{ave} in W/m²	t in s	Fluence in J/m²		
1.22	1.14	42.3	48		
1.21	1.13	84.5	96		
1.20	1.12	126.8	142		
1.20	1.12	169.0	189		
1.21	1.13	253.5	286		
1.21	1.13	295.8	333		
logN0	5.98	irradiation day 5			
Fluence in J/m²	Dilution	Aliquot	Count	logN	logI
48	-4	1	99	6.00	-0.01
48	-4	1	71	5.85	0.13
48	-4	1	67	5.83	0.16
96	-4	1	52	5.72	0.27
96	-4	1	31	5.49	0.49
96	-4	1	34	5.53	0.45
142	-3	1	168	5.23	0.76
142	-3	1	153	5.18	0.80
142	-3	1	151	5.18	0.81
189	-3	1	62	4.79	1.19
189	-3	1	51	4.71	1.28
189	-3	1	65	4.81	1.17
286	-2	1	86	3.93	2.05
286	-2	1	55	3.74	2.24
286	-2	1	61	3.79	2.20
333	-1	1	328	3.52	2.47
333	-1	1	330	3.52	2.47
333	-1	1	316	3.50	2.49

Bacillus subtilis spores: Batch 1

Laser-based setup with wavelength 275 nm, #4

Date	12.04.2022				
PF	0.9800				
WF	0.9959				
RF	0.9750				
DF	0.9824				
λ in nm	275				
UVT in %	98.2				
S in W/m²	S_{ave} in W/m²	t in s	Fluence in J/m²		
1.00	0.94	53.6	50		
1.00	0.94	107.0	100		
1.01	0.94	160.3	151		
1.01	0.94	213.7	201		
1.02	0.95	320.4	305		
1.01	0.95	373.8	354		
logN0	6.13	irradiation day 6			
Fluence in J/m²	Dilution	Aliquot	Count	logN	logI
50	-4	1	101	6.00	0.13
50	-4	1	63	5.80	0.33
50	-4	1	70	5.85	0.29
100	-4	1	55	5.74	0.39
100	-4	1	58	5.76	0.37
100	-4	1	54	5.73	0.40
151	-4	1	25	5.40	0.74
151	-4	1	21	5.32	0.81
151	-4	1	31	5.49	0.64
201	-3	1	68	4.83	1.30
201	-3	1	49	4.69	1.44
201	-3	1	62	4.79	1.34
305	-2	1	71	3.85	2.28
305	-2	1	59	3.77	2.36
305	-2	1	58	3.76	2.37
354	-1	1	223	3.35	2.79
354	-1	1	202	3.31	2.83
354	-2	1	31	3.49	2.64

Bacillus subtilis spores: Batch 1

Laser-based setup with wavelength 277 nm, #1

Date	12.04.2022				
PF	0.9800				
WF	0.9961				
RF	0.9750				
DF	0.9824				
λ in nm	277				
UVT in %	98.2				
S in W/m²	S_{ave} in W/m²	t in s	Fluence in J/m²		
1.11	1.04	48.5	50		
1.11	1.03	96.8	100		
1.10	1.03	145.1	149		
1.11	1.03	193.4	200		
1.10	1.03	290.0	298		
1.10	1.03	338.3	349		
logN0	6.13	irradiation day 6			
Fluence in J/m²	Dilution	Aliquot	Count	logN	logI
50	-4	1	117	6.07	0.07
50	-4	1	68	5.83	0.30
50	-4	1	67	5.83	0.31
100	-4	1	34	5.53	0.60
100	-4	1	36	5.56	0.58
100	-4	1	36	5.56	0.58
149	-3	1	180	5.26	0.88
149	-3	1	153	5.18	0.95
149	-3	1	134	5.13	1.01
200	-3	1	38	4.58	1.55
200	-3	1	36	4.56	1.58
200	-3	1	46	4.66	1.47
298	-2	1	52	3.72	2.42
298	-2	1	45	3.65	2.48
298	-2	1	31	3.49	2.64
349	-1	1	100	3.00	3.13
349	-1	1	95	2.98	3.16
349	-1	1	111	3.05	3.09

Bacillus subtilis spores: Batch 1

Laser-based setup with wavelength 280 nm, #1

Date	28.10.2021				
PF	0.9800				
WF	0.9939				
RF	0.9750				
DF	0.9824				
λ in nm	280				
UVT in %	97.2				
S in W/m²	S_{ave} in W/m²	t in s	Fluence in J/m²		
1.79	1.67	56.8	95		
1.78	1.66	85.2	141		
1.77	1.65	113.6	188		
1.78	1.66	170.5	283		
1.77	1.66	227.3	376		
logN0	6.09	irradiation day 1			
Fluence in J/m²	Dilution	Aliquot	Count	logN	logI
95	-4	1	51	5.71	0.39
95	-4	1	39	5.59	0.50
95	-4	1	28	5.45	0.65
141	-3	1	122	5.09	1.01
141	-3	1	128	5.11	0.99
141	-3	1	108	5.03	1.06
188	-3	1	51	4.71	1.39
188	-3	1	49	4.69	1.40
188	-3	1	61	4.79	1.31
283	-2	1	107	4.03	2.06
283	-2	1	101	4.00	2.09
283	-2	1	90	3.95	2.14
376	-1	1	144	3.16	2.94
376	-1	1	160	3.20	2.89
376	-1	1	154	3.19	2.91

Bacillus subtilis spores: Batch 1

Laser-based setup with wavelength 280 nm, #2

Date	30.11.2021				
PF	0.9800				
WF	0.9926				
RF	0.9750				
DF	0.9824				
λ in nm	280				
UVT in %	96.7				
S in W/m²	S_{ave} in W/m²	t in s	Fluence in J/m²		
1.78	1.65	54.8	91		
1.75	1.64	82.3	135		
1.78	1.66	109.7	182		
1.77	1.65	164.5	272		
1.77	1.65	219.4	361		
logN0	6.00	irradiation day 2			
Fluence in J/m²	Dilution	Aliquot	Count	logN	logI
91	-4	1	37	5.57	0.43
91	-4	1	21	5.32	0.67
91	-4	1	28	5.45	0.55
135	-3	1	168	5.23	0.77
135	-3	1	135	5.13	0.87
135	-3	1	122	5.09	0.91
182	-3	1	52	4.72	1.28
182	-3	1	37	4.57	1.43
182	-3	1	46	4.66	1.33
272	-2	1	108	4.03	1.96
272	-2	1	80	3.90	2.09
272	-2	1	77	3.89	2.11
361	-1	1	171	3.23	2.76
361	-1	1	150	3.18	2.82
361	-1	1	171	3.23	2.76

Bacillus subtilis spores: Batch 1

Laser-based setup with wavelength 280 nm, #3

Date	02.02.2022				
PF	0.9800				
WF	0.9948				
RF	0.9750				
DF	0.9824				
λ in nm	280				
UVT in %	97.7				
S in W/m²	S_{ave} in W/m²	t in s	Fluence in J/m²		
1.49	1.40	64.5	90	Sample tube was broken	
1.49	1.39	96.7	135		
1.48	1.39	129.0	179		
1.49	1.40	193.5	270		
1.49	1.39	258.0	359		
logN0	5.98	irradiation day 5			
Fluence in J/m²	Dilution	Aliquot	Count	logN	logI
135	-3	1	144	5.16	0.83
135	-3	1	128	5.11	0.88
135	-3	1	144	5.16	0.83
179	-3	1	68	4.83	1.15
179	-3	1	64	4.81	1.18
179	-3	1	44	4.64	1.34
270	-2	1	62	3.79	2.19
270	-2	1	82	3.91	2.07
270	-2	1	73	3.86	2.12
359	-1	1	164	3.21	2.77
359	-1	1	152	3.18	2.80
359	-1	1	163	3.21	2.77

Bacillus subtilis spores: Batch 1

Laser-based setup with wavelength 282 nm, #1

Date	02.02.2022				
PF	0.9800				
WF	0.9950				
RF	0.9750				
DF	0.9824				
λ in nm	282				
UVT in %	97.7				
S in W/m²	S_{ave} in W/m²	t in s	Fluence in J/m²		
1.48	1.38	65.4	90		
1.47	1.37	130.9	180		
1.48	1.38	196.3	271		
1.48	1.38	229.0	316		
1.47	1.37	261.8	360		
1.48	1.39	327.2	453		
logN0	5.98	irradiation day 5			
Fluence in J/m²	Dilution	Aliquot	Count	logN	logI
90	-4	1	70	5.85	0.14
90	-4	1	67	5.83	0.16
90	-4	1	64	5.81	0.18
180	-3	1	190	5.28	0.71
180	-3	1	204	5.31	0.68
180	-3	1	198	5.30	0.69
271	-3	1	80	4.90	1.08
271	-3	1	68	4.83	1.15
271	-3	1	72	4.86	1.13
316	-2	1	383	4.58	1.40
316	-2	1	382	4.58	1.40
316	-2	1	336	4.53	1.46
360	-2	1	150	4.18	1.81
360	-2	1	171	4.23	1.75
360	-2	1	157	4.20	1.79
453	-1	1	487	3.69	2.30
453	-1	1	539	3.73	2.25
453	-1	1	506	3.70	2.28

Bacillus subtilis spores: Batch 1

Laser-based setup with wavelength 285 nm, #1

Date	30.11.2021				
PF	0.9800				
WF	0.9936				
RF	0.9750				
DF	0.9824				
λ in nm	285				
UVT in %	97.1				
S in W/m²	S_{ave} in W/m²	t in s	Fluence in J/m²		
1.31	1.22	77.5	94		
1.31	1.22	155.0	189		
1.30	1.22	232.4	283		
1.30	1.21	309.9	376		
1.32	1.23	387.4	475		
logN0	6.00	irradiation day 2			
Fluence in J/m²	Dilution	Aliquot	Count	logN	logI
94	-4	1	107	6.03	-0.03
94	-4	1	100	6.00	0.00
94	-4	1	89	5.95	0.05
189	-4	1	85	5.93	0.07
189	-4	1	61	5.79	0.21
189	-4	1	86	5.93	0.06
283	-3	1	382	5.58	0.41
283	-3	1	411	5.61	0.38
283	-3	1	322	5.51	0.49
376	-3	1	310	5.49	0.51
376	-3	1	309	5.49	0.51
376	-3	1	285	5.45	0.54
475	-2	1	971	4.99	1.01
475	-2	1	1010	5.00	0.99
475	-2	1	898	4.95	1.04

Bacillus subtilis spores: Batch 1

Laser-based setup with wavelength 285 nm, #2

Date	01.12.2021				
PF	0.9800				
WF	0.9936				
RF	0.9750				
DF	0.9824				
λ in nm	285				
UVT in %	97.1				
S in W/m²	S_{ave} in W/m²	t in s	Fluence in J/m²		
1.24	1.15	77.5	89		
1.25	1.16	155.0	180		
1.25	1.16	232.4	271		
1.24	1.16	309.9	360		
1.25	1.16	387.4	450		
logN0	6.07	irradiation day 3			
Fluence in J/m²	Dilution	Aliquot	Count	logN	logI
89	-4	1	119	6.08	0.00
89	-4	1	131	6.12	-0.05
89	-4	1	88	5.94	0.13
180	-4	1	94	5.97	0.10
180	-4	1	128	6.11	-0.04
180	-4	1	98	5.99	0.08
271	-3	1	502	5.70	0.37
271	-3	1	477	5.68	0.39
271	-3	1	419	5.62	0.45
360	-3	1	310	5.49	0.58
360	-3	1	313	5.50	0.58
360	-3	1	316	5.50	0.57
450	-2	1	1210	5.08	0.99
450	-2	1	1370	5.14	0.93
450	-2	1	1130	5.05	1.02

Bacillus subtilis spores: Batch 1

Laser-based setup with wavelength 285 nm, #3

Date	02.02.2022				
PF	0.9800				
WF	0.9951				
RF	0.9750				
DF	0.9824				
λ in nm	285				
UVT in %	97.8				
S in W/m²	S_{ave} in W/m²	t in s	Fluence in J/m²		
1.07	1.00	227.9	227		
1.05	0.98	455.9	449		
1.06	0.99	729.4	720		
1.06	0.99	911.7	902		
logN0	5.98	irradiation day 5			
Fluence in J/m²	Dilution	Aliquot	Count	logN	logI
227	-4	1	60	5.78	0.21
227	-4	1	52	5.72	0.27
227	-4	1	74	5.87	0.12
449	-4	1	28	5.45	0.54
449	-4	1	28	5.45	0.54
449	-4	1	16	5.20	0.78
720	-3	1	59	4.77	1.21
720	-3	1	40	4.60	1.38
720	-3	1	52	4.72	1.27
902	-2	1	184	4.26	1.72
902	-2	1	178	4.25	1.73
902	-2	1	174	4.24	1.74

Bacillus subtilis spores: Batch 1

Laser-based setup with wavelength 290 nm, #1

Date	28.10.2021				
PF	0.9800				
WF	0.9950				
RF	0.9750				
DF	0.9824				
λ in nm	290				
UVT in %	97.8				
S in W/m²	S_{ave} in W/m²	t in s	Fluence in J/m²		
0.98	0.92	204.1	187		
0.99	0.93	408.2	378		
0.98	0.92	612.2	561		
0.99	0.93	816.3	756		
logN0	6.09	irradiation day 1			
Fluence in J/m²	Dilution	Aliquot	Count	logN	logI
187	-4	1	118	6.07	0.02
187	-4	1	90	5.95	0.14
187	-4	1	100	6.00	0.09
378	-4	1	90	5.95	0.14
378	-4	1	90	5.95	0.14
378	-4	1	108	6.03	0.06
561	-4	1	95	5.98	0.12
561	-4	1	89	5.95	0.14
561	-4	1	77	5.89	0.21
756	-4	1	116	6.06	0.03
756	-4	1	93	5.97	0.13
756	-4	1	126	6.10	-0.01

Bacillus subtilis spores: Batch 1

Laser-based setup with wavelength 290 nm, #2

Date	30.11.2021				
PF	0.9800				
WF	0.9943				
RF	0.9750				
DF	0.9824				
λ in nm	290				
UVT in %	97.4				
S in W/m²	S_{ave} in W/m²	t in s	Fluence in J/m²		
0.97	0.91	214.4	195		
0.98	0.91	428.7	390		
0.98	0.91	643.1	588		
0.97	0.91	1071.8	975		
logN0	6.00	irradiation day 2			
Fluence in J/m²	Dilution	Aliquot	Count	logN	logI
195	-4	1	123	6.09	-0.09
195	-4	1	89	5.95	0.05
195	-4	1	95	5.98	0.02
390	-4	1	88	5.94	0.05
390	-4	1	89	5.95	0.05
390	-4	1	92	5.96	0.03
588	-4	1	89	5.95	0.05
588	-4	1	122	6.09	-0.09
588	-4	1	65	5.81	0.18
975	-4	1	71	5.85	0.15
975	-4	1	64	5.81	0.19
975	-4	1	62	5.79	0.20

Bacillus subtilis spores: Batch 1

Laser-based setup with wavelength 300 nm, #1

Date	28.10.2021				
PF	0.9800				
WF	0.9957				
RF	0.9750				
DF	0.9824				
λ in nm	300				
UVT in %	98.1				
S in W/m²	S_{ave} in W/m²	t in s	Fluence in J/m²		
3.40	3.18	58.8	187		
3.36	3.14	117.6	370		
3.34	3.12	176.5	551		
3.32	3.10	235.3	730		
logN0	6.09	irradiation day 1			
Fluence in J/m²	Dilution	Aliquot	Count	logN	logI
187	-4	1	126	6.10	-0.01
187	-4	1	119	6.08	0.02
187	-4	1	116	6.06	0.03
370	-4	1	127	6.10	-0.01
370	-4	1	117	6.07	0.03
370	-4	1	106	6.03	0.07
551	-4	1	153	6.18	-0.09
551	-4	1	146	6.16	-0.07
551	-4	1	120	6.08	0.01
730	-4	1	137	6.14	-0.04
730	-4	1	136	6.13	-0.04
730	-4	1	139	6.14	-0.05

Bacillus subtilis spores: Batch 1

Laser-based setup with wavelength 310 nm, #1

Date	28.10.2021				
PF	0.9800				
WF	0.9960				
RF	0.9750				
DF	0.9824				
λ in nm	310				
UVT in %	98.2				
S in W/m²	S_{ave} in W/m²	t in s	Fluence in J/m²		
4.15	3.88	50.0	194		
4.17	3.90	100.0	390		
4.18	3.90	150.0	586		
4.19	3.91	200.0	783		
logN0	6.09	irradiation day 1			
Fluence in J/m²	Dilution	Aliquot	Count	logN	logI
194	-4	1	129	6.11	-0.02
194	-4	1	108	6.03	0.06
194	-4	1	116	6.06	0.03
390	-4	1	172	6.24	-0.14
390	-4	1	150	6.18	-0.08
390	-4	1	124	6.09	0.00
586	-4	1	150	6.18	-0.08
586	-4	1	151	6.18	-0.09
586	-4	1	126	6.10	-0.01
783	-4	1	120	6.08	0.01
783	-4	1	107	6.03	0.06
783	-4	1	122	6.09	0.01

Bacillus subtilis spores: Batch 1

Laser-based setup with wavelength 320 nm, #1

Date	28.10.2021				
PF	0.9800				
WF	0.9961				
RF	0.9750				
DF	0.9824				
λ in nm	320				
UVT in %	98.3				
S in W/m²	S_{ave} in W/m²	t in s	Fluence in J/m²		
4.76	4.45	43.5	194		
4.76	4.45	87.0	387		
4.79	4.48	130.4	584		
4.78	4.47	173.9	777		
logN0	6.09	irradiation day 1			
Fluence in J/m²	Dilution	Aliquot	Count	logN	logI
194	-4	1	108	6.03	0.06
194	-4	1	91	5.96	0.13
194	-4	1	94	5.97	0.12
387	-4	1	126	6.10	-0.01
387	-4	1	92	5.96	0.13
387	-4	1	112	6.05	0.04
584	-4	1	169	6.23	-0.13
584	-4	1	172	6.24	-0.14
584	-4	1	149	6.17	-0.08
777	-4	1	111	6.05	0.05
777	-4	1	137	6.14	-0.04
777	-4	1	128	6.11	-0.01

Bacillus subtilis spores: Batch 1

LP-CB irradiation at TZW, #1

Date	28.10.2021	Calculation $logN_0$			
		Dilution	Aliquot	Count	$logN_0$
PF	0.9790	-4	1	93	5.97
WF	0.9979	-4	1	110	6.04
RF	0.9750	-4	1	92	5.96
DF	0.9938	-4	1	71	5.85
		-4	1	58	5.76
λ in nm	253.7	-4	1	77	5.89
UVT in %	99.0	-4	1	85	5.93
		-4	1	56	5.75
		-4	1	69	5.84
				$logN_0$ average	5.89
S in W/m²	S_{ave} in W/m²	t in s	Fluence in J/m²		
2.30	2.19	46.5	102		
2.31	2.20	91.5	201		
2.30	2.20	137.0	301		
2.30	2.20	182.5	401		
2.31	2.21	227.5	502		
2.31	2.20	273.0	601		
2.31	2.21	318.0	701		
Fluence in J/m²	Dilution	Aliquot	Count	logN	logI
102	-4	1	79	5.90	-0.01
102	-4	1	81	5.91	-0.02
102	-4	1	65	5.81	0.08
201	-3	1	174	5.24	0.65
201	-3	1	114	5.06	0.83
201	-3	1	122	5.09	0.80
301	-3	1	45	4.65	1.23
301	-3	1	33	4.52	1.37
301	-3	1	24	4.38	1.51
401	-2	1	97	3.99	1.90
401	-2	1	88	3.94	1.94
401	-2	1	82	3.91	1.97
502	-1	1	177	3.25	2.64
502	-1	1	162	3.21	2.68
502	-1	1	177	3.25	2.64
601	-1	1	71	2.85	3.04
601	-1	1	59	2.77	3.12
601	-1	1	59	2.77	3.12
701	0	1	132	2.12	3.77
701	0	1	147	2.17	3.72
701	0	1	124	2.09	3.79

Bacillus subtilis spores: Batch 1

LP-CB irradiation at TZW, #2

Date	06.12.2021	Calculation $logN_0$			
		Dilution	Aliquot	Count	$logN_0$
PF	0.9790	-4	1	102	6.01
WF	0.9979	-4	1	82	5.91
RF	0.9750	-4	1	83	5.92
DF	0.9938	-4	1	77	5.89
		-4	1	71	5.85
λ in nm	253.7	-4	1	71	5.85
UVT in %	99.0	-4	1	62	5.79
		-4	1	85	5.93
		-4	1	57	5.76
				$logN_0$ average	5.88
S in W/m²	S_{ave} in W/m²	t in s	Fluence in J/m²		
2.31	2.20	46.0	101		
2.31	2.20	91.5	202		
2.32	2.21	136.5	302		
2.32	2.21	181.5	401		
2.32	2.22	226.5	502		
2.32	2.21	271.5	601		
2.32	2.21	317.0	702		
Fluence in J/m²	Dilution	Aliquot	Count	logN	logI
101	-4	1	61	5.79	0.09
101	-4	1	52	5.72	0.16
101	-4	1	63	5.80	0.08
202	-3	1	157	5.20	0.68
202	-3	1	147	5.17	0.71
202	-3	1	138	5.14	0.74
302	-3	1	42	4.62	1.26
302	-3	1	30	4.48	1.40
302	-3	1	26	4.41	1.46
401	-2	1	82	3.91	1.96
401	-2	1	79	3.90	1.98
401	-2	1	70	3.85	2.03
502	-1	1	220	3.34	2.54
502	-1	1	241	3.38	2.50
502	-1	1	177	3.25	2.63
601	-1	1	73	2.86	3.02
601	-1	1	59	2.77	3.11
601	-1	1	64	2.81	3.07
702	0	1	156	2.19	3.69
702	0	1	196	2.29	3.59
702	0	1	174	2.24	3.64

Bacillus subtilis spores: Batch 1

LP-CB irradiation at TZW, #3

Date	01.02.2022	Calculation $logN_0$			
		Dilution	Aliquot	Count	$logN_0$
PF	0.9870	-4	1	123	6.09
WF	0.9965	-4	1	82	5.91
RF	0.9750	-4	1	122	6.09
DF	0.9938	-4	1	114	6.06
		-4	1	108	6.03
λ in nm	253.7	-4	1	98	5.99
UVT in %	98.3	-4	1	85	5.93
		-4	1	137	6.14
		-4	1	94	5.97
				$logN_0$ average	6.02
S in W/m²	S_{ave} in W/m²	t in s	Fluence in J/m²		
2.32	2.22	46.0	102		
2.32	2.21	91.0	201		
2.33	2.22	135.5	301		
2.33	2.23	180.5	402		
2.33	2.22	226.0	502		
2.32	2.22	271.5	602		
Fluence in J/m²	Dilution	Aliquot	Count	logN	logI
102	-4	1	55	5.74	0.28
102	-4	1	70	5.85	0.18
102	-4	1	49	5.69	0.33
201	-3	1	239	5.38	0.65
201	-3	1	192	5.28	0.74
201	-3	1	162	5.21	0.81
301	-3	1	37	4.57	1.46
301	-3	1	46	4.66	1.36
301	-3	1	49	4.69	1.33
402	-2	1	119	4.08	1.95
402	-2	1	134	4.13	1.90
402	-2	1	143	4.16	1.87
502	-1	1	285	3.45	2.57
502	-1	1	284	3.45	2.57
502	-1	1	294	3.47	2.56
602	-1	1	86	2.93	3.09
602	-1	1	142	3.15	2.87
602	-1	1	75	2.88	3.15

Bacillus subtilis spores: Batch 1

LP-CB irradiation at TZW, #4

Date	12.04.2022	Calculation $logN_0$			
		Dilution	Aliquot	Count	$logN_0$
PF	0.9870	-4	1	73	5.86
WF	0.9978	-4	1	89	5.95
RF	0.9750	-4	1	91	5.96
DF	0.9938	-4	1	80	5.90
		-4	1	77	5.89
λ in nm	253.7	-4	1	83	5.92
UVT in %	98.9	-4	1	64	5.81
		-4	1	70	5.85
		-4	1	93	5.97
				$logN_0$ average	5.90
S in W/m²	S_{ave} in W/m²	t in s	Fluence in J/m²		
2.28	2.18	46.5	101		
2.29	2.19	92.0	201		
2.29	2.19	138.0	302		
2.30	2.19	183.0	402		
2.30	2.19	228.5	501		
2.30	2.20	274.0	602		
2.30	2.19	320.5	702		
Fluence in J/m²	Dilution	Aliquot	Count	logN	logI
101	-4	1	35	5.54	0.36
101	-4	1	41	5.61	0.29
101	-4	1	46	5.66	0.24
201	-3	1	110	5.04	0.86
201	-3	1	89	4.95	0.95
201	-3	1	114	5.06	0.84
302	-3	1	39	4.59	1.31
302	-3	1	20	4.30	1.60
302	-3	1	29	4.46	1.44
402	-2	1	49	3.69	2.21
402	-2	1	45	3.65	2.25
402	-2	1	56	3.75	2.15
501	-1	1	152	3.18	2.72
501	-1	1	178	3.25	2.65
501	-1	1	150	3.18	2.72
602	-1	1	39	2.59	3.31
602	-1	1	37	2.57	3.33
602	-1	1	56	2.75	3.15
702	0	1	177	2.25	3.65
702	0	1	154	2.19	3.71
702	0	1	116	2.06	3.84

Bacillus subtilis spores: Batch 1

LP-CB irradiation at TZW, #5

Date	12.04.2022	Calculation $logN_0$			
		Dilution	Aliquot	Count	$logN_0$
PF	0.9870	-4	1	62	5.79
WF	0.9978	-4	1	59	5.77
RF	0.9750	-4	1	56	5.75
DF	0.9938	-4	1	76	5.88
		-4	1	88	5.94
λ in nm	253.7	-4	1	77	5.89
UVT in %	98.9	-4	1	100	6.00
		-4	1	76	5.88
		-4	1	83	5.92
				$logN_0$ average	5.87
S in W/m²	S_{ave} in W/m²	t in s	Fluence in J/m²		
2.29	2.19	46.5	102		
2.30	2.19	92.0	202		
2.30	2.19	137.5	302		
2.30	2.19	183.5	402		
2.30	2.19	229.0	502		
2.30	2.19	274.0	601		
2.30	2.19	320.0	702		
Fluence in J/m²	Dilution	Aliquot	Count	logN	logI
102	-4	1	34	5.53	0.34
102	-4	1	37	5.57	0.30
102	-4	1	46	5.66	0.21
202	-3	1	141	5.15	0.72
202	-3	1	119	5.08	0.79
202	-3	1	122	5.09	0.78
302	-2	1	218	4.34	1.53
302	-2	1	186	4.27	1.60
302	-2	1	193	4.29	1.58
402	-2	1	64	3.81	2.06
402	-2	1	70	3.85	2.02
402	-2	1	65	3.81	2.06
502	-1	1	107	3.03	2.84
502	-1	1	135	3.13	2.74
502	-1	1	119	3.08	2.79
601	-1	1	25	2.40	3.47
601	-1	1	33	2.52	3.35
601	-1	1	43	2.63	3.24
702	0	1	131	2.12	3.75
702	0	1	122	2.09	3.78
702	0	1	120	2.08	3.79

Bacillus subtilis spores: Batch 2

Laser-based setup with wavelength 254 nm, #1

Date	01.02.2022				
PF	0.9800				
WF	0.9883				
RF	0.9750				
DF	0.9824				
λ in nm	254				
UVT in %	94.8				
S in W/m²	S_{ave} in W/m²	t in s	Fluence in J/m²		
1.77	1.64	112.5	184		
1.75	1.63	168.8	274		
1.74	1.61	225.0	363		
1.74	1.61	281.3	454		
logN0	6.03				
Fluence in J/m²	Dilution	Aliquot	Count	logN	logI
184	-3	1	245	5.39	0.64
184	-3	1	252	5.40	0.63
184	-3	1	153	5.18	0.84
274	-2	1	149	4.17	1.85
274	-2	1	171	4.23	1.79
274	-2	1	172	4.24	1.79
363	-2	1	54	3.73	2.29
363	-2	1	45	3.65	2.37
363	-2	1	42	3.62	2.40
454	-1	1	46	2.66	3.36
454	-1	1	46	2.66	3.36
454	0	1	492	2.69	3.34

Bacillus subtilis spores: Batch 2

Laser-based setup with wavelength 260 nm, #1

Date	01.02.2022				
PF	0.9800				
WF	0.9883				
RF	0.9750				
DF	0.9824				
λ in nm	260				
UVT in %	94.8				
S in W/m²	S_{ave} in W/m²	t in s	Fluence in J/m²		
1.80	1.67	57.6	96		
1.79	1.66	86.3	144		
1.80	1.67	115.1	192		
1.79	1.66	143.9	239		
1.80	1.67	172.7	288		
1.80	1.67	201.5	336		
logN0	6.03				
Fluence in J/m²	Dilution	Aliquot	Count	logN	logI
96	-4	1	110	6.04	-0.01
96	-4	1	45	5.65	0.37
96	-4	1	51	5.71	0.32
144	-3	1	230	5.36	0.67
144	-3	1	232	5.37	0.66
144	-3	1	232	5.37	0.66
192	-3	1	105	5.02	1.01
192	-3	1	51	4.71	1.32
192	-3	1	47	4.67	1.35
239	-2	1	142	4.15	1.87
239	-2	1	106	4.03	2.00
239	-2	1	149	4.17	1.85
288	-1	1	736	3.87	2.16
288	-1	1	600	3.78	2.25
288	-1	1	600	3.78	2.25
336	-1	1	90	2.95	3.07
336	-1	1	160	3.20	2.82
336	-1	1	152	3.18	2.85

Bacillus subtilis spores: Batch 2

Laser-based setup with wavelength 270 nm, #1

Date	01.02.2022				
PF	0.9800				
WF	0.9884				
RF	0.9750				
DF	0.9824				
λ in nm	270				
UVT in %	94.8				
S in W/m²	S_{ave} in W/m²	t in s	Fluence in J/m²		
1.81	1.68	55.8	94		
1.83	1.70	83.6	142		
1.83	1.70	111.5	189		
1.83	1.70	139.4	237		
1.83	1.70	167.3	284		
logN0	6.03				
Fluence in J/m²	Dilution	Aliquot	Count	logN	logI
94	-4	1	45	5.65	0.37
94	-4	1	21	5.32	0.70
94	-4	1	31	5.49	0.54
142	-3	1	28	4.45	1.58
142	-3	1	30	4.48	1.55
142	-2	1	288	4.46	1.57
189	-2	1	190	4.28	1.75
189	-2	1	107	4.03	2.00
189	-2	1	102	4.01	2.02
237	-1	1	95	2.98	3.05
237	-1	1	145	3.16	2.87
237	-1	1	292	3.47	2.56
284	0	1	156	2.19	3.83
284	0	1	134	2.13	3.90
284	0	1	260	2.41	3.61

Bacillus subtilis spores: Batch 2

Laser-based setup with wavelength 280 nm, #1

Date	01.02.2022				
PF	0.9800				
WF	0.9891				
RF	0.9750				
DF	0.9824				
λ in nm	280				
UVT in %	95.1				
S in W/m²	S_{ave} in W/m²	t in s	Fluence in J/m²		
1.58	1.46	96.7	142		
1.57	1.45	129.0	187		
1.57	1.46	161.2	235		
1.57	1.46	193.5	282		
1.56	1.45	225.7	327		
logN0	6.03				
Fluence in J/m²	Dilution	Aliquot	Count	logN	logI
142	-3	1	138	5.14	0.89
142	-3	1	136	5.13	0.89
142	-3	1	210	5.32	0.70
187	-3	1	42	4.62	1.40
187	-3	1	41	4.61	1.41
187	-2	1	364	4.56	1.47
235	-2	1	121	4.08	1.94
235	-2	1	208	4.32	1.71
235	-2	1	112	4.05	1.98
282	-1	1	268	3.43	2.60
282	-1	1	156	3.19	2.83
282	-1	1	176	3.25	2.78
327	-1	1	18	2.26	3.77
327	-1	1	34	2.53	3.50
327	-1	1	51	2.71	3.32

Bacillus subtilis spores: Batch 1

LP-CB irradiation at TZW for comparison between LP-CB and MP-CB

Date	09.06.2022	Calculation $logN_0$			
		Dilution	Aliquot	Count	$logN_0$
PF	0.9870	-4	1	91	5.96
WF	0.9980	-4	1	76	5.88
RF	0.9750	-4	1	59	5.77
DF	0.9938	-4	1	94	5.97
		-4	1	107	6.03
λ in nm	253.7	-4	1	88	5.94
UVT in %	99.0	-4	1	107	6.03
		-4	1	79	5.90
		-4	1	94	5.97
				$logN_0$ average	5.94
S in W/m²	S_{ave} in W/m²	t in s	Fluence in J/m²		
2.25	2.15	47.5	102		
2.26	2.15	93.5	201		
2.28	2.17	139.0	302		
2.27	2.17	185.5	402		
2.27	2.17	231.5	502		
2.27	2.17	277.0	601		
Fluence in J/m²	Dilution	Aliquot	Count	logN	logI
102	-4	1	67	5.83	0.11
102	-4	1	58	5.76	0.18
102	-4	1	59	5.77	0.17
201	-3	1	146	5.16	0.78
201	-3	1	128	5.11	0.83
201	-3	1	133	5.12	0.82
302	-3	1	33	4.52	1.42
302	-3	1	25	4.40	1.54
302	-3	1	34	4.53	1.41
402	-2	1	52	3.72	2.22
402	-2	1	48	3.68	2.26
402	-2	1	42	3.62	2.32
502	-1	1	177	3.25	2.69
502	-1	1	177	3.25	2.69
502	-1	1	149	3.17	2.77
601	-1	1	55	2.74	3.20
601	-1	1	49	2.69	3.25
601	-1	1	46	2.66	3.28

Bacillus subtilis spores: Batch 1

MP-CB irradiation at TZW for comparison between LP-CB and MP-CB

Date	09.06.2022	Calculation $logN_0$			
		Dilution	Aliquot	Count	$logN_0$
PF	0.9210	-4	1	74	5.87
WF	0.9980	-4	1	95	5.98
RF	0.9750	-4	1	88	5.94
DF	0.9951	-4	1	122	6.09
		-4	1	111	6.05
λ in nm	253.7	-4	1	86	5.93
UVT in %	99.0	-4	1	95	5.98
		-4	1	49	5.69
		-4	1	85	5.93
				$logN_0$ average	5.94
S in W/m²	S_{ave} in W/m²	t in s	Fluence in J/m²		
3.33	3.18	32.0	102		
3.33	3.18	63.5	202		
3.33	3.18	95.0	302		
3.33	3.18	126.5	402		
3.33	3.18	158.0	502		
3.33	3.18	189.5	602		
Fluence in J/m²	Dilution	Aliquot	Count	logN	logI
102	-4	1	51	5.71	0.23
102	-4	1	43	5.63	0.31
102	-4	1	40	5.60	0.34
202	-3	1	46	4.66	1.28
202	-3	1	51	4.71	1.23
202	-3	1	71	4.85	1.09
302	-2	1	92	3.96	1.98
302	-2	1	91	3.96	1.98
302	-2	1	88	3.94	1.99
402	-1	1	174	3.24	2.70
402	-1	1	132	3.12	2.82
402	-1	1	135	3.13	2.81
502	0	1	294	2.47	3.47
502	-1	1	37	2.57	3.37
502	-1	1	36	2.56	3.38
602	0	1	122	2.09	3.85
602	0	1	138	2.14	3.80
602	0	1	100	2.00	3.94

Bacillus subtilis spores: Batch 1

Laser-based setup with wavelength 254 nm at low irradiances

Date	12.0.2022				
PF	0.9800				
WF	0.9978				
RF	0.9750				
DF	0.9824				
λ in nm	254				
UVT in %	99.0				
S in W/m²	S_{ave} in W/m²	t in s	Fluence in J/m²		
0.08	0.08	1123.2	86		
0.08	0.08	4504.7	339		
logN0	6.13	Irradiation day 6			
Fluence in J/m²	Dilution	Aliquot	Count	logN	logI
86	-4	1	101	6.00	0.13
86	-4	1	74	5.87	0.26
86	-4	1	99	6.00	0.14
339	-2	1	200	4.30	1.83
339	-2	1	199	4.30	1.83
339	-2	1	255	4.41	1.73

Bacillus subtilis spores: Batch 1

Laser-based setup with wavelength 265 nm at low irradiances

Date	12.0.2022				
PF	0.9800				
WF	0.9972				
RF	0.9750				
DF	0.9824				
λ in nm	265				
UVT in %	98.7				
S in W/m²	S_{ave} in W/m²	t in s	Fluence in J/m²		
0.11	0.10	974.0	102		
0.11	0.10	3459.4	362		
logN0	6.13	Irradiation day 6			
Fluence in J/m²	Dilution	Aliquot	Count	logN	logI
102	-4	1	41	5.61	0.52
102	-4	1	52	5.72	0.42
102	-4	1	54	5.73	0.40
362	-1	1	150	3.18	2.96
362	-1	1	126	3.10	3.03
362	-1	1	143	3.16	2.98

Bacillus subtilis spores: Batch 1

Laser-based setup with wavelength 270 nm at low irradiances

Date	12.0.2022				
PF	0.9800				
WF	0.9965				
RF	0.9750				
DF	0.9824				
λ in nm	270				
UVT in %	98.4				
S in W/m²	S_{ave} in W/m²	t in s	Fluence in J/m²		
0.10	0.10	979.3	94		
0.10	0.10	2942.6	281		
logN0	6.13	Irradiation day 6			
Fluence in J/m²	Dilution	Aliquot	Count	logN	logI
94	-4	1	31	5.49	0.64
94	-4	1	44	5.64	0.49
94	-4	1	34	5.53	0.60
281	-2	1	37	3.57	2.57
281	-2	1	34	3.53	2.60
281	-2	1	46	3.66	2.47

MS2 phage

Laser-based setup with wavelength 254 nm, #1

Date	29.11.2022				
PF	0.9800				
WF	0.9933				
RF	0.9750				
DF	0.9824				
λ in nm	254				
UVT in %	97.0				
S in W/m²	S_{ave} in W/m²	t in s	Fluence in J/m²		
2.77	2.53	37.3	95		
2.74	2.50	111.5	279		
2.73	2.50	148.6	371		
2.72	2.49	185.7	462		
2.72	2.49	223.2	555		
2.71	2.48	297.0	736		
logN0	5.58				
Fluence in J/m²	Dilution	Aliquot	Count	logN	logI
0	-4	1	36	5.56	0.02
0	-4	1	40	5.60	-0.02
95	-3	1	51	4.71	0.87
95	-3	1	47	4.67	0.91
279	-2	1	139	4.14	1.44
279	-2	1	148	4.17	1.41
371	-1	1	194	3.29	2.29
371	-1	1	186	3.27	2.31
462	-1	1	98	2.99	2.59
462	-1	1	72	2.86	2.72
555	-1	1	60	2.78	2.80
555	-1	1	76	2.88	2.70
736	0	1	106	2.03	3.55
736	0	1	129	2.11	3.47

MS2 phage

Laser-based setup with wavelength 254 nm, #2

Date	30.11.2022				
PF	0.9800				
WF	0.9933				
RF	0.9750				
DF	0.9824				
λ in nm	254				
UVT in %	97.0				
S in W/m²	S_{ave} in W/m²	t in s	Fluence in J/m²		
2.75	2.51	37.3	94		
2.72	2.49	111.5	277		
2.70	2.47	148.6	367		
2.70	2.47	185.7	458		
2.70	2.46	223.1	550		
2.70	2.46	297.0	732		
logN0	6.29				
Fluence in J/m²	Dilution	Aliquot	Count	logN	logI
0	-4	1	178	6.25	0.04
0	-4	1	214	6.33	-0.04
94	-4	1	33	5.52	0.77
94	-4	1	40	5.60	0.69
277	-2	1	221	4.34	1.95
277	-2	1	225	4.35	1.94
367	-2	1	62	3.79	2.50
367	-2	1	61	3.79	2.51
458	-2	1	35	3.54	2.75
458	-2	1	33	3.52	2.77
550	-1	1	86	2.93	3.36
550	-1	1	111	3.05	3.25
732	0	1	101	2.00	4.29
732	0	1	97	1.99	4.30

MS2 phage

Laser-based setup with wavelength 254 nm, #3

Date	21.02.2023				
PF	0.9800				
WF	0.9929				
RF	0.9750				
DF	0.9824				
λ in nm	254				
UVT in %	96.8				
S in W/m²	S_{ave} in W/m²	t in s	Fluence in J/m²		
2.68	2.44	39.4	96		
2.63	2.40	117.7	283		
2.63	2.40	156.8	377		
2.63	2.40	196.0	471		
2.62	2.39	235.1	563		
2.63	2.40	313.5	754		
logN0	6.62				
Fluence in J/m²	Dilution	Aliquot	Count	logN	logI
0	-5	1	39	6.59	0.03
0	-5	1	45	6.65	-0.03
96	-4	1	34	5.53	1.09
96	-4	1	33	5.52	1.10
283	-3	1	41	4.61	2.01
283	-3	1	51	4.71	1.91
377	-2	1	188	4.27	2.35
377	-2	1	177	4.25	2.37
471	-2	1	74	3.87	2.75
471	-2	1	91	3.96	2.66
563	-1	1	121	3.08	3.54
563	-1	1	195	3.29	3.33
754	-1	1	29	2.46	4.16
754	-1	1	47	2.67	3.95

MS2 phage

Laser-based setup with wavelength 260 nm, #1

Date	29.11.2022				
PF	0.9800				
WF	0.9944				
RF	0.9750				
DF	0.9824				
λ in nm	260				
UVT in %	97.5				
S in W/m²	S_{ave} in W/m²	t in s	Fluence in J/m²		
2.61	2.39	38.2	91		
2.62	2.40	76.1	183		
2.62	2.40	114.0	274		
2.64	2.41	151.9	367		
2.63	2.41	189.8	457		
2.63	2.41	227.7	548		
logN0	5.79				
Fluence in J/m²	Dilution	Aliquot	Count	logN	logI
0	0	-4	1	71.00	5.85
0	0	-4	1	54.00	5.73
91	8282	-3	1	74.00	4.87
91	8282	-3	1	76.00	4.88
183	33315	-2	1	206.00	4.31
183	33315	-2	1	213.00	4.33
274	74894	-2	1	87.00	3.94
274	74894	-2	1	77.00	3.89
367	134486	-2	1	36.00	3.56
367	134486	-2	1	35.00	3.54
457	208552	-1	1	45.00	2.65
457	208552	-1	1	58.00	2.76
548	300478	-1	1	20.00	2.30
548	300478	-1	1	31.00	2.49

MS2 phage

Laser-based setup with wavelength 260 nm, #2

Date	21.02.2023				
PF	0.9800				
WF	0.9938				
RF	0.9750				
DF	0.9824				
λ in nm	260				
UVT in %	97.2				
S in W/m²	S_{ave} in W/m²	t in s	Fluence in J/m²		
2.37	2.17	42.7	93		
2.39	2.19	85.2	186		
2.39	2.19	127.6	279		
2.40	2.19	170.1	373		
2.39	2.18	212.5	464		
2.39	2.18	255.0	557		
logN0	6.33				
Fluence in J/m²	Dilution	Aliquot	Count	logN	logI
0	0	-4	1	195.00	6.29
0	0	-4	1	238.00	6.38
93	8581	-4	1	48.00	5.68
93	8581	-4	1	48.00	5.68
186	34753	-3	1	49.00	4.69
186	34753	-3	1	63.00	4.80
279	77963	-3	1	41.00	4.61
279	77963	-3	1	48.00	4.68
373	138938	-2	1	84.00	3.92
373	138938	-2	1	99.00	4.00
464	215552	-1	1	442.00	3.65
464	215552	-1	1	302.00	3.48
557	309946	-1	1	208.00	3.32
557	309946	-1	1	218.00	3.34

MS2 phage

Laser-based setup with wavelength 265 nm, #1

Date	29.11.2022				
PF	0.9800				
WF	0.9949				
RF	0.9750				
DF	0.9824				
λ in nm	265				
UVT in %	97.7				
S in W/m²	S_{ave} in W/m²	t in s	Fluence in J/m²		
2.63	2.41	38.6	93		
2.63	2.41	77.1	186		
2.64	2.42	115.5	279		
2.64	2.42	153.9	373		
2.63	2.41	193.0	466		
2.63	2.41	230.7	557		
logN0	5.58				
Fluence in J/m²	Dilution	Aliquot	Count	logN	logI
0	0	-4	1	30.00	5.48
0	0	-4	1	48.00	5.68
93	8649	-2	1	279.00	4.45
93	8649	-2	1	297.00	4.47
186	34531	-2	1	128.00	4.11
186	34531	-2	1	128.00	4.11
279	77927	-1	1	180.00	3.26
279	77927	-1	1	174.00	3.24
373	138848	-1	1	119.00	3.08
373	138848	-1	1	92.00	2.96
466	216914	-1	1	37.00	2.57
466	216914	-1	1	49.00	2.69
557	309774	0	1	185.00	2.27
557	309774	0	1	187.00	2.27

MS2 phage

Laser-based setup with wavelength 265 nm, #2

Date	21.02.2023				
PF	0.9800				
WF	0.9940				
RF	0.9750				
DF	0.9824				
λ in nm	265				
UVT in %	97.3				
S in W/m²	S_{ave} in W/m²	t in s	Fluence in J/m²		
2.49	2.28	41.3	94		
2.49	2.28	82.4	188		
2.47	2.27	123.5	280		
2.48	2.27	164.5	374		
2.47	2.27	205.6	466		
2.47	2.26	247.2	559		
logN0	6.72				
Fluence in J/m²	Dilution	Aliquot	Count	logN	logI
0	0	-5	1	47.00	6.67
0	0	-5	1	58.00	6.76
94	8882	-4	1	71.00	5.85
94	8882	-4	1	78.00	5.89
188	35249	-3	1	157.00	5.20
188	35249	-3	1	168.00	5.23
280	78241	-3	1	57.00	4.76
280	78241	-3	1	58.00	4.76
374	139583	-2	1	230.00	4.36
374	139583	-2	1	200.00	4.30
466	217004	-2	1	91.00	3.96
466	217004	-2	1	92.00	3.96
559	313037	-1	1	204.00	3.31
559	313037	-1	1	218.00	3.34

MS2 phage

Laser-based setup with wavelength 267 nm, #1

Date	29.11.2022				
PF	0.9800				
WF	0.9950				
RF	0.9750				
DF	0.9824				
λ in nm	267				
UVT in %	97.8				
S in W/m²	S_{ave} in W/m²	t in s	Fluence in J/m²		
2.64	2.42	39.9	96		
2.65	2.42	79.5	193		
2.65	2.43	119.1	289		
2.65	2.42	158.7	385		
2.66	2.43	199.0	484		
2.65	2.42	238.0	577		
logN0	5.53				
Fluence in J/m²	Dilution	Aliquot	Count	logN	logI
0	-4	1	32	5.51	0.03
0	-4	1	36	5.56	-0.03
96	-3	1	125	5.10	0.43
96	-3	1	127	5.10	0.43
193	-2	1	126	4.10	1.43
193	-2	1	89	3.95	1.58
289	-2	1	52	3.72	1.81
289	-2	1	42	3.62	1.91
385	-1	1	148	3.17	2.36
385	-1	1	138	3.14	2.39
484	-1	1	15	2.18	3.35
484	-1	1	19	2.28	3.25
577	0	1	177	2.25	3.28
577	0	1	160	2.20	3.33

MS2 phage

Laser-based setup with wavelength 267 nm, #2

Date	21.02.2023				
PF	0.9800				
WF	0.9941				
RF	0.9750				
DF	0.9824				
λ in nm	267				
UVT in %	97.3				
S in W/m²	S_{ave} in W/m²	t in s	Fluence in J/m²		
2.57	2.35	41.3	97		
2.57	2.35	82.5	194		
2.58	2.36	123.6	292		
2.58	2.36	164.7	388		
2.58	2.36	205.8	486		
2.58	2.36	247.2	584		
logN0	6.69				
Fluence in J/m²	Dilution	Aliquot	Count	logN	logI
0	-5	1	50	6.70	-0.01
0	-5	1	47	6.67	0.01
97	-4	1	22	5.34	1.34
97	-4	1	27	5.43	1.25
194	-3	1	127	5.10	1.58
194	-3	1	108	5.03	1.65
292	-3	1	17	4.23	2.46
292	-3	1	29	4.46	2.22
388	-2	1	157	4.20	2.49
388	-2	1	169	4.23	2.46
486	-1	1	468	3.67	3.02
486	-1	1	432	3.64	3.05
584	-1	1	182	3.26	3.43
584	-1	1	218	3.34	3.35

MS2 phage

Laser-based setup with wavelength 270 nm, #1

Date	29.11.2022				
PF	0.9800				
WF	0.9952				
RF	0.9750				
DF	0.9824				
λ in nm	270				
UVT in %	97.8				
S in W/m²	S_{ave} in W/m²	t in s	Fluence in J/m²		
2.82	2.58	39.4	102		
2.81	2.57	78.6	202		
2.82	2.58	117.7	304		
2.83	2.59	156.9	406		
2.82	2.59	196.0	507		
2.83	2.59	235.2	610		
logN0	5.73				
Fluence in J/m²	Dilution	Aliquot	Count	logN	logI
0	-4	1	47	5.67	0.06
0	-4	1	61	5.79	-0.06
102	-3	1	61	4.79	0.94
102	-3	1	69	4.84	0.89
202	-2	1	135	4.13	1.60
202	-2	1	169	4.23	1.50
304	-2	1	39	3.59	2.14
304	-2	1	33	3.52	2.21
406	-1	1	79	2.90	2.83
406	-1	1	87	2.94	2.79
507	-1	1	15	2.18	3.55
507	-1	1	25	2.40	3.33
610	0	1	163	2.21	3.52
610	0	1	146	2.16	3.56

MS2 phage

Laser-based setup with wavelength 270 nm, #2

Date	21.02.2023				
PF	0.9800				
WF	0.9941				
RF	0.9750				
DF	0.9824				
λ in nm	270				
UVT in %	97.3				
S in W/m²	S_{ave} in W/m²	t in s	Fluence in J/m²		
2.75	2.52	38.8	98		
2.76	2.52	77.4	195		
2.76	2.52	116.0	292		
2.76	2.52	154.5	389		
2.76	2.52	193.1	487		
2.76	2.52	231.7	585		
logN0	6.40				
Fluence in J/m²	Dilution	Aliquot	Count	logN	logI
0	-5	1	28	6.45	-0.04
0	-5	1	23	6.36	0.04
98	-4	1	49	5.69	0.71
98	-4	1	65	5.81	0.59
195	-3	1	75	4.88	1.53
195	-3	1	74	4.87	1.54
292	-2	1	215	4.33	2.07
292	-2	1	263	4.42	1.98
389	-2	1	81	3.91	2.50
389	-2	1	95	3.98	2.43
487	-2	1	39	3.59	2.81
487	-2	1	42	3.62	2.78
585	-1	1	119	3.08	3.33
585	-1	1	112	3.05	3.36

MS2 phage

Laser-based setup with wavelength 275 nm, #1

Date	29.11.2022				
PF	0.9800				
WF	0.9955				
RF	0.9750				
DF	0.9824				
λ in nm	275				
UVT in %	98.0				
S in W/m²	S_{ave} in W/m²	t in s	Fluence in J/m²		
2.09	1.92	58.8	113		
2.10	1.92	117.3	225		
2.10	1.92	175.8	338		
2.09	1.92	235.3	451		
2.10	1.93	292.9	564		
2.10	1.93	351.4	677		
logN0	5.51				
Fluence in J/m²	Dilution	Aliquot	Count	logN	logI
0	-4	1	30	5.48	0.03
0	-4	1	35	5.54	-0.03
113	-3	1	39	4.59	0.92
113	-3	1	44	4.64	0.87
225	-2	1	201	4.30	1.21
225	-2	1	180	4.26	1.26
338	-1	1	159	3.20	2.31
338	-1	1	222	3.35	2.16
451	-1	1	80	2.90	2.61
451	-1	1	98	2.99	2.52
564	-1	1	23	2.36	3.15
564	-1	1	22	2.34	3.17
677	0	1	185	2.27	3.24
677	0	1	193	2.29	3.23

MS2 phage

Laser-based setup with wavelength 275 nm, #2

Date	21.02.2023				
PF	0.9800				
WF	0.9942				
RF	0.9750				
DF	0.9824				
λ in nm	275				
UVT in %	97.4				
S in W/m²	S_{ave} in W/m²	t in s	Fluence in J/m²		
2.26	2.07	52.7	109		
2.23	2.04	105.1	214		
2.22	2.03	157.6	321		
2.22	2.03	210.0	427		
2.23	2.04	262.5	535		
2.22	2.03	314.9	641		
logN0	6.41				
Fluence in J/m²	Dilution	Aliquot	Count	logN	logI
0	-4	1	248	6.39	0.02
0	-4	1	266	6.42	-0.02
109	-4	1	54	5.73	0.68
109	-4	1	67	5.83	0.58
214	-3	1	118	5.07	1.34
214	-3	1	122	5.09	1.32
321	-3	1	63	4.80	1.61
321	-3	1	63	4.80	1.61
427	-2	1	173	4.24	2.17
427	-2	1	163	4.21	2.20
535	-1	1	202	3.31	3.10
535	-1	1	200	3.30	3.11
641	-1	1	65	2.81	3.60
641	-1	1	85	2.93	3.48

MS2 phage

Laser-based setup with wavelength 277 nm, #1

Date	29.11.2022				
PF	0.9800				
WF	0.9957				
RF	0.9750				
DF	0.9824				
λ in nm	277				
UVT in %	98.0				
S in W/m²	S_{ave} in W/m²	t in s	Fluence in J/m²		
2.26	2.07	54.0	112		
2.26	2.07	107.8	223		
2.27	2.08	161.5	336		
2.26	2.07	215.3	446		
2.26	2.07	269.0	558		
2.27	2.08	322.8	672		
logN0	5.69				
Fluence in J/m²	Dilution	Aliquot	Count	logN	logI
0	-4	1	62	5.79	-0.11
0	-4	1	38	5.58	0.11
112	-3	1	62	4.79	0.89
112	-3	1	48	4.68	1.00
223	-2	1	137	4.14	1.55
223	-2	1	152	4.18	1.50
336	-2	1	38	3.58	2.11
336	-2	1	28	3.45	2.24
446	-2	1	22	3.34	2.34
446	-2	1	25	3.40	2.29
558	-1	1	40	2.60	3.08
558	-1	1	42	2.62	3.06
672	-1	1	10	2.00	3.69
672	-1	1	20	2.30	3.39

MS2 phage

Laser-based setup with wavelength 277 nm, #2

Date	21.02.2023				
PF	0.9800				
WF	0.9943				
RF	0.9750				
DF	0.9824				
λ in nm	277				
UVT in %	97.4				
S in W/m²	S_{ave} in W/m²	t in s	Fluence in J/m²		
2.32	2.12	49.7	105		
2.32	2.12	99.1	210		
2.33	2.13	148.6	317		
2.32	2.12	198.1	421		
2.33	2.13	247.5	526		
2.33	2.13	297.0	632		
logN0	6.20				
Fluence in J/m²	Dilution	Aliquot	Count	logN	logI
0	-4	1	162	6.21	-0.01
0	-4	1	157	6.20	0.01
105	-4	1	15	5.18	1.03
105	-4	1	16	5.20	1.00
210	-3	1	96	4.98	1.22
210	-3	1	115	5.06	1.14
317	-2	1	149	4.17	2.03
317	-2	1	154	4.19	2.02
421	-2	1	110	4.04	2.16
421	-2	1	114	4.06	2.15
526	-2	1	38	3.58	2.62
526	-2	1	38	3.58	2.62
632	-1	1	137	3.14	3.07
632	-1	1	96	2.98	3.22

MS2 phage

Laser-based setup with wavelength 280 nm, #1

Date	29.11.2022				
PF	0.9800				
WF	0.9958				
RF	0.9750				
DF	0.9824				
λ in nm	280				
UVT in %	98.1				
S in W/m²	S_{ave} in W/m²	t in s	Fluence in J/m²		
2.52	2.30	38.0	88		
2.67	2.45	75.8	186		
2.68	2.45	113.6	278		
2.68	2.46	151.3	372		
2.67	2.45	189.1	463		
logN0	5.04				
Fluence in J/m²	Dilution	Aliquot	Count	logN	logI
0	-4	1	12	5.08	-0.04
0	-4	1	10	5.00	0.04
88	-3	1	30	4.48	0.56
88	-3	1	39	4.59	0.45
186	-3	1	32	4.51	0.53
186	-3	1	30	4.48	0.56
278	-2	1	142	4.15	0.89
278	-2	1	134	4.13	0.91
372	-2	1	113	4.05	0.99
372	-2	1	91	3.96	1.08
463	-2	1	19	3.28	1.76
463	-2	1	18	3.26	1.78

MS2 phage

Laser-based setup with wavelength 280 nm, #2

Date	21.02.2023				
PF	0.9800				
WF	0.9943				
RF	0.9750				
DF	0.9824				
λ in nm	280				
UVT in %	97.4				
S in W/m²	S_{ave} in W/m²	t in s	Fluence in J/m²		
2.52	2.31	40.1	92		
2.51	2.29	80.0	184		
2.52	2.31	119.8	276		
2.51	2.29	159.7	366		
2.52	2.30	199.6	460		
logN0	6.22				
Fluence in J/m²	Dilution	Aliquot	Count	logN	logI
0	-4	1	173	6.24	-0.01
0	-4	1	162	6.21	0.01
92	-3	1	112	5.05	1.17
92	-3	1	112	5.05	1.17
184	-3	1	53	4.72	1.50
184	-3	1	72	4.86	1.37
276	-3	1	39	4.59	1.63
276	-3	1	57	4.76	1.47
366	-2	1	114	4.06	2.17
366	-2	1	103	4.01	2.21
460	-2	1	248	4.39	1.83
460	-2	1	289	4.46	1.76

MS2 phage

Laser-based setup with wavelength 290 nm, #1

Date	30.11.2022				
PF	0.9800				
WF	0.9964				
RF	0.9750				
DF	0.9824				
λ in nm	290				
UVT in %	98.4				
S in W/m²	S_{ave} in W/m²	t in s	Fluence in J/m²		
1.69	1.55	260.3	402		
1.70	1.55	520.4	809		
1.71	1.56	780.5	1220		
logN0	6.06				
Fluence in J/m²	Dilution	Aliquot	Count	logN	logI
0	-4	1	117	6.07	-0.01
0	-4	1	112	6.05	0.01
402	-3	1	114	5.06	1.00
402	-3	1	106	5.03	1.03
809	-2	1	103	4.01	2.05
809	-2	1	106	4.03	2.03
1220	-1	1	170	3.23	2.83
1220	-1	1	180	3.26	2.80

MS2 phage

Laser-based setup with wavelength 290 nm, #2

Date	21.02.2023				
PF	0.9800				
WF	0.9948				
RF	0.9750				
DF	0.9824				
λ in nm	290				
UVT in %	97.7				
S in W/m²	S_{ave} in W/m²	t in s	Fluence in J/m²		
1.67	1.53	249.2	381		
1.67	1.53	498.1	763		
1.67	1.53	747.5	1144	Sample tube broken	
logN0	5.74				
Fluence in J/m²	Dilution	Aliquot	Count	logN	logI
0	-4	1	49	5.69	0.05
0	-4	1	61	5.79	-0.05
381	-3	1	80	4.90	0.83
381	-3	1	63	4.80	0.94
763	-2	1	18	3.26	2.48
763	-2	1	17	3.23	2.51

MS2 phage

LP-CB irradiation at TZW, #1

Date	30.11.2022				
PF	0.9730				
WF	0.9950				
RF	0.9750				
DF	0.9838				
λ in nm	254				
UVT in %	97.6				
S in W/m²	S_{ave} in W/m²	t in s	Fluence in J/m²		
2.28	2.14	47.5	102		
2.32	2.18	138.5	302		
2.32	2.18	184.0	401		
2.33	2.19	229.5	502		
2.33	2.19	275.0	601		
2.33	2.19	366.5	802		
logN0	6.14				
Fluence in J/m²	Dilution	Aliquot	Count	logN	logI
0	-4	1	133	6.12	0.02
0	-4	1	143	6.16	-0.02
102	-3	1	127	5.10	1.04
102	-3	1	118	5.07	1.07
302	-2	1	155	4.19	1.95
302	-2	1	123	4.09	2.05
401	-2	1	66	3.82	2.32
401	-2	1	77	3.89	2.25
502	-2	1	28	3.45	2.69
502	-2	1	31	3.49	2.65
601	-1	1	99	3.00	3.14
601	-1	1	99	3.00	3.14
802	0	1	115	2.06	4.08
802	0	1	133	2.12	4.02

MS2 phage

LP-CB irradiation at TZW, #2

Date	30.11.2022				
PF	0.9730				
WF	0.9950				
RF	0.9750				
DF	0.9838				
λ in nm	254				
UVT in %	97.6				
S in W/m²	S_{ave} in W/m²	t in s	Fluence in J/m²		
2.28	2.14	47.5	102		
2.32	2.18	138.5	302		
2.32	2.18	184.0	401		
2.33	2.19	229.5	502		
2.33	2.19	275.0	601		
2.33	2.19	366.5	802		
logN0	5.52				
Fluence in J/m²	Dilution	Aliquot	Count	logN	logI
0	-4	1	36	5.56	-0.04
0	-4	1	30	5.48	0.04
102	-3	1	49	4.69	0.83
102	-3	1	60	4.78	0.74
302	-2	1	50	3.70	1.82
302	-2	1	35	3.54	1.97
401	-1	1	152	3.18	2.33
401	-1	1	178	3.25	2.27
502	-1	1	90	2.95	2.56
502	-1	1	91	2.96	2.56
601	-1	1	41	2.61	2.90
601	-1	1	50	2.70	2.82
802	0	1	91	1.96	3.56
802	0	1	74	1.87	3.65

MS2 phage

LP-CB irradiation at TZW, #3

Date	22.02.2023				
PF	0.98721				
WF	0.9952				
RF	0.9750				
DF	0.9838				
λ in nm	254				
UVT in %	97.7				
S in W/m²	S_{ave} in W/m²	t in s	Fluence in J/m²		
2.25	2.13	47.5	101		
2.29	2.17	139.0	301		
2.30	2.18	184.5	401		
2.30	2.18	230.5	501		
2.30	2.18	276.5	602		
2.30	2.18	368.0	802		
logN0	6.13				
Fluence in J/m²	Dilution	Aliquot	Count	logN	logI
0	-4	1	144	6.16	-0.03
0	-4	1	128	6.11	0.03
101	-3	1	292	5.47	0.67
101	-3	1	320	5.51	0.63
301	-3	1	65	4.81	1.32
301	-3	1	77	4.89	1.25
401	-2	1	135	4.13	2.00
401	-2	1	145	4.16	1.97
501	-2	1	77	3.89	2.25
501	-2	1	114	4.06	2.08
602	-2	1	40	3.60	2.53
602	-2	1	26	3.41	2.72
802	-1	1	118	3.07	3.06
802	-1	1	165	3.22	2.92

Appendix D: Chapter 4: COMSOL Multiphysics®

Equations for Turbulent flow calculations using realizable k-ε model:

Equation

Equation form:

Study controlled

Show equation assuming:

Studie 1, Stationär

$$\rho(\mathbf{u}\cdot\nabla)\mathbf{u} = \nabla\cdot[-p\mathbf{I}+\mathbf{K}]+\mathbf{F}$$

$$\rho\nabla\cdot\mathbf{u} = 0$$

$$\mathbf{K} = (\mu+\mu_T)\left(\nabla\mathbf{u}+(\nabla\mathbf{u})^T\right)$$

$$\rho(\mathbf{u}\cdot\nabla)k = \nabla\cdot\left[\left(\mu+\frac{\mu_T}{\sigma_k}\right)\nabla k\right]+P_k - \rho\epsilon$$

$$\rho(\mathbf{u}\cdot\nabla)\epsilon = \nabla\cdot\left[\left(\mu+\frac{\mu_T}{\sigma_\epsilon}\right)\nabla\epsilon\right]+C_1\rho S\epsilon - C_{\epsilon 2}\frac{\rho\epsilon^2}{k+\sqrt{\nu\epsilon}}, \quad \epsilon = \text{ep}$$

$$C_1 = max\left\{0.43,\frac{\eta}{5+\eta}\right\},\ \eta = \frac{Sk}{\epsilon},\ S = \sqrt{2\mathbf{S}:\mathbf{S}},\ \mathbf{S} = \frac{1}{2}\left(\nabla\mathbf{u}+(\nabla\mathbf{u})^T\right)$$

$$\mu_T = \rho C_\mu\frac{k^2}{\epsilon},\ C_\mu = \frac{1}{A_0+A_s U^{(\star)}\frac{k}{\epsilon}},\ A_s = \sqrt{6}\cos\left(\frac{1}{3}\arccos\left(\sqrt{6}W\right)\right)$$

$$W = \frac{2\sqrt{2}\mathbf{S}:(\mathbf{S}\cdot\mathbf{S})}{|\mathbf{S}|^3},\ U^{(\star)} = \sqrt{\mathbf{S}:\mathbf{S}+\mathbf{\Omega}:\mathbf{\Omega}},\ \mathbf{\Omega} = \frac{1}{2}\left(\nabla\mathbf{u}-(\nabla\mathbf{u})^T\right)$$

$$P_k = \mu_T\left[\nabla\mathbf{u}:\left(\nabla\mathbf{u}+(\nabla\mathbf{u})^T\right)\right]$$

Model constants:

Variables

Name	Expression	Unit	Description
spf.T_stress_uz	up(spf.T_stress_tensorzx)*spf.unx...	N/m²	Total traction, interior boundar...
spf.sigmaw	0.2	1	Smoothing parameter
spf.sigmak	1	1	Turbulence model parameter
spf.sigmaeps_Rkeps	1.2	1	Turbulence model parameter
spf.RkepsC2	1.9	1	Turbulence model parameter
spf.A0	4	1	Turbulence model parameter
spf.kappav	0.41	1	Turbulence model parameter
spf.B	5.2	1	Law of the wall constant
spf.usePseudoTimeStepping	1	1	Help variable